Dynamic Optimization
of Gas Transmission Networks
for Storage of Renewable Energy

Von der Fakultät für Mathematik und Physik
der Gottfried Wilhelm Leibniz Universität Hannover

zur Erlangung des Grades
Doktor der Naturwissenschaften
Dr. rer. nat.

genehmigte Dissertation
von

M.Sc. Jan Thiedau

2018

Abstract

To ensure security of supply in the presence of highly volatile generation of renewable electric energy, extensive storage is required. In this thesis the application of mathematical optimization methods to gas transmission networks with electricity driven compressor stations, operated as electricity storage, is discussed.

Therefore, a transient network model that incorporates the gas dynamics described by the isothermal Euler equations as well as technical network elements is introduced and reviewed as coupled systems of hyperbolic balance laws. For optimization problems on networks these PDEs are commonly discretized by finite differences using an implicit box-scheme. The comparison with finite volume simulations, obtained using a high order ADER method, shows that the finite difference approximations represent sufficiently well the gas dynamics for typical flow situations on transmission networks while requiring much less computational effort.

The optimization model is then applied to realistic test problems abstracting parts of the German gas transmission network. The results for different price scenarios, which are used as indicator for the availability of renewable energy, show the potential of using pipelines as short term storage for electric energy but also the limitations.

The thesis is concluded by a discussion of the recently proposed distributed optimization algorithm ALADIN and its application to the structured gas network optimization problems. Therefore, an implementation of this algorithm as well as the experiences applying it to the introduced model are presented. Compared to a general purpose interior-point method, this approach of exploiting the problem structure shows promising performance for simple examples but fails for more complicated model instances.

Keywords: gas transmission networks, nonlinear optimization, hyperbolic balance laws on networks, finite volume schemes, distributed optimization algorithms

Kurzzusammenfassung

Um die Versorgungssicherheit auch bei stark fluktuierender Stromerzeugung aus regenerativen Quellen sicherzustellen, werden umfangreiche Speicher benötigt. In dieser Arbeit wird die Anwendung mathematischer Optimierungsmethoden auf Gasnetze mit elektrisch betriebenen Verdichtern diskutiert, die als Stromspeicher eingesetzt werden sollen.

Dafür wird ein transientes Netzmodell, das sowohl die Gasdynamik in Form der isothermen Euler-Gleichungen als auch weitere technische Netzelemente umfasst, eingeführt und anschließend im Kontext von hyperbolischer Erhaltungsgleichungen auf Netzen besprochen. Für Optimierungsprobleme auf Netzen werden diese partiellen Differentialgleichungen üblicherweise mit Finiten Differenzen eines impliziten Boxschemas diskretisiert. Der Vergleich mit den Ergebnissen von Finite-Volumen-Simulationen, die mit einem ADER-Verfahren höherer Ordnung bestimmt werden, zeigt, dass diese Finite-Differenzen-Approximationen die typische Dynamik in Gastransportnetzen genügend genau darstellen und dafür erheblich weniger Rechenaufwand benötigen.

Dieses Optimierungsmodell wird dann auf realistische Testprobleme angewendet, die Teile des deutschen Gastransportnetzes abstrahieren. Die Ergebnisse für verschiedene Preissituationen, die als Indikator für das Angebot an erneuerbarer Energie genutzt werden, zeigen das Potential der Nutzung von Gasleitungen als kurzfristiger Stromspeicher aber auch die Einschränkungen.

Zum Abschluss dieser Arbeit werden der kürzlich vorgestellte, verteilte Optimierungsalgorithmus ALADIN und seine Anwendung auf die strukturierten Gasnetzoptimierungsprobleme diskutiert. Dazu werden eine konkrete Implementation des Algorithmus und die Erfahrungen aus deren Einsatz für die vorgestellten Netzmodelle präsentiert. Im Vergleich zu einem Standardverfahren zeigt dieser Vorschlag einer Struktur ausnutzenden Lösungsmethode für einfache Beispiele ein vielversprechendes Verhalten, scheitert jedoch für kompliziertere Modellinstanzen.

Schlagworte: Gastransportnetze, Nichtlineare Optimierung, Hyperbolische Erhaltungsgleichungen auf Netzen, Finite-Volumen-Verfahren, Verteilte Optimierungsalgorithmen

Acknowledgments

I would like to thank my supervisor Marc Steinbach for the opportunity to be part of his work group and his mentoring during my work on this thesis.

Special thanks go to Jochen Kall and Raul Borsche for their offer to use their implementation of the ADER approach and answering my questions on how to get it to work for my problem.

I want to thank my current and former colleagues at the Institute of Applied Mathematics for the uncountable discussions and for providing me with new challenges, close as well as far away from my research topic. I am especially in debt with my AO-Lieblingskollegin Lisa Hegerhorst for proofreading drafts of this thesis.

Additionally, I want to thank my family for their support without ever really understanding on what I have been working all this time. Finally but most important, I would like to thank my wife Masiel for her endless support and believe in me that made this thesis possible.

Contents

List of Figures

List of Tables

Chapter 1

Introduction

1.1 Gas Pipelines as Storage for Renewable Energy

The activities to face climate change and the decision on the nuclear power phaseout in Germany have necessarily led to the extension of electric energy generation from so-called renewable sources. The generation from alternative sources like wind and solar energy is highly volatile and difficult to control such that the necessity for big and reliable short- and midterm storage has increased in similar manner. The requirements of huge storage evoked a variety of ideas. The use of natural gas infrastructure has undergone big popularity. Among the most advanced approaches is to convert electric energy into hydrogen or even methane by water electrolysis possibly followed by a methanation. The synthesized gas can be induced into the natural gas systems or used by special engines directly. Despite the relatively low efficiency of these approaches and the problems of introducing for example molecular hydrogen into the natural gas infrastructure, there are already working test plants[19].

In this work we discuss an alternative approach that considers the existing natural gas infrastructure as electricity storage presented by our project partners Derlien and Müller-Kirchenbauer [18]. Electric compressor drives in gas transmission networks could couple gas and electricity networks. They are able to use a surplus of renewable electricity generation to increase the pressure in subsequent pipelines. This operation policy will be called "power-to-compression" in the spirit of the above mentioned "power-to-gas" technologies. The compression with electric drives in time periods of high availability of renewable energy is a direct alternative to these technologies because the electric energy is stored in terms of the saved natural fuel gas that would otherwise have been used in gas turbines for compression. Like the synthesized gas, the saved fuel gas can be used by domestic and industrial customers or in modern gas power plants to generate electric energy in times of insufficient renewable energy generation. Additionally to this temporal separation of generation and utilization of electric energy a spatial shift by gas transport is included in this approach, too.

Derlien and Müller-Kirchenbauer [18] show the potential of this approach based on the

observation that about 0.8% of the annual gas consumption in Germany in 2010 is consumed for the compression in gas transmission networks. They also state that the new approach has a considerably higher efficiency compared to the "power-to-gas" approach. Nevertheless, in Germany almost all compressor in gas transmission networks are gas driven. Beside historic reasons, a handicap for electric drives due to the German tax legislation is mentioned, too. This might explain why in other countries more electric drives have already been installed. However, it is also mentioned that the implementation of the "power-to-compression" approach is restricted to existing and planned gas compressor stations and therefore not arbitrarily scalable.

On the other hand, the "power-to-compression" approach can also be interpreted as so-called *line packing* operation policy. In times of lower demand the compressors are operated above the mandatory, pushing more gas into subsequent pipelines. This policy is usually employed to be prepared for volatile and unexpected withdrawal of natural gas from the transmission networks. The electric drives could be operated considering the current generation of renewable electric energy by increasing the pressure in subsequent pipelines in periods of high availability. In exchange, in periods of less availability of renewable energy the compressor operation can be reduced or even stopped. This electricity induced load shift can also be interpreted as short- or mid-term storage for renewable electric energy using already existing infrastructure. To rate the compressor operation with respect to the objective to store electric energy in periods with an overage of renewable electric energy in the network, an indicator for these periods is required. We assume a strong correlation between the high generation of renewable energy and the electricity price (see [26] for associated statistics) and utilize the electricity market price to weight the availability. Hence, we expect that high availability usually implies lower energy prices and higher prices correspond to periods with less generation of renewable energy.

This motivation of this thesis has been part of the joint research project "Development of optimization methods for compressor operation in gas infrastructure for the storage of renewable energy" (German: „Entwicklung von Optimierungsverfahren für den Verdichtereinsatz in der Erdgasinfrastruktur zur Speicherung regenerativer Energien") with the authors of the above mentioned article, at that time part of the workgroup for Gas Supply Systems of the Institute of Oil and Gas Technology at Technical University Clausthal. The objective of the project was to evaluate this potential benefit of the presented approach using methods from mathematical optimization to provide foundations for the investigation on related economic questions.

1.2 Mathematical Optimization of Gas Networks

The idea to couple gas and electricity networks is a popular approach to address the new challenges in the presence of volatile energy generation. Just like changes in regulatory rules on the European gas market this implies more and more actors with different goals in the gas transmission network operation. The operation corresponding to these new goals might be far away from known operations. Hence, it becomes more difficult to find a feasible operation of the gas transmission network by procedures based on the experience of the network operators. Therefore, the usage of numerical optimization techniques to automatically determine a feasible or even optimal network operation without explicit knowledge is a very appealing approach.

The flow of natural gas in networks has been subject of scientific investigation at the interface between mathematics and engineering in the last decades. There are also early approaches to use mathematical optimization on gas networks that use strong simplifications on simple tree structured networks [12, 74, 75] while pure simulation results already included more realistic gas dynamics and network elements. Established simulation software like SIMONE [47, 46] or PSIGANESI [72, 60], that is commonly employed by network operators, evolved from these investigations.

More recently, the detailed models are also considered for mathematical optimization. There have been two branches using different simplifications, since the direct full mixed-integer nonlinear programming approach is not tractable. One branch assumes fixed discrete decisions but uses detailed nonlinear models for the transient [22, 23, 64] and the stationary case [57, 69, 76]. The other branch includes discrete decisions directly but handles nonlinearities by approximations, e.g. [30, 50].

A joint research project of different German universities, industry and public institutions merged these branches for the stationary case, addressing problems originated in the deregulation process in the European gas market. In particular, this project aimed for an automatic procedure which provides feasible controls with respect to the gas network model used in simulations. The results of this project, published in [44], document the progress in optimization of the stationary case. We refer to this publication and others related for more details on this particular issue as well as for a more comprehensive overview on gas network operation in general.

A related theoretical approach to the flow on networks deals with the stability and controllability of the governing isothermal Euler equations [34]. There are published results assuming smooth solutions [32, 33, 35] as well as general weak solutions in the context of hyperbolic balance laws [1, 8, 14, 14, 34]. The incorporation of these theoretical results in

numerical optimization has been presented in [37] for a semilinear simplification of the Euler equations.

Outline and Contributions

This thesis is structured as follows. Chapter 2 is devoted to the model for a transient description of gas flow on networks. After introducing the most important model relations the analytic solution structure is analyzed generalizing well known results for ideal gases to the more complicated description as real gases. Built on this basis, eventually high order finite volume discretization schemes as well as a finite difference discretization scheme are presented.

In Chapter 3 a survey on the theory and algorithmic concepts for nonlinear optimization problems is given.

For the mathematical optimization on gas networks the introduced finite difference scheme is one of the most detailed descriptions commonly considered for the dynamics on the pipes. However, in comparison with high resolution finite volume schemes this approach is still very coarse. In the first part of Chapter 4 we present a novel comparison of the optimization solution corresponding to the finite difference approximation with simulation results using a high order finite volume scheme. Comparing the discretized solutions for typical dynamics on a gas transmission pipeline provides information on the required discretization technique for the description of complete transmission pipelines. In a second part of this chapter we discuss the potential of the proposal to use gas networks as electricity storage as introduced in Section 1.1. These investigations are based on numerical case studies for simple networks abstracted from real German gas transmission networks.

In this thesis up to that point the numerical optimization results are computed by a general purpose nonlinear optimization solver. In Chapter 5 we introduce a solver tailored to structured nonlinear problems like the cost optimization problem on gas networks. We describe our implementation of the distributed algorithm proposed in [39] and discuss advantages and shortcomings based on our computational experiences.

Chapter 2

Modeling Gas Flow on Networks

To evaluate the potential of the approach introduced in Section 1.1 of using the gas transmission networks as storage, a description of the transient dynamics on the networks is required. This is in contrast to the models investigated in [44] which are restricted to the stationary case.

First, in Section 2.1 the considered physical and technical aspects of the basic model used through the thesis are stated. To get an insight to the structure of analytic solutions to this model we discuss briefly questions of existence of solutions and optimal network controls in Section 2.2. Section 2.3 is devoted to the discretization of the governing partial differential equations (PDE) with respect to the coupling algebraic equations as well. Using the analytic solution structure, in Section 2.3.1 we present the basic ideas of a high order finite volume scheme to discretize the dynamics on the network. This chapter is concluded by the presentation of a finite difference scheme in Section 2.3.2.

2.1 Physical and Technical Model

In this section the model aspects investigated through this thesis are presented. For the modeling of flow on gas networks there exist already a huge number of proposals and investigation on different scales. From a three dimensional modeling (in space) of the gas dynamics inside the pipeline to approximations for the stationary flow there are a wide range of scales and model aspects as well as mathematical and technical fields to be covered. For the flow on complete transmission networks it is commonly accepted to base the model on a one dimensional view on pipes which are, at least in comparison to its diameter, long one-dimensional objects. The model presented here follows directly the lines of the previous investigation [23, 62] and is a selection of the modeled aspects as described in the Chapters [27] and [63] of the already mentioned book [44]. We refer also to the book of Cerbe [13] for details about gas transport and storage from an engineer's point of view.

We only consider an isothermal model for the gas flow. The inner energy of the gas, usually

expressed in terms of temperature, introduces further difficulties to the model like nonsmooth relations for the temperature mixing. Additionally, the temperature is strongly influenced by the surrounding temperature. Hence, a good data basis is required to compute meaningful results. To avoid these and other difficulties, we concentrate on the isothermal case.

A further decision to make is if the model should explicitly include discrete decisions. The state of the art optimization methods are not able to solve the resulting problems so far. In [44] there have been various approaches towards a solution procedure for the stationary case but investigation for the transient case, to the best of our knowledge, have not yet advanced sufficiently. We therefore externally prescribe the discrete decisions like switching compressors on or off as well as changes of the topology modeled by closing or opening valves. This can be justified up to some point by the assumptions that the general flow situation over the time horizon to consider is known and therefore the discrete decisions can be made in advance, for example by a solution for the stationary case using one of the procedures presented in [44].

For the short time horizons we also assume the boundary profiles for flow and pressure which represent the customer and provider behavior, to be deterministic and do not consider any stochastic. Clearly, it would be preferable to include all these effects directly into the model to get rid of these assumptions which in many situation are at least questionable. However, an integrated algorithm would probably consist of some sort of alternating solution of simplified subproblems. Therefore, optimization models with simplifications similar to ours have to be considered anyway.

2.1.1 Characterizing Gas Flow

Given a fixed gas network topology and the assumed fixed in- and outflow profile the task, for the network operation is to find a control for all controllable network elements such that the physical and technical relations as well as the prescribed boundary conditions are satisfied. Under the given assumptions the flow on the network is mainly described by the amount of gas present at a given time inside a space interval. Hence, the gas density ρ and the mass flow q are chosen as main characterizing quantities in this thesis to characterize the gas flow through the network. For clearer presentation not all relations are directly expressed in these quantities but for example via the related pressure. The model relations include the influence of gas composition and the gas temperature which are both assumed to be constant. Table 2.1 gives an overview on the main quantities used to describe the state of the network.

Equation of State   One of the most important aspects is the relation between the thermo-dynamic quantities pressure p, temperature T and density ρ. The most simple approximation

Quantity	Symbol	Unit
Density	ρ	kg/m^3
Mass flow	q	kg/s
Pressure	p	$\text{Pa} = 10^{-5}\,\text{bar}$
Temperature	T	K
Universal gas constant	R	$8.314\,462\,1\,\text{J/(mol K)}$

Table 2.1: Principal quantities and constants

is the *ideal gas law*

$$p = R_{\text{s}} T \rho, \tag{2.1}$$

characterizing a so-called ideal gas with homogeneous composition. The specific gas constant $R_{\text{s}} = R/m$ as proportionality constant is only dependent on the molar mass m of the gas mixture whereas $R = 8.314\,462\,1\,\text{J/(mol K)}$ is the universal gas constant. The deviation of the behavior of a *real gas* from relation (2.1) for ideal gases can be described by a *compressibility factor*

$$z = \frac{pV}{R_{\text{s}} T}.$$

The *standard equation of state for real gases*

$$p = R_{\text{s}} T \rho z. \tag{2.2}$$

then includes ideal gases by $z \equiv 1$. In [27] a power series expansion for the compressibility factor is introduced which can be used for the derivation of approximate formulas. Moreover, there exist a great number of possibilities to describe the characteristics of real gases. In this thesis, additional to the ideal gas approximation two common empirical relations are used that only depend on pressure, temperature and the pseudocritical point of a gas mixture, that is characteristic for each gas composition. The equation of Papay [56] stated in terms of the reduced pressure $p_{\text{r}} = p/p_c$ and reduced temperature $T_{\text{r}} = T/T_c$

$$z(p, T) = 1 - 3.52\,p_{\text{r}}\exp(-2.26 T_{\text{r}}) + 0.274\,p_{\text{r}}^2\exp(-1.878 T_{\text{r}}) \tag{2.3}$$

can be applied reasonably up to $150\,\text{bar}$, whereas the formula of the American Gas Association (AGA)

$$z(p, T) = 1 + 0.257\,p_{\text{r}} - 0.533\,\frac{p_{\text{r}}}{T_{\text{r}}} \tag{2.4}$$

(a) Compressibility $z(p, T)$ (b) Pressure as function of density $p(\rho)$
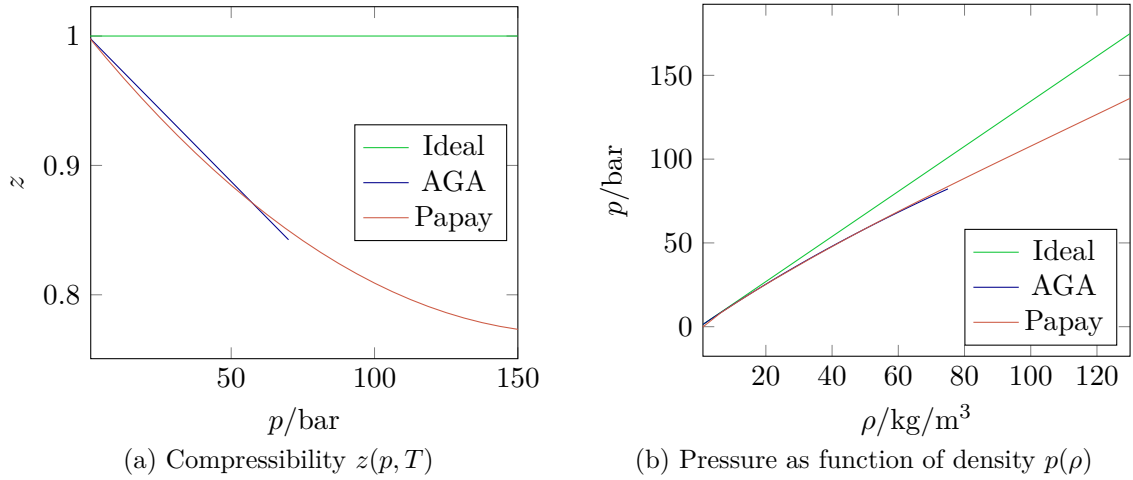
Figure 2.1: Comparison of compressibility factors at $T = 283.15\,\mathrm{K}$

is known to be sufficiently accurate only in a smaller pressure range up to about $70\,\mathrm{bar}$. In Figure 2.1 a comparison for these three different models is illustrated by an example for a typical natural gas composition at fixed temperature.

2.1.2 Network Model

The above selected quantities have to be tracked over the network. The network is divided in logical units representing technical facilities like pipelines or compressors. Additionally, some virtual elements are added to the model that help to state the model in a clearer fashion. The network itself is formally represented by a directed graph $\mathbb{G} = (\mathbb{V}, \mathbb{A})$. The set of nodes or vertices $\mathbb{V}$ comprise interior nodes $\mathbb{V}_0$ as well as entries $\mathbb{V}_+$ and exits $\mathbb{V}_-$ as boundary nodes. The pipelines $\mathbb{A}_{\mathrm{pi}}$, compressor stations $\mathbb{A}_{\mathrm{cs}}$ and control valves $\mathbb{A}_{\mathrm{cv}}$ together with virtual short pipes $\mathbb{A}_{\mathrm{sc}}$ form the set $\mathbb{A}$ of network arcs or edges. In order to state the model, we fix some conventions. For the models associated with edges any quantity describing a movement along the edge $a = ij$, for example the velocity v_{ij} or mass flow q_{ij}, is defined to be positive if it is directed from node i to j. The outgoing or negative incident arcs to node i are denoted by $\delta_i^- = \{a \in \mathbb{A} \colon a = ij\}$ and the ingoing or positive incident arcs by $\delta_i^+ = \{a \in \mathbb{A} \colon a = ji\}$. An index to denote the association of a quantity to an arc or node class is only added when necessary for the presentation and suppressed otherwise. The following paragraphs provide the models for each of these network element types.

Quantity	Symbol	Unit
Velocity	v	m/s
Friction acceleration	λ	m/s
Length	L	m
Diameter	D	m
Integral roughness	k	m
Dynamic viscosity	η	m s/kg

Table 2.2: Pipe model: Additional model quantities and parameters

Pipeline Model

Pipelines are the fundamental part of gas transmission networks connecting customers and providers of natural gas over possibly large distances. Pipelines are typically build from preconstructed pipeline segments that are connected on site and installed underground. The flow in pipes is mainly pressure driven. Hence, the gas usually moves from higher to lower pressure. The pipe walls have to resist the high pressure values in the pipelines.

For many problems the relations between flow and pressures at the pipeline endpoints are of interest and have to be properly described by the model. Clearly, the pipe length L plays an important role in the description of the gas dynamics. In transmission networks pipe length can be more than $100\,\mathrm{km}$ but also quite short pipes of only about $10\,\mathrm{m}$ can occur. The longer the pipe is, the larger will be the pressure drop along the direction of flow. The pressure drop along the pipe is mainly due to friction effects. Hence, the diameter D of the cylindrical pipe and the integral pipe roughness k summarizing the effects of the pipe surface material and imperfections, for example dirt or pipe curvature, also have strong impact in the gas flow relations.

The flow inside the pipeline is obviously on a three dimensional domain and can be investigated as it. The detailed flow situation is, for example, topic in computational fluid dynamics. Since the pipe diameter of the, in our case always cylindrical, cross sectional area of the pipeline is small in comparison to the typical pipe length we only consider a model in one space dimension. Three-dimensional dynamic effects like turbulence and nonhomogeneous flow over the cross section are combined in a friction source term to represent their effect in the 1-D model.

The mathematical description of the gas dynamics is then expressed in terms of velocity $v(x,t)$, density $\rho(x,t)$ and pressure $p(x,t)$. The set of hyperbolic balance laws often referred to as *isothermal Euler equations*

$$\frac{\partial \rho}{\partial t} + \frac{\partial(\rho v)}{\partial x} = 0, \tag{2.5a}$$

$$\frac{\partial(\rho v)}{\partial t} + \frac{\partial(\rho v^2)}{\partial x} + \frac{\partial p}{\partial x} + g\rho s + \tilde{\lambda}(v)\frac{|v|v}{2D}\rho = 0, \tag{2.5b}$$

where $s = \frac{\partial h}{\partial x}$ denotes the constant slope of the pipeline segment, is deviated from conservation of mass and momentum in the pipeline. The above mentioned friction relation $\tilde{\lambda}(v)$ will be addressed below. Using the constant cross sectional area $A = \frac{\pi D^2}{4}$ the equations can be expressed in terms of the mass flow $q = A\rho v$. Scaling the second equation with A then leads to:

$$\frac{\partial \rho}{\partial t} + \frac{1}{A}\frac{\partial q}{\partial x} = 0, \tag{2.6a}$$

$$\frac{\partial q}{\partial t} + \frac{1}{A}\frac{\partial}{\partial x}\left(\frac{q^2}{\rho}\right) + A\frac{\partial p}{\partial x} + gA\rho s + \lambda(q)\frac{|q|q}{2AD\rho} = 0. \tag{2.6b}$$

The qualitative behavior of this system of hyperbolic PDEs is discussed in more detail in Section 2.2. The full set of Euler equations as presented for example in [27] contains a further PDE originating from energy conservation which is neglected here since we use the isothermal simplification, i.e. constant gas temperature.

Friction Model and Approximation   The pressure function $\lambda(q)$ has to cover all the effects of interior and boundary friction. All common descriptions are empirical physical laws and depend on the current flow situation. *Laminar* flow shows much less friction influence than *turbulent* flows. The transition between these two regimes depends on the flow velocity as well as on the fluid properties, especially the viscosity. The point of transition is not sharp but however characterized by the so-called *Reynolds number*

$$\mathrm{Re}(|q|) = \frac{D}{A\eta}|q|, \tag{2.7}$$

where η is the dynamic viscosity of the gas. If the Reynolds number of the flow state is below the critical value $\mathrm{Re_{crit}} \approx 2320$, then laminar flow can be assumed. In this state the friction can be characterized by the exact physical law of Hagen-Poiseuille

$$\lambda^{\mathrm{HP}}(q) = \frac{64}{\mathrm{Re}(q)}. \tag{2.8}$$

For bigger Reynolds numbers $\mathrm{Re}(|q|) > \mathrm{Re_{crit}}$ the flow is turbulent. There is no exact physical law for the friction in that case. The implicit equation of *Prandtl-Colebrook* which relates the friction with the pipe diameter D and integrated pipe roughness k

$$\frac{1}{\sqrt{\lambda^{\mathrm{PC}}(q)}} = -2\log_{10}\left(\frac{2.51}{\mathrm{Re}(q)\sqrt{\lambda^{\mathrm{PC}}(q)}} + \frac{k}{3.71D}\right) \tag{2.9}$$

is usually considered as most exact in this situation. Combining the formula (2.8) for laminar flows and equation (2.9) we obtain the piecewise defined friction function

$$\lambda^{\text{HP-PC}}(q) = \begin{cases} \lambda^{\text{HP}}(q), & \text{Re}(q) \leq \text{Re}_{\text{crit}}, \\ \lambda^{\text{PC}}(q), & \text{Re}(q) > \text{Re}_{\text{crit}}. \end{cases} \tag{2.10}$$

This can be directly extended to negative flows by

$$\lambda^{\text{HP-PC}}(-|q|) := \lambda^{\text{HP-PC}}(|q|). \tag{2.11}$$

The resulting friction term

$$\lambda^{\text{HP-PC}}(q) \frac{q|q|}{2AD} \tag{2.12}$$

has discontinuities at the transitions between the two cases. Additionally, there is a jump in the second derivatives w.r.t. q at $q = 0$ due to the absolute value function. Burgschweiger et al. [9] proposed for drinking water networks the global smooth approximation

$$\phi(q) = r \left(\sqrt{q^2 + a^2} + b + \frac{c}{\sqrt{q^2 + d2}} \right) q, \tag{2.13}$$

which has been adapted to the gas case [62]. The constants $a, d > 0$ have to be chosen related to the approximation around $q = 0$ and the further parameters are then computed according to

$$r = \frac{\tilde{\lambda}}{2AD}, \quad \tilde{\lambda} = (2 \log_{10} \beta)^{-2}, \quad b = 2\delta, \quad c = (\ln \beta + 1) \delta^2 - \frac{a^2}{2},$$
$$\alpha = \frac{2.51 A \eta}{D}, \quad \beta = \frac{k}{3.71 D}, \quad \delta = \frac{2\alpha}{\beta \ln 10}.$$

It is shown in [9] that this approximation is asymptotically correct for large $|q|$. Resuming the above we have

$$\phi(q) \approx \frac{\lambda^{\text{HP-PC}}(q)}{2AD} q|q|. \tag{2.14}$$

Further simplifications Depending on the observed situation, more assumption or simplification are commonly applied to get simpler systems of partial differential equations. For example, the first terms of the momentum equation (2.6b) could be neglected in some situations since in earlier studies [73] it has been observed that their contribution to the momentum balance equation is often very small:

$$\frac{\partial \rho}{\partial t} + \frac{1}{A} \frac{\partial q}{\partial x} = 0, \tag{2.15a}$$

Symbol	Explanation	Unit
H_{ad}	Adiabatic head	J/kg
n	Compressor speed	1/s
P	Compressor input power	W
η_{ad}	Adiabatic efficiency	1
κ	Isentropic exponent	1

Table 2.3: Compressor model: Physical and technical quantities

$$A\frac{\partial p}{\partial x} + gA\rho s + \frac{\phi(q)}{\rho} = 0. \tag{2.15b}$$

In this case the hyperbolic behavior is replaced by a parabolic one as already remarked in [72].

For the stationary case there exist even an explicit solution and a well known quadratic approximation (cf. [27]) for the pressure drop along the flow direction. We will not use this approximation in this study but it clearly helps as rule of thumb for a first check of the results.

Compressor Model

The pressure loss in pipelines due to the friction is balanced by compressor machines which increase the pressure from a lower incoming pressure to high outflow pressure, making gas transmission over long distances possible. Real-world compressor facilities, which may be composed of different elements installed in complicated subnetwork structures, can be characterized on different levels of abstraction. In this work we will only consider a basic compressor modeling. For more complex versions and a comprehensive overview on aspects to model in compressor stations we again refer to the general modeling chapter [27] in [44].

There are different types of compressors used in the gas transmission networks but we restrict ourselves to the most common turbo compressors. The gas is accelerated increasing the kinetic energy which is then converted into a pressure increase by a diffuser. Every turbo compressor is modeled in combination with a gas turbine or an electric motor as drive. The compressor model describes the feasible combination of pressure increase in terms of the increase of adiabatic enthalpy

$$H_{\mathrm{ad}}(T_{\mathrm{in}}, T_{\mathrm{out}}, p_{\mathrm{in}}, p_{\mathrm{out}}) = z_{\mathrm{in}} T_{\mathrm{in}} R_{\mathrm{s}} \frac{\kappa}{\kappa - 1}\left(\left(\frac{p_{\mathrm{out}}}{p_{\mathrm{in}}}\right)^{\frac{\kappa-1}{\kappa}} - 1\right), \tag{2.16}$$

and the gas flow through the compressor expressed as volumetric flow

$$q = Q\rho_{\text{in}}, \tag{2.17}$$

as well as the required power

$$P = \frac{qH_{\text{ad}}}{\eta_{\text{ad}}}. \tag{2.18}$$

Here ρ_{in} and z_{in} denote the incoming density and associated compressibility, respectively. The isentropic exponent $\kappa(T_{\text{in}}, T_{\text{out}}, p_{\text{in}}, p_{\text{out}})$ is here approximated by the constant value $\kappa = 1.296$ whereas the adiabatic efficiency $\eta_{\text{ad}} \in (0, 1]$ depends on the operation state in general.

Ideal Compressor The most simple model choice to describe the feasible operation range is denominated ideal compressor. This model assumes a constant adiabatic efficiency $\eta_{\text{ad}} \in (0, 1]$ independent of the operation point. Additionally, only simple bounds on the operation range are assumed. The energy consumption rate of the drive is also modeled as constant efficiency factor

$$b(P) = c_{\text{drive}}P, \tag{2.19}$$

while the maximal drive power is given by a constant upper bound:

$$P \in [0, P^{\text{max}}] \tag{2.20}$$

Characteristic Diagrams Clearly, the ideal compressor is a very coarse description of the feasible operation range and the energy consumption of the drive. Technically the turbo compressor can be controlled by manipulating the rotation speed n that has an impact on flow as well as enthalpy increase. The operation range of a compressor is usually given by so-called *characteristic diagrams*. Figure 2.2 gives an example for such a visualization of the feasible operation range.

These relations are characteristic for each compressor machine and usually given only in terms of different measurements. To get a continuous description of the operation range and the efficiency function, the mentioned measurements are used to derive least squares based quadratic or biquadratic approximations. Analogously, the energy consumption and maximal drive power are often also given in that form. We refer once more to [27] for the complete model including the characteristic diagrams.

Operation costs and further compressor station model elements For a given energy cost profile $e(t)$, i.e. the electric energy or gas price profile, the operation cost over a time horizon
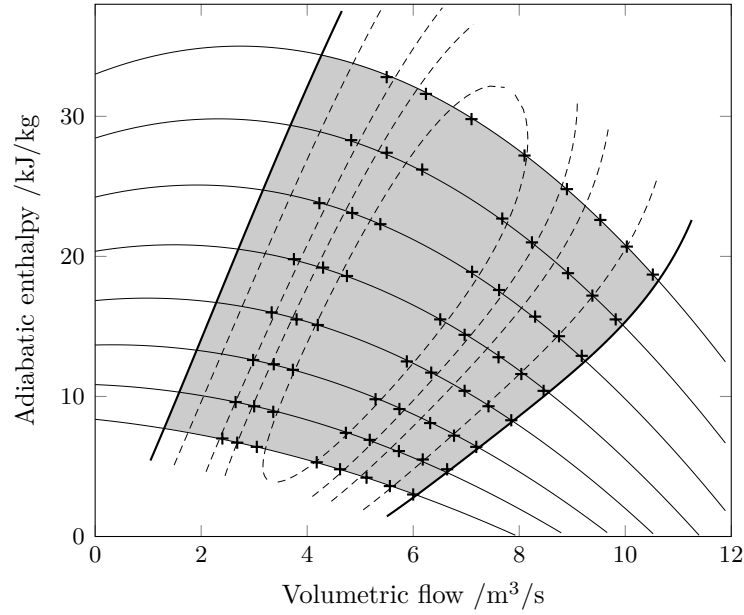
Figure 2.2: Example of a characteristic diagram of a turbo compressor(Source: [62]); straight
          lines for constant rotation speed (increasing from bottom to top); dashed lines
          for constant efficiency (increasing to the center); measurements given at '+'.

$[\underline{t}, \overline{t}]$ of the compressor is then computed as

$$\int_{\underline{t}}^{\overline{t}} e(t)b(P(t))\,\mathrm{d}t. \tag{2.21}$$

The discrete control decision for compressor are modeled by three operation modes: closed,
bypass and active. The active mode is characterized by the relations introduced above. A
closed compressor acts like a closed valve, i.e. it decouples the two nodes connected by the
closed compressor station as if there were no connecting arc. If a compressor group is in
bypass mode, it is equivalent to a short pipe which couples directly via equality the flow and
pressure quantities at the edge endpoints. In this model the mode selection is assumed to
be externally prescribed. To model the compressor stations in more detail, in- and output
resistors representing the resistance of gadgets, filters and piping could be added to the
network.

Control Valves

At transition points between high pressurized transmission networks and distribution networks
on lower pressure levels the pressure has to be decreased technically. This takes place in
control valves which are usually part of larger control valve stations. These consist not only

of control valves but also other gadgets, filters and especially preheaters providing heating energy to balance the temperature loss due to the gas expansion. Again the discrete decisions are modeled by the three modes closed, bypass and active which we assume to be externally prescribed. We model the active control valves by a controllable pressure drop over the edge

$$p_{\text{in}} - p_{\text{out}} = \Delta p \geq 0 \tag{2.22}$$

and a fixed flow direction $q \geq 0$. The bypass and closed state for the control valves are modeled like in the compressor model.

Short Pipes

Short pipes are artificial network elements used to simplify the presentation, e.g. by dividing one physical node into various logical nodes. For that purpose there should be no pressure loss over the short pipe:

$$p_{\text{in}} = p_{\text{out}} \tag{2.23}$$

There are no further bounds on flow or pressures. We do not model any spatial extension by short pipes.

Valves

The valve allows to model a change of the network geometry and is characterized by its two discrete modes: open and closed. An open valve behaves like a short pipe while the closed valve is described by

$$q = 0 \tag{2.24}$$

which corresponds to a nonexisting edge.

Node model

The above presented edge models have to be connected at the nodes of the gas network. The dynamics in the junctions is again simplified and characterized by the mass conservation

$$q^{\text{ext}} + \sum_{a \in \delta^+} q_a - \sum_{a \in \delta^-} q_a = 0, \tag{2.25}$$

coupling the in- and outgoing mass flows of incident arcs, where q_i^{ext} is the external in- or outflow to the network. We remark that in- and outgoing edges are fixed by the network structure as directed graph and not dependent on the actual flow direction. Interior nodes are

characterized by the lack of external inflow. For entry and exit nodes the external mass flow is bounded to nonnegative and nonpositive values, respectively. Additionally, the pressure at the ends of the incident edges are set to be equal to the node pressure

$$p = p_a, \text{ for all incident arcs } a \in \delta^+ \cup \delta^-. \tag{2.26}$$

The first coupling equation for mass flow is directly related to the mass conservation in pipes whereas the pressure equality conditions are a simplification of the dynamic processes in junctions. Comparisons to other approaches to couple the dynamic energy of the gas flow have been presented in [38] for junctions with three incident edges.

2.1.3 Measuring the State of the Network

To prepare the optimization problems built upon the introduced model for the gas network we present here a selection of functionals that measure the current state of the network. One possibility is to measure the deviation of the actual flow or pressure profile from prescribed profiles q^{fix} or p^{fix} for the boundary values

$$\int_{\underline{t}}^{\bar{t}} |q^{\text{ext}}(t) - q^{\text{fix}}(t)| \, \mathrm{d}t \quad \text{or} \quad \int_{\underline{t}}^{\bar{t}} |p(t) - p^{\text{fix}}(t)| \, \mathrm{d}t, \tag{2.27}$$

in the desired integral norm, respectively. Another possibility is to measure the distance to a desired flow profile $q^{\text{ext}}(x)$ at a particular time point $\tilde{t}$ in a pipe of length L

$$\int_0^L |q(x, \tilde{t}) - q^{\text{ext}}(x)| \, \mathrm{d}x \tag{2.28}$$

or the mass contained inside the pipeline at time point $\tilde{t}$

$$\int_0^L \rho(x, \tilde{t}) \, \mathrm{d}x. \tag{2.29}$$

Together with the operational costs of the compressors modeled as in equation (2.21) these functionals are commonly used as possible objective functions for optimization tasks on gas networks.

2.2 Transient Gas Network Model as coupled System of Hyperbolic Balance Laws

The model presented above can be investigated from different points of view. To get computational solutions to the modeling equations a discretized version is required. In this section we will give a summary of results that are more emphasized in the qualitative

behavior of the solutions for the Euler equations on gas networks. We first state the model in the usual setting for coupled systems of hyperbolic balance laws on networks and then present some statements on well-posedness and controllability. The section introduces the general theoretical steps and applies it to our case of the isothermal Euler equations. The presentation on the general theory of hyperbolic conservation laws follows the lines of the textbooks of LeVeque [49] and Toro [66]. The results for the network case are extensions to those for the ideal gas law that can be found in the survey of Bressan et al. [8] and the references therein [14, 15, 33, 34]. In addition to a better understanding of the solution structure, this section also provides the foundations for the numerical schemes presented in the next section.

We set $\boldsymbol{u}^T = (\rho, q)$ as model variable, the *flux function* as

$$\boldsymbol{f}(\boldsymbol{u})^T = (q/A, \frac{q^2}{A\rho} + Ap(\rho)) \tag{2.30}$$

and source term $\boldsymbol{s}(\boldsymbol{u})^T = (0, -gsA\rho - \frac{\phi(q)}{\rho})$, where $p(\rho)$ is the pressure function associated with one of the three presented compressibility laws and $\phi(q)$ the friction approximation. Then, the system of Euler equations (2.6) has the form of a general system of balance laws in one spatial dimension

$$\frac{\partial \boldsymbol{u}}{\partial t} + \frac{\partial \boldsymbol{f}(\boldsymbol{u})}{\partial x} = \boldsymbol{s}(\boldsymbol{u}). \tag{2.31}$$

As in our case, these systems are often derived from conservation principles and which can be described more naturally by the integral form

$$\frac{\mathrm{d}}{\mathrm{d}t} \int_{x_l}^{x_r} \boldsymbol{u}(x, t)\,\mathrm{d}x + \boldsymbol{f}(\boldsymbol{u}(x_r, t)) - \boldsymbol{f}(\boldsymbol{u}(x_l, t)) = \int_{x_l}^{x_r} \boldsymbol{s}(\boldsymbol{u}(x, t))\,\mathrm{d}x \tag{2.32}$$

for any space interval (x_l, x_u). If the solution is sufficiently smooth, this integral form is equivalent to the differential form (2.31). Solution to the integral forms of the balance laws are called *weak solutions*. They also admit solutions that are not differentiable, which thus cannot be solutions to the differential form (2.31) in the classical sense. Integration of (2.32) over a test volume in time, i.e. an interval $(\underline{t}, \bar{t})$, leads to a second integral form of (2.31):

$$\int_{x_l}^{x_r} \boldsymbol{u}(x, \bar{t}) - \boldsymbol{u}(x, \underline{t})\,\mathrm{d}x + \int_{\underline{t}}^{\bar{t}} \boldsymbol{f}(\boldsymbol{u}(x_r, t)) - \boldsymbol{f}(\boldsymbol{u}(x_l, t))\,\mathrm{d}t = \int_{\underline{t}}^{\bar{t}} \int_{x_l}^{x_r} \boldsymbol{s}(\boldsymbol{u}(x, t))\,\mathrm{d}x\,\mathrm{d}t. \tag{2.33}$$

Hyperbolicity of problem A system is called *strictly hyperbolic* if the Jacobian matrix of the flux function $J(\boldsymbol{u}) = \partial_{\boldsymbol{u}}\boldsymbol{f}(\boldsymbol{u})$ has two distinct real eigenvalues. It is well known and easy

to compute that the eigenvalues of the Jacobian matrix of the flux (2.30)

$$J(\rho, q) = \begin{bmatrix} 0 & \frac{1}{A} \\ -\frac{q^2}{A\rho^2} + Ap'(\rho) & \frac{2q}{A\rho} \end{bmatrix} \tag{2.34}$$

are given by

$$\lambda_{1/2}(\boldsymbol{u}) = \frac{q}{A\rho} \mp a(\rho) = v \mp a(\rho) \tag{2.35}$$

where $a(\rho) = \sqrt{p'(\rho)}$ denotes the *speed of sound*. The corresponding right eigenvectors are given by

$$\boldsymbol{r}_{1/2}(\boldsymbol{u}) = \begin{pmatrix} 1 \\ A\,\lambda_{1/2}(\boldsymbol{u}) \end{pmatrix}. \tag{2.36}$$

The chosen model variables, density and mass flow, are called *conservative variables* in this context since they correspond to the balance law in the form (2.31). For some calculations it is more convenient to express the Euler equations in terms of density and velocity, the so-called *physical variables* $\boldsymbol{w} = (\rho, v)$. We assume that the solution $\boldsymbol{u}$ is differentiable and derive from (2.6) the quasilinear system of PDEs for the physical variables:

$$\frac{\partial \rho}{\partial t} + v\frac{\partial \rho}{\partial x} + \rho\frac{\partial v}{\partial x} = 0, \tag{2.37a}$$

$$\frac{\partial v}{\partial t} + \frac{p'(\rho)}{\rho}\frac{\partial \rho}{\partial x} + v\frac{\partial v}{\partial x} = -gsA\rho - \frac{\phi(A\rho v)}{\rho}. \tag{2.37b}$$

The corresponding Jacobian

$$J(\boldsymbol{w}) = \begin{bmatrix} v & \rho \\ \frac{a^2(\rho)}{\rho} & v \end{bmatrix},$$

has eigenvalues and corresponding right eigenvectors

$$\lambda_{1/2}(\boldsymbol{w}) = v \mp a(\rho), \qquad r_{1/2}(\boldsymbol{w})^T = (\, 1, \mp\frac{a(\rho)}{\rho} \,). \tag{2.38}$$

Equation of state   Before going on, we have a closer look on the selected equations of state (2.2). As seen above, the equation of state has to be solvable as a function $p(\rho)$. To show that the isothermal Euler equations indeed form a hyperbolic system, the pressure equation is required to have positive derivative $p'(\rho) > 0$. We will check this for our choices and state some observations useful for the forthcoming computations. Taking the ideal gas

law (2.1) as equation of state, we get

$$\frac{p}{\rho} = a^2 \iff p(\rho) = a^2 \rho \tag{2.39}$$

with speed of sound $a^2 = R_{\mathrm{s}}T$. For the case of the AGA equation (2.4) we have

$$0 = p - R_{\mathrm{s}}T\rho z(p, T) = p - R_{\mathrm{s}}T\rho(1 - c_2 p)$$
$$\implies p_{\mathrm{AGA}}(\rho) = \frac{a^2 \rho}{1 + a^2 c_2 \rho}, \tag{2.40}$$

with $c_2 = -\frac{0.257}{p_c} + 0.533\frac{T_c}{Tp_c} > 0$. For Papay's equations the pressure function can be expressed as a solution of a quadratic equation:

$$0 = p - R_{\mathrm{s}}T\rho z(p, T) = p - R_{\mathrm{s}}T\rho(1 - C_2 p + C_3 p^2)$$

with positive constants $C_2 = \frac{3.52}{p_c}\exp(-2.26\frac{T}{T_c})$, $C_3 = \frac{0.274}{p_c^2}\exp(-1.878\frac{T}{T_c})$. Solving for ρ yields

$$\rho = \frac{p}{a^2 z(p, T)} = \frac{p}{a^2(1 - C_2 p + C_3 p^2)}$$
$$\implies \rho'(p) = \frac{1 - C_3 p^2}{a^2(1 - C_2 p + C_3 p^2)^2}$$

The inverse function exists on intervals with monotonicity, e.g.

$$\rho'(p) \overset{!}{>} 0 \iff p < \frac{1}{\sqrt{C_3}}$$

So for $p \in [0, \frac{1}{\sqrt{C_3}}]$ we have an inverse function. An explicit expression can be derived solving the quadratic equation for p and selecting the "$-$" solution:

$$p_{\mathrm{Papay}}(\rho) = \frac{1 + a^2 C_2 \rho - \sqrt{(1 + a^2 C_2 \rho)^2 - 4a^4 C_3 \rho^2}}{2a^2 C_3 \rho}$$
$$= \frac{1 + a^2 C_2 \rho}{2a^2 C_3 \rho} - \sqrt{\frac{(1 + a^2 C_2 \rho)^2}{4a^4 C_3^2 \rho^2} - \frac{1}{C_3}}.$$

Using Vieta's formulas we get the alternative formulation

$$p_{\mathrm{Papay}}(\rho) = \frac{2a^2 \rho}{1 + a^2 C_2 \rho + \sqrt{(1 + a^2 C_2 \rho)^2 - 4a^4 C_3 \rho^2}}$$
$$= \frac{2a^2 \rho}{1 + a^2 C_2 \rho + \sqrt{D(\rho)}}, \tag{2.41}$$

(a) Pressure functions of density   (b) Speed of sound
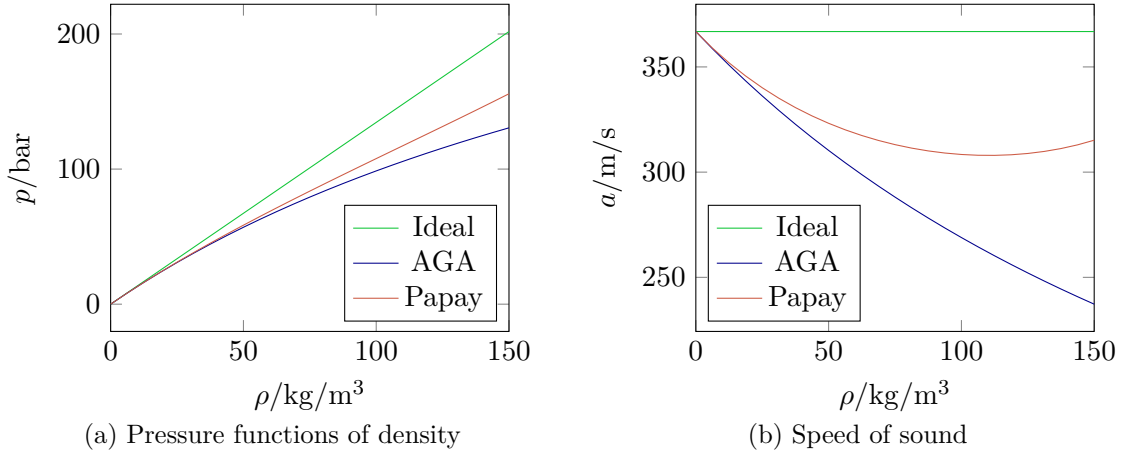
Figure 2.3: Structural comparison of pressure functions and associated speed of sound

with abbreviation $D(\rho) = (1 + a^2 C_2 \rho)^2 - 4 a^4 C_3 \rho^2$. These expression imply the condition $D(\rho) > 0$ to ensure a real solution. For a typical gas compositions these bounds are beyond the assumed valid range for the equation of Papay.

For later results it is convenient to observe that $\sqrt{D(\rho)} < 1 + a^2 C_2 \rho$. This implies a comparison of the AGA and Papay type of pressure equation for fixed ρ:

$$p_{\text{Papay}}(\rho) \geq p_{\text{AGA}}(\rho)$$

We emphasize that this is not an inequality on the real pressures since the constants are computed in a different manner from the gas parameters and the temperature. The inequality holds only for the algebraic relations as if both constants were the same. To illustrate this Figure 2.3 compares the different functions for computation of pressure and speed of sound as functions of density with coefficients C_2, C_3 computed by the formulas for the Papay case. We again point out that this does not show real pressures computed by the AGA equation (cf. Figure 2.1).

To finally decide if the isothermal Euler system is hyperbolic, we need the derivatives for the three cases. For the ideal gas it holds

$$p_{\text{ideal}}(\rho) = a^2 \rho \implies p'_{\text{ideal}}(\rho) = a^2 > 0, \tag{2.42}$$

i.e. in this case the system is clearly hyperbolic. For the AGA equation basic calculation shows that

$$p'_{\text{AGA}}(\rho) = \frac{a^2}{(1 + a^2 c_2 \rho)^2} = \frac{p_{\text{AGA}}(\rho)}{t(\rho)\rho} > 0, \tag{2.43}$$

$$p''_{\mathrm{AGA}}(\rho) = -\frac{2a^4 c_2}{(1 + a2c_2\rho)^3} = \frac{p_{\mathrm{AGA}}(\rho)}{t(\rho)^2 \rho^2}(1 - t(\rho) - \rho t'(\rho)), \tag{2.44}$$

where the abbreviation $t(\rho) = 1 + a^2 c_2 \rho$ is used. For the Papay equation we get

$$p'_{\mathrm{Papay}}(\rho) = \frac{2a^2}{\sqrt{D(\rho)}(1 + a^2 C_2 \rho + \sqrt{D(\rho)})} = \frac{p_{\mathrm{Papay}}(\rho)}{\sqrt{D(\rho)}\rho} > 0, \tag{2.45}$$

$$p''_{\mathrm{Papay}}(\rho) = \frac{p_{\mathrm{Papay}}(\rho)}{D(\rho)\rho^2}(1 - \sqrt{D(\rho)} - \rho\frac{D'(\rho)}{2\sqrt{D(\rho)}}). \tag{2.46}$$

In both cases the first derivatives are positive which eventually proves that the system is hyperbolic in all three cases. In the following we assume a subsonic flow situation, i.e. $|v| < a(\rho)$. Hence, the first eigenvalue is negative and the second positive.

Hyperbolic Balance Laws on Networks

So far, the results concentrate only on single pipelines. To extend these to networks we consider a vertex coupling m pipes which are all modeled by the isothermal Euler equations (2.6). We present the abstract coupling setting and show that the remaining model relations from Section 2.1 fit into that form.

For a simpler statement of the system generalizing (2.31) to junctions we re-parametrize the problem on each of the edge to the open real intervals $(0, \infty)$. Hence, all edges are outgoing for the connecting vertex, on all these incident edges located at $x = 0$. The problem of coupled systems of balance laws is then given by:

$$\left. \begin{aligned} \partial_t \boldsymbol{u}^1 + \partial_x \boldsymbol{f}^1(\boldsymbol{u}^1) &= \boldsymbol{s}^1(\boldsymbol{u}^1) \\ &\vdots \\ \partial_t \boldsymbol{u}^m + \partial_x \boldsymbol{f}^m(\boldsymbol{u}^m) &= \boldsymbol{s}^m(\boldsymbol{u}^m) \end{aligned} \right\} \quad \text{for } x \geq 0, \tag{2.47a}$$

$$\Psi(\boldsymbol{u}^1(0+, t), \dots, \boldsymbol{u}^m(0+, t)) = \Pi(t), \tag{2.47b}$$

for $t \geq 0$, where the state on edge $i \in \{1, \dots, m\}$ is indexed as $\boldsymbol{u}^i$. For the isothermal Euler equations on each pipe we have, just as before, $\boldsymbol{u}^i = (\rho^i, q^i)$, flux functions $\boldsymbol{f}^i(\boldsymbol{u}^i)^T = (q^i/A^i, \frac{q^i}{A\rho^i} + A^i p(\rho^i))$ and sources $\boldsymbol{s}^i(\boldsymbol{u}^i)^T = (0, -gs^i A^i \rho^i - \frac{\phi^i(q^i)}{\rho^i})$. The function Ψ contains the coupling relations at the vertex.

The coupling conditions (2.25) and (2.26) at a node coupling m pipes are directly adapted as

$$
\Psi(\boldsymbol{u}^1, \ldots, \boldsymbol{u}^m) = \begin{pmatrix} \sum_{i=1}^m q^i \\ p(\rho^2) - p(\rho^1) \\ \vdots \\ p(\rho^m) - p(\rho^1) \end{pmatrix}, \quad \Pi(t) = \begin{pmatrix} q^{\mathrm{ext}}(t) \\ 0 \\ \vdots \\ 0 \end{pmatrix}, \tag{2.48}
$$

where the first component models mass conservation and the other $m-1$ equations model equality of the pressures at the vertex. The external flow $q^{\mathrm{ext}}(t)$ can be chosen to be zero on interior nodes.

In contrast to the model introduced in Section 2.1, in publications on hyperbolic conservation laws on networks the compressors are usually modeled as nodes coupling two pipes. An ideal compressor is then modeled as a special vertex with coupling functions

$$
\Psi(\boldsymbol{u}^1, \boldsymbol{u}^2) = \begin{bmatrix} q^1 + q^2 \\ q^2/\eta_{\mathrm{ad}} \cdot H_{\mathrm{ad}}\left(p(\rho^2), p(\rho^1)\right) \end{bmatrix} \tag{2.49}
$$

and right hand side

$$
\Pi(t) = \begin{bmatrix} 0 \\ P(t) \end{bmatrix}. \tag{2.50}
$$

where H_{ad} is the function given in Equation 2.16 for constant temperatures and $P(t)$ the given power consumption of the compression. The direction implied by the orientation of the arc is fixed here by the enumeration of the two pipes. Since the function H_{ad} is not symmetric in its inputs the coupling model is not symmetric, too.

In the same manner, an active control valve is also modeled as node coupling two pipes by adapting directly the relation (2.22) and the mass conservation at its input and output node as

$$
\Psi(\boldsymbol{u}^1, \boldsymbol{u}^2) = \begin{bmatrix} q^1 + q^2 \\ p(\rho^1) - p(\rho^2) \end{bmatrix}, \quad \Pi(t) = \begin{bmatrix} 0 \\ \Delta p(t) \end{bmatrix}. \tag{2.51}
$$

The flow direction on the active control valve is again fixed by the enumeration of the incident edges.

2.2.1 Existence of Solution and Well-Posedness

In this subsection we will review basic results on the well-posedness of the previously stated model of coupled systems of hyperbolic balance laws. Again, we first concentrate on single pipelines and then present the extensions to networks.

It is well known that the solutions to nonlinear hyperbolic PDEs do not exist in the classical sense of (2.54a) even if the initial data is smooth. The solution can become discontinuous after finite time which makes other solution concepts necessary. In the case of physical conservation or balance laws the PDE is often derived from the integral form first. Hence, it is natural to search for solutions of the integral equation that admits nonsmooth and even discontinuous solutions. It can be shown that this is equivalent to weak solutions in the sense of distributions for the system of PDEs. To obtain uniqueness of solutions to the integral equations, additional conditions are required that are usually referred to as *entropy conditions*. Below a condition convenient for the isothermal Euler equations will be presented.

We start with the *Rankine-Hugoniot condition* that characterizes discontinuities of solutions to the integral form (2.33) of the balance law. A jumps of the solution $\boldsymbol{u}^+ - \boldsymbol{u}^-$ must satisfy

$$s(\boldsymbol{u}^+ - \boldsymbol{u}^-) = \boldsymbol{f}(\boldsymbol{u}^+) - \boldsymbol{f}(\boldsymbol{u}^-) \tag{2.52}$$

where s is the speed at which the discontinuity is propagating in x-t-space. In the context of hyperbolic balance laws discontinuities in the solution are often called *shocks*.

The structure of the solution to hyperbolic PDEs is easier understood for the case of homogeneous linear systems of the form

$$\partial_t \boldsymbol{u} + J \, \partial_x \boldsymbol{u} = 0. \tag{2.53}$$

Corresponding to a strictly hyperbolic system, the matrix J has n eigenvalues $\lambda_1, \ldots, \lambda_n$ with linear independent eigenvectors $\boldsymbol{r}_1, \ldots, \boldsymbol{r}_n$. Using the transformed variables $\boldsymbol{z} = R^{-1}\boldsymbol{u}$, where R is the matrix of eigenvectors, the system can be equivalently rewritten as

$$\partial_t \boldsymbol{z} + \Lambda \, \partial_x \boldsymbol{z} = 0,$$

where Λ is the diagonal matrix of eigenvalues. Since the system is now decoupled, the initial value for each characteristic variable $\boldsymbol{z}_p$, $p \in 1, \ldots, n$, is simply advected. In this case the *characteristic curves* $X(t) = x_0 + \lambda_p t$ associated with eigenvalue λ_p, i.e. the curves of finite and constant speed along which the information propagates unchanged, are straight lines. The curves corresponding to λ_p and $\boldsymbol{r}_p$ are often denominated p^{th} *characteristic family* or *field*.

In the general case the matrix of the quasilinear form $J(\boldsymbol{u}) = \partial_{\boldsymbol{u}} \boldsymbol{f}(\boldsymbol{u})$ is a function of $\boldsymbol{u}$ and as a consequence the corresponding eigenvalues λ_p and eigenvectors $\boldsymbol{r}_p$, too. However, the solution structure is similar to the linear case. The information as well propagates along the characteristic curves with finite speed associated to the eigenvalues of $\partial_{\boldsymbol{u}} \boldsymbol{f}(\boldsymbol{u})$. Since the slope of the characteristics now depends on the solution $\boldsymbol{u}$, the characteristic curves associated with

different initial points can intersect or diverge leading to more difficult solution structures than in the linear case. If the system is not homogeneous, the solution along each characteristic curve is not constant any more but has to satisfy a nontrivial ordinary differential equation. This information propagation with finite speed is commonly considered as wave-like. This motivates the denomination *wave* for state changes in the solution traveling through the x-t-space. Since the information moves at finite speed, the solution at a point $(\bar{x}, \bar{t})$ is only influenced by the initial values on a bounded subset of the observed domain. We call all points (x, t) whose image under $\boldsymbol{u}$ influences $\boldsymbol{u}(\bar{x}, \bar{t})$, the (analytic) *domain of dependency.*

Riemann Problem

As a common building block for the investigation of a system of hyperbolic PDEs we will now concentrate on the so-called *Riemann* problem. This denominates the initial value problem for the homogeneous PDE associated with (2.31)

$$\frac{\partial \boldsymbol{u}}{\partial t} + \frac{\partial \boldsymbol{f}(\boldsymbol{u})}{\partial x} = 0, \tag{2.54a}$$

equipped with the so-called *Riemann initial conditions*

$$\boldsymbol{u}(x, 0) = \begin{cases} \boldsymbol{u}_{\mathrm{L}} & = (\rho_{\mathrm{L}}, q_{\mathrm{L}}), \quad x < 0, \\ \boldsymbol{u}_{\mathrm{R}} & = (\rho_{\mathrm{R}}, q_{\mathrm{R}}), \quad x > 0. \end{cases} \tag{2.54b}$$

These problems are principal ingredients for existence proofs and give further insight into the solution strategy. For the general overview we take a look on the linear case (2.53) and the depicted solution structure first. If there is an initial discontinuity in the transformed variable $\boldsymbol{z}_p$, then this is transported with the constant velocity λ_p. The complete solution is hence a set of constant states separated by n discontinuities or shock waves leaving the origin at the speed given by the eigenvalues. Any jump has to satisfy the Rankine-Hugoniot condition which means here that the jump $\boldsymbol{u}^+ - \boldsymbol{u}^-$ corresponding to the pth wave needs to be a multiple of $\boldsymbol{r}_p$.

Like in the linear case, the solution for the nonlinear Riemann problem consists of a set of constant values connected by a transition or wave for each characteristic family. It is constant on rays with fixed values for x/t. Such solutions are called *self-similar*. In contrast to the linear case, the transitions are not all discontinuities but can be of one of the three possible types: *shocks*, *contact discontinuities* or continuous *rarefactions*.

In Figure 2.4 a solution with two waves like for the isothermal Euler equations is visualized in the x-t-space. In the so-called subsonic case ($|v| < a(\rho)$) one wave is moving to the left and the other wave to the right. The first step is to determine whether the characteristic
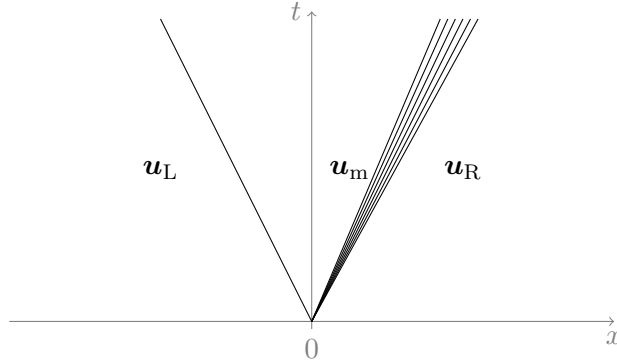
Figure 2.4: Schematic overview of solution to Riemann problem

fields are *genuinely nonlinear* or *linear degenerate*. This helps to decide which of the three transition types are possibly part of the solution structure.

Definition ([48] §7.3). *A characteristic field associated with the pth family is called* genuinely nonlinear *if*

$$\nabla \lambda_p(\boldsymbol{u})^T \cdot \boldsymbol{r}_p(\boldsymbol{u}) \neq 0, \quad \text{for all } \boldsymbol{u} \tag{2.55}$$

where λ_p and $\boldsymbol{r}_p$ are the eigenvalue and right eigenvector associated with the field. If for all $\boldsymbol{u}$ the converse relation $\nabla \lambda_p(\boldsymbol{u})^T \cdot \boldsymbol{r}_p(\boldsymbol{u}) = 0$ holds then the corresponding field is said to be linearly degenerate.

Genuine nonlinearity generalizes the convexity requirement on the flux function in one dimension. It implies that the eigenvalue $\lambda(\boldsymbol{u})$ is strictly monotone on integral curves of the field associated with $r(\boldsymbol{u})$. In a linearly degenerate field the eigenvalue is constant on these integral curves. If the characteristic field is genuinely nonlinear, the associated transition can only be a shock or rarefaction. If the field is linear degenerate, its transition is a contact discontinuity. The consequences of these observations applied to the Euler equations are formulated in the following lemma.

Lemma 2.1. *The solution of the Riemann problem* (2.54) *for the isothermal Euler equations with equation of state* (2.2) *and the compressibility factor calculated according to $z \equiv 1$ for an ideal gas, by the AGA-formula* (2.4) *or by Papay's formula* (2.3)*, consists of three constant states connected by shock or rarefaction waves.*

Proof. To prove the lemma we only have to check the condition (2.55) for genuine nonlinearity of the two characteristic fields for all three pressure expressions. Using the above computed

eigenvalues in physical variables (2.38) the condition reads

$$\nabla \lambda_{1/2}^T(\boldsymbol{w}) \cdot \boldsymbol{r}_{1/2}(\boldsymbol{w}) = \begin{pmatrix} \mp a'(\rho) \\ 1 \end{pmatrix}^T \begin{pmatrix} 1 \\ \mp \frac{a(\rho)}{\rho} \end{pmatrix} = \mp(a'(\rho) + \frac{a(\rho)}{\rho})$$

$$= \mp \left(\frac{p''(\rho)}{2\sqrt{p'(\rho)}} + \frac{\sqrt{p'(\rho)}}{\rho} \right) \tag{2.56}$$

For the ideal gas this simplifies to

$$\nabla \lambda_{1/2}^T(\boldsymbol{w}) \cdot \boldsymbol{r}_{1/2}(\boldsymbol{w}) = \mp \frac{a}{\rho} \lessgtr 0.$$

For the AGA equation we get from (2.43), (2.44)

$$\nabla \lambda_{1/2}^T(\boldsymbol{w}) \cdot \boldsymbol{r}_{1/2}(\boldsymbol{w}) = \mp \frac{1}{a(\rho)} \left(\frac{p''(\rho)}{2} + \frac{p'(\rho)}{\rho} \right)$$

$$= \mp \frac{p(\rho)}{a(\rho)} \left(\frac{1 - t(\rho) - \rho t'(\rho)}{2\rho^2 t(\rho)^2} + \frac{1}{\rho^2 t(\rho)} \right)$$

$$= \mp \frac{p(\rho)}{a(\rho)} \frac{1 + t(\rho) - \rho t'(\rho)}{2\rho^2 t(\rho)^2} = \mp \frac{p(\rho)}{a(\rho)} \frac{2}{2\rho^2 t(\rho)^2} \lessgtr 0.$$

Similar computations for the Papay equation yield

$$\nabla \lambda_{1/2}^T(\boldsymbol{w}) \cdot \boldsymbol{r}_{1/2}(\boldsymbol{w}) = \mp \frac{p(\rho)}{2a(\rho)D(\rho)\rho^2} \left(1 + \sqrt{D(\rho)} - \rho \frac{D'(\rho)}{2\sqrt{D(\rho)}} \right).$$

The term in parenthesis is positive since by basic computation one gets

$$D(\rho) - \tfrac{\rho}{2} D'(\rho) = 1 + a^2 C_2 \rho > 0.$$

This proves genuine nonlinearity for the Papay case and hence the statement for all three choices for the compressibility factor. $\qquad\square$

Shock waves   Next the wave structure is analyzed in more detail and we focus first on the case of a discontinuous transition or shock wave. As already noted above, a jump in the solution has to satisfy the Rankine-Hugoniot condition (2.52) which for the isothermal Euler equation is given by

$$(\rho v)^- - (\rho v)^+ = s(\rho^- - \rho^+), \tag{2.57a}$$

$$(\rho v^2 + p(\rho))^- - (\rho v^2 + p(\rho))^+ = s((\rho v)^- - (\rho v)^+). \tag{2.57b}$$

This condition can now be exploited to get a more detailed view on the solution of the Riemann problem (2.54). Rearranging the first term to get an expression for s and plugging this into the second equation yields after some simplifications

$$(v^- - v^+)^2 = \frac{(p(\rho^-) - p(\rho^+))\,(\rho^- - \rho^+)}{\rho^- \rho^+}$$

$$\Longleftrightarrow\ v^- - v^+ = \pm\sqrt{\frac{(p(\rho^-) - p(\rho^+))\,(\rho^- - \rho^+)}{\rho^- \rho^+}}. \tag{2.58}$$

The set of all points (ρ, v) in phase space satisfying the Rankine-Hugoniot condition are called *Hugoniot locus.*

For shock waves there are different conditions to distinguish admissible shocks from the nonphysical ones. If all fields are genuine nonlinear, the physical shocks satisfy the *Lax entropy condition* as stated in [48, §7.4]:

$$\lambda(\boldsymbol{u}^-) > s > \lambda(\boldsymbol{u}^+), \tag{2.59}$$

where s is again the shock speed. A shock is physical only if the characteristics run into the shock and disappear. There are no characteristics leaving the shock.

This entropy condition helps to identify the entropy-violating branches of the solutions to the Rankine-Hugoniot conditions. We consider a 2-shock and use the above equation (2.58) to get all velocities $v(\rho)$ as functions of density such that the point $\boldsymbol{u}(\rho) = (\rho, A\rho v(\rho))^T$ is connected by a 2-shock to the right initial state $\boldsymbol{u}_{\mathrm{R}}$:

$$v(\rho) = v_{\mathrm{R}} \pm \sqrt{\frac{(p(\rho_{\mathrm{R}}) - p(\rho)) \pm (\rho_{\mathrm{R}} - \rho)}{\rho_{\mathrm{R}}\rho}}$$

Clearly $\boldsymbol{u}(\rho)$ and $\boldsymbol{u}_{\mathrm{R}}$ satisfy the Rankine-Hugoniot condition. Derivation of this condition w.r.t. ρ and considering the parametrization via ρ we get that

$$\boldsymbol{u}'(\rho_{\mathrm{R}}) = \alpha \boldsymbol{r}_2(\boldsymbol{u}_{\mathrm{R}}), \ \text{with}\ \alpha > 0.$$

It follows then from the genuine nonlinearity (cf. Lemma 2.1)

$$\nabla \lambda_2^T(\boldsymbol{u}_{\mathrm{R}})\boldsymbol{u}'(\rho_{\mathrm{R}}) = \alpha \nabla \lambda_2^T(\boldsymbol{u}_{\mathrm{R}})\boldsymbol{r}_2(\boldsymbol{u}_{\mathrm{R}}) > 0$$

which means that locally $\lambda_2(\boldsymbol{u}(\rho))$ increases with ρ around ρ_{R}. Because the Lax entropy condition (2.59) requires that $\lambda(\boldsymbol{u}(\rho)) > \lambda(\boldsymbol{u}_{\mathrm{R}})$ only the part for $\rho \geq \rho_{\mathrm{R}}$ gives physically feasible post-shock states. It remains to determine which sign in (2.58) is the correct for 2-shocks. Using the first jump condition (2.57a), it follows that it has to hold $v(\rho) \geq v_{\mathrm{R}}$ if $\rho \geq \rho_{\mathrm{R}}$ which fixes the "+"- sign for the 2-shock. Summarizing the previous results we have

for shocks associated to the second field

$$v(\rho) = v_{\mathrm{R}} + \sqrt{\frac{\left(p(\rho_{\mathrm{R}}) - p(\rho)\right)\left(\rho_{\mathrm{R}} - \rho\right)}{\rho_{\mathrm{R}}\rho}} \quad \text{for } \rho \geq \rho_{\mathrm{R}}. \tag{2.60}$$

For a shock associated with the first characteristic field we get an analog parametrization for all post-shock states for the left initial value $\boldsymbol{u}_{\mathrm{L}}$ by

$$v(\rho) = v_{\mathrm{L}} - \sqrt{\frac{\left(p(\rho_{\mathrm{L}}) - p(\rho)\right)\left(\rho_{\mathrm{L}} - \rho\right)}{\rho_{\mathrm{L}}\rho}} \quad \text{for } \rho \geq \rho_{\mathrm{L}}. \tag{2.61}$$

Rarefactions   While shocks are discontinuities satisfying the jump condition, rarefaction waves are continuous and differentiable transitions between the two constant states to the left and right of the wave. Parametrized by $\xi = x/t$, the self similar solution inside the transition, associated with the pth wave, is a solution to the ordinary differential equation

$$\tilde{\boldsymbol{u}}'(\xi) = g(\xi)\boldsymbol{r}_p(\tilde{\boldsymbol{u}}(\xi)), \tag{2.62}$$

where g depends on the parametrization. Solutions to initial value problems for this ODE are called integral curves of the vector field $\boldsymbol{r}_p$ since in each point the tangent to the curve is a multiple of $\boldsymbol{r}_p$. Assuming that the constant states $\boldsymbol{u}^-$ and $\boldsymbol{u}^+$ lie on one integral curve to the pth field, the solution has the form

$$\boldsymbol{u}(x, t) = \begin{cases} \boldsymbol{u}^- & \text{if } x/t \leq \lambda_p(\boldsymbol{u}^-), \\ \tilde{\boldsymbol{u}}(x/t) & \text{if } \lambda_p(\boldsymbol{u}^-) < x/t < \lambda_p(\boldsymbol{u}^+), \\ \boldsymbol{u}^+ & \text{if } x/t \geq \lambda_p(\boldsymbol{u}^+). \end{cases}$$

This definition is only useful if the characteristic curves diverge as the time advances. Hence, it must hold

$$\lambda_p(\boldsymbol{u}^-) < \lambda_p(\boldsymbol{u}^+). \tag{2.63}$$

To solve the Riemann problem, an explicit expression for two states on the same integral curve is required. We again use the physical variables $\boldsymbol{w} = (\rho, v)$, set $g(\xi) \equiv 1$ to fix a particular parametrization and solve

$$\tilde{\boldsymbol{w}}'(\xi) = \boldsymbol{r}_i(\tilde{\boldsymbol{w}}'(\xi)) = \begin{pmatrix} 1 \\ \mp \frac{a(\rho(\xi))}{\rho(\xi)} \end{pmatrix}, \quad i = 1, 2.$$

Clearly, $\rho(\xi) = \xi + c$ is a solution to the first equation which enables us to parametrize the solution in terms of the density ρ. The corresponding solution to second equation is:

$$v(\rho^+) - v(\rho^-) = \mp \int_{\rho^-}^{\rho^+} \frac{a(\tilde{\rho})}{\tilde{\rho}} \, \mathrm{d}\tilde{\rho}.$$

Using that relation we get for all states that can be connected over a 2-rarefaction to the right initial value:

$$v(\rho) = v_{\mathrm{R}} - \int_{\rho}^{\rho_{\mathrm{R}}} \frac{a(\tilde{\rho})}{\tilde{\rho}} \, \mathrm{d}\tilde{\rho}, \quad \text{for } \rho \leq \rho_{\mathrm{R}}. \tag{2.64}$$

The restriction to the case $\rho \leq \rho_R$ follows from the principle of diverging characteristics (2.63) using the genuine nonlinearity. For the 1-rarefaction the analog result holds:

$$v(\rho) = v_{\mathrm{L}} - \int_{\rho_{\mathrm{L}}}^{\rho} \frac{a(\tilde{\rho})}{\tilde{\rho}} \, \mathrm{d}\tilde{\rho}, \quad \text{for } \rho \leq \rho_{\mathrm{L}}. \tag{2.65}$$

Lax curves Putting together the results (2.60)–(2.65) for each wave, we get

$$v(\rho) = v_{\mathrm{L}} - \begin{cases} \sqrt{\frac{(p(\rho_{\mathrm{L}}) - p(\rho))(\rho_{\mathrm{L}} - \rho)}{\rho_{\mathrm{L}}\rho}} & \text{, for } \rho > \rho_{\mathrm{L}}, \\ -\int_{\rho}^{\rho_{\mathrm{L}}} \frac{a(\tilde{\rho})}{\tilde{\rho}} \, \mathrm{d}\tilde{\rho} & \text{, for } \rho \leq \rho_{\mathrm{L}}, \end{cases} \tag{2.66}$$

for the 1-wave and analogously for the 2-wave:

$$v(\rho) = v_{\mathrm{R}} + \begin{cases} \sqrt{\frac{(p(\rho_{\mathrm{R}}) - p(\rho))(\rho_{\mathrm{R}} - \rho)}{\rho_{\mathrm{R}}\rho}} & \text{, for } \rho > \rho_{\mathrm{R}}, \\ -\int_{\rho}^{\rho_{\mathrm{R}}} \frac{a(\tilde{\rho})}{\tilde{\rho}} \, \mathrm{d}\tilde{\rho} & \text{, for } \rho \leq \rho_{\mathrm{R}}. \end{cases} \tag{2.67}$$

The *Lax curve* corresponding to the waves consists of all points that can be connected to the left or right initial state, respectively, by an admissible shock or rarefaction. Parametrizing the Lax curves, in this case by the density ρ, yields

$$\mathcal{L}_1(\rho, \boldsymbol{u}_{\mathrm{L}}) = \{\boldsymbol{u} = (\rho, \rho A v)^T \colon v = v(\rho) \text{ by } (2.66)\}, \tag{2.68}$$

$$\mathcal{L}_2(\rho, \boldsymbol{u}_{\mathrm{R}}) = \{\boldsymbol{u} = (\rho, \rho A v)^T \colon v = v(\rho) \text{ by } (2.67)\}. \tag{2.69}$$

Now two characterizations for the constant middle state of the solution for the Riemann Problem are available. To solve the Riemann-Problem (2.54), one needs to find a state $\boldsymbol{u}_{\mathrm{m}} = (\rho_{\mathrm{m}}, v_{\mathrm{m}})$ which can be connected to $\boldsymbol{u}_L$ by an 1-wave and to $\boldsymbol{u}_R$ by an 2-wave, i.e. such that both relations (2.66) and (2.67) hold. Thus, the question if the Riemann Problem has a solution, reduces to the task of finding a density ρ_{m} such that the velocities computed according to (2.66) and (2.67) coincide. Geometrically, we search for an intersection of
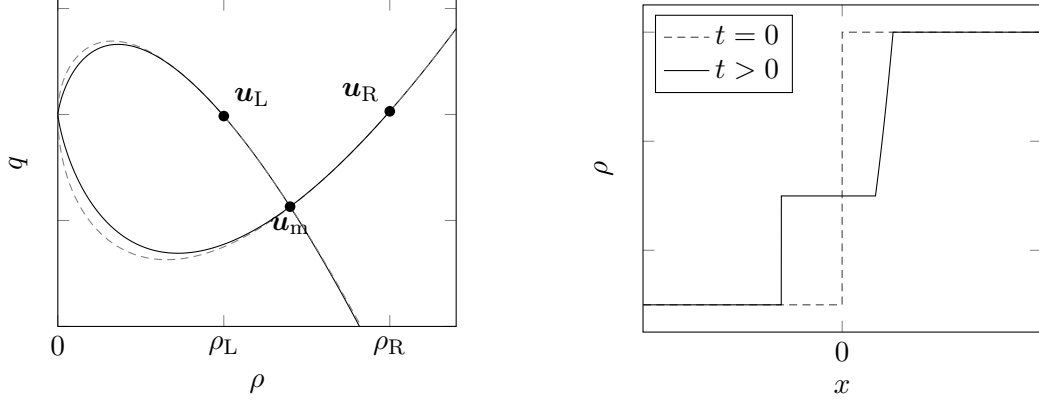
(a) Solution in phase space; the dotted lines are   (b) Density part of solution at $t = 0$ and $t_1 > 0$.
the nonphysical branches of the integral curves
or Hugoniot loci, respectively.

Figure 2.5: Solution of Riemann problem

the Lax curves in the phase space connected to the initial values $\boldsymbol{u}_{\mathrm{L}}$ and $\boldsymbol{u}_{\mathrm{R}}$, respectively. Figure 2.5 illustrates the solution of a Riemann problem for the isothermal Euler equation in the phase space as sketched before. This can be expressed by finding a root for the auxiliary function

$$\psi(\rho) = v_{\mathrm{R}} - v_{\mathrm{L}} + f_{\mathrm{L}}(\rho) + f_{\mathrm{R}}(\rho) \tag{2.70}$$

$$\text{with } f_{\mathrm{K}}(\rho) = \begin{cases} \sqrt{\dfrac{(p(\rho_{\mathrm{K}}) - p(\rho))(\rho_{\mathrm{K}} - \rho)}{\rho_{\mathrm{K}}\rho}} & \text{, for } \rho > \rho_{\mathrm{K}} \\ -\int_{\rho}^{\rho_{\mathrm{K}}} \dfrac{a(\tilde{\rho})}{\tilde{\rho}} \, \mathrm{d}\tilde{\rho} & \text{, for } \rho < \rho_{\mathrm{K}} \end{cases} \quad \mathrm{K} \in \{\mathrm{L}, \mathrm{R}\}. \tag{2.71}$$

The functions $f_{\mathrm{K}}(\rho)$ for $\mathrm{K} \in \{\mathrm{L}, \mathrm{R}\}$ are monotonically increasing, thus $\psi(\rho)$ is monotonically increasing. Hence, if there exist a root ρ_{m}, i.e. an intermediate state, then it is unique. To show the existence of the root for each combination of initial values is not possible for all cases. It can be shown that $\psi(\rho)$ diverges to $-\infty$ for $\rho \to 0$. Hence, if $v_{\mathrm{R}} - v_{\mathrm{L}} > 0$ holds, then there must exist a root of ψ. However, it is possible to construct examples of Riemann problems at least for the Papay pressure equation that do not have a solution: Since ρ has to be such that $D(\rho) > 0$, this implies an upper bound for ρ. If we assume $v_{\mathrm{R}} - v_{\mathrm{L}} \ll 0$ and $\rho_{\mathrm{R}} = \rho_{\mathrm{L}} \lessapprox \rho_{\max}$, the solution must have two shocks. Hence, ρ_{m} might leaves the feasible range for ρ since it has to be greater than ρ_{L}. These cases seem to be far away from real operation states of pipelines so we will not investigate further on these cases.

The initial value problem for general initial values is analytically treated by so-called wave-front tracking techniques. The strategy starts with a piecewise constant approximation of the initial state. Then Riemann problems are solved for any jump point. Whenever any of the emerging waves interact, a new Riemann problem appears and has to be solved. Iterating

this procedure gives the complete solution. To state results for the limit case for decreasing initial approximation grid sizes, the number and strength of emerging Riemann problems have to be controlled. For details on the analytic techniques we refer to [7] since these techniques go much beyond the scope of this thesis. Instead, we continue with the extension of the ideas of Riemann problems to connected pipes in networks.

Solution on Networks   The first point to notice is that only a particular network with just one vertex coupling various edges has to be discussed. Again the fact that the waves propagate with finite speed can be used to extend the discussion to general networks. The results necessary for this generalization can be found for the example of traffic networks in [28].

Just like for the case of single pipelines, the theoretical treatment of hyperbolic systems on networks uses wave-front tracking techniques based on solutions to Riemann problems. Additionally to the classical Riemann problem on the edge domains (2.54), a Riemann problem for the coupled problem at the junction (2.47) is therefore required and usually defined as

$$\partial_t \boldsymbol{u}^1 + \partial_x \boldsymbol{f}^1(\boldsymbol{u}^1) = 0,$$

$$\vdots \tag{2.72a}$$

$$\partial_t \boldsymbol{u}^m + \partial_x \boldsymbol{f}^m(\boldsymbol{u}^m) = 0,$$

$$\Psi(\boldsymbol{u}^1(0+,t), \dots, \boldsymbol{u}^m(0+,t)) = \bar{\Pi}, \tag{2.47b}$$

$$\boldsymbol{u}^1(x,0) = \boldsymbol{u}^1_{\mathrm{R}}, \text{ for } x \geq 0,$$

$$\vdots \tag{2.72b}$$

$$\boldsymbol{u}^m(x,0) = \boldsymbol{u}^m_{\mathrm{R}}, \text{ for } x \geq 0,$$

with constant right initial states $\boldsymbol{u}^i_{\mathrm{R}}$ and constant control $\bar{\Pi}$. We set the image space of the solution $\boldsymbol{u}^i$ on edge i to be an open set $\Omega^i \subset \mathbb{R}^n$, with $n = 2$ for the isothermal Euler equations. The concatenation is denoted by $\boldsymbol{u} = (\boldsymbol{u}^1, \dots, \boldsymbol{u}^m) \in \boldsymbol{\Omega} = \Omega^1 \times \cdots \times \Omega^m$. To solve the problem (2.72), we need to determine m intermediate states $\boldsymbol{u}^1_{\mathrm{G}}, \dots \boldsymbol{u}^m_{\mathrm{G}}$ such that the coupling conditions are satisfied

$$\Psi(\boldsymbol{u}^1_{\mathrm{G}}, \dots \boldsymbol{u}^m_{\mathrm{G}}) = \bar{\Pi}$$

and for all incident edges i the state $\boldsymbol{u}^i_{\mathrm{G}}$ is connected by a feasible wave to the right initial state $\boldsymbol{u}^i_{\mathrm{R}}$. This is a direct generalizing of solving the classical Riemann problems. Hence, for the Euler equations it corresponds to the determination of parameters $\xi^1, \dots, \xi^m$ for the

(a) Initial state

(b) Solution in phase space
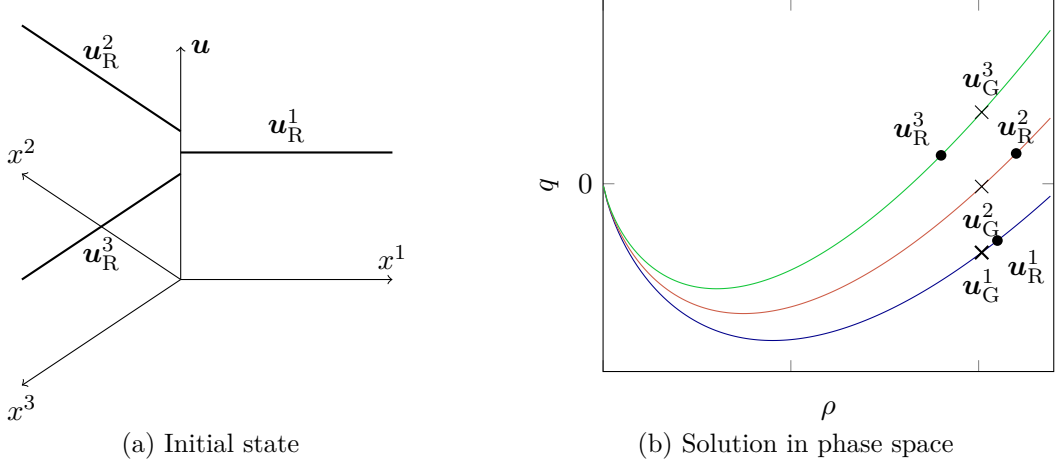
Figure 2.6: Riemann problem at simple junction coupling three pipes; first edge is ingoing, second and third are outgoing edges.

2-Lax curves as introduced in (2.69) on each edge such that

$$\Psi\big(\mathcal{L}_2^1(\xi^1, \boldsymbol{u}_\mathrm{R}^1), \ldots, \mathcal{L}_2^m(\xi^m, \boldsymbol{u}_\mathrm{R}^m)\big) = \bar{\bar{\Pi}}. \tag{2.73}$$

In Figure 2.6 the Riemann problem and its solution in phase space are illustrated for a junction of one outgoing and two ingoing edges. We note that only 2-Lax curves appear because of the local reparametrization.

The well-posedness result provided in [15] and [8] for systems of two unknowns for each edge, which fits to our case, depends on two basic assumptions we discuss first.

(**F**) The flux function $\boldsymbol{f}^i$ is smooth on each edge and every problem is strictly hyperbolic with $\lambda_1^i(\boldsymbol{u}^i) < 0 < \lambda_2^i(\boldsymbol{u}^i)$. Additionally, all characteristic fields of $\boldsymbol{f}^i$ are either genuinely nonlinear or linear degenerate.

(**Ψ**) This condition is said to hold in $\bar{\boldsymbol{u}} \in \boldsymbol{\Omega}$ if the function $\Psi \in \mathcal{C}^1$ satisfies

$$\det\Big[D_{\boldsymbol{u}_1}\Psi(\bar{\boldsymbol{u}})r_2^1(\bar{\boldsymbol{u}}^1), \ldots, D_{\boldsymbol{u}_m}\Psi(\bar{\boldsymbol{u}})r_2^1(\bar{\boldsymbol{u}}^m) \Big] \neq 0 \tag{2.74}$$

The condition (**F**) has been treated in the previous paragraph. We have shown that the isothermal Euler equations with each of the three choices for the compressibility is genuinely nonlinear. The condition on the eigenvalues means that the solutions stay in the subsonic domain which we have assumed earlier in this thesis. In this context this especially means that on each edge only the characteristic associated with the positive eigenvalue emerge from the vertex and thus the number of leaving or entering characteristics does not change. It is well known for boundary value problems for hyperbolic conservation laws that one boundary

condition is required for any characteristic leaving the boundary. From the interpretation of the coupling problem (2.47) as one big boundary value problem it follow that the number of coupling conditions must equal the constant number of leaving characteristics.

The second condition $(\boldsymbol{\Psi})$ offers some more insight in the local solvability of the coupling Riemann problem at the junction. Considering the above sketched solution structure, this condition ensures that the implicit function theorem can be applied to guarantee the local solvability of the coupling conditions if the distance between the initial states is sufficiently small. Additionally, the condition includes that no characteristic velocity can be zero leading to badly posed boundary conditions.

In [34] it has been shown that the coupling conditions for gas nodes (2.48) as well as the coupling relations for a 1-to-1 coupling representing a compressor (2.49) satisfy condition $(\boldsymbol{\Psi})$ in every subsonic state $\boldsymbol{u}$. Similar computations show that this also holds true for vertices representing a control valve.

To state the well-posedness result for the initial value problem to the coupled systems of hyperbolic balance laws (2.47) in detail as given in the survey [8], we only need some more notation. Solutions of hyperbolic PDEs for every time point t, considered as functions of the space variable $x \in \mathbb{R}^m_{\geq 0} =: \mathbb{R}^+$, are usually measured using the norm in $\boldsymbol{L}^1(\mathbb{R}^+, \boldsymbol{\Omega})$

$$\|\boldsymbol{u}\|_{\boldsymbol{L}^1} = \int_{\mathbb{R}^+} \|\boldsymbol{u}(x)\| \, \mathrm{d}x$$

or by the *total variation* defined as

$$TV(\boldsymbol{u}) = \sum_i \mathrm{TV}(\boldsymbol{u}^i)$$

$$\text{with} \quad \mathrm{TV}(\boldsymbol{u}^i) = \sup \sum_{j=1}^N \|\boldsymbol{u}^i(\xi_j) - \boldsymbol{u}^i(\xi_{j-1})\|,$$

where the supremum is taken over all subdivisions $0 \leq \xi_1 < \cdots < \xi_N = \infty$ of the positive real axis.

Theorem 2.2 (Theorem 2.13. in [8], Well-Posedness)**.** *Let $m \in \mathbb{N}$, $m \geq 2$ and assumption* $(\mathbf{F})$ *hold. Fix a state $\bar{\boldsymbol{u}}_0 \in \boldsymbol{\Omega}$ such that the Riemann problem (2.72) with initial values $\bar{\boldsymbol{u}}_0$ has as weak solution $\boldsymbol{u} = \bar{\boldsymbol{u}}_0$. Let the coupling assumption $(\boldsymbol{\Psi})$ be satisfied at point $\bar{\boldsymbol{u}}_0$. Then there exist positive δ, L and a map $S\colon [0, \infty] \times D \to D$ such that*

1. *$D \supseteq \{\boldsymbol{u} \in \bar{\boldsymbol{u}}_0 + \boldsymbol{L}^1(\mathbb{R}^+, \boldsymbol{\Omega})\colon \mathrm{TV}(u) \leq \delta\}$;*

2. *for $\boldsymbol{u} \in D$ holds $S(0)\,\boldsymbol{u} = \boldsymbol{u}$ and for $s, t \geq 0$ the relation $S(s)\,S(t)\,\boldsymbol{u} = S(s+t)\,\boldsymbol{u}$;*

3. *for $\boldsymbol{u}, \tilde{\boldsymbol{u}} \in D$ and $s, t \geq 0$ it holds $\|S(t)\boldsymbol{u} - S(s)\tilde{\boldsymbol{u}}\|_{\boldsymbol{L}^1} \leq L \left(\|\boldsymbol{u} - \tilde{\boldsymbol{u}}\|_{[\boldsymbol{L}^1} + |t - s| \right)$;*

4. *if $\boldsymbol{u} \in D$ is piecewise constant, then for $t < 0$ sufficiently small $S(t)\boldsymbol{u}$ coincides with the juxtaposition of the solution to Riemann problem centered at the points of the jumps or at the junction.*

Moreover, for every $\boldsymbol{u} \in D$, the map $t \mapsto S(t)\boldsymbol{u}$ is a weak solution to the initial value problem for (2.47).

As we have remarked above the conditions of this theorem are satisfied for the gas flow in pipelines with coupling by nodes, control valves and compressor station. Hence, the analytic problems arising from the modeling are well-posed in this sense.

For the case of a compressor coupling two pipes Colombo et al. [14] extend this result and show that the solution is also Lipschitz continuous w.r.t. the compressor control in suitable function spaces. This ensures existence of minimizers in this setting if the initial value problem is used as constraints for optimization. For the presentation of the details for this result we refer to [14] as well as to [8].

2.3 Discretization Strategies

This section is devoted to the discretization of the isothermal Euler equation considering the coupling algebraic equations. We start with *finite volume* discretization schemes that are designed to capture the solution structure discussed in the previous chapter. Some of the techniques are directly based on the theoretical ideas used for the analytic investigation. To conclude this section, we present a simpler approaches to discretize the Euler equations with *finite differences.* The introduced numerical schemes are compared in Section 4.2 for examples of realistic flows in gas transmission networks. Both schemes approximate the solution $\boldsymbol{u}(x, t)$ by a finite dimensional vector $\boldsymbol{U}$ where each entry is associated with finite dimensional grids in time $t_0 < t_1 < \cdots < t_M$ and space $\cdots < x_{i-1} < x_i < x_{i+1} < \cdots$.

2.3.1 Finite Volume Methods

In one spatial dimension finite volume methods are based on subdividing the spatial domain into nonoverlapping subintervals and approximate the true solution by a piecewise constant function representing the integral mean on each subinterval. Based on the integral form (2.32) the approximation is then updated for each time step using the (numerical approximation of the) flux on the subinterval boundaries. The discussion is first restricted to the homogeneous case of a single infinite, one dimensional domain and then extended to the network structure, higher order approximations and finally to source term treatment. We remark that only a small selection of techniques and methods, used for the numerical computations later,

is presented here. There is a huge number of related topics not covered in this surveying section. For more details and a much more extensive overview we refer to the text books of LeVeque [49] and Toro [66] from where this presentation is principally adapted, as well as to the dissertation of J. Kall [43] for the results on higher order methods on networks.

The subintervals or *cells* are denoted by $\mathcal{C}_i = [x_{i-1/2}, x_{i+1/2}]$, $i \in \mathbb{Z}$ where the cell width $x_{i+1/2} - x_{i-1/2} = \Delta x$ is assumed to be constant for all cells. We set $t_{n+1} = t_n + \Delta t$ to describe the time grid for the numerical approximation. The time step size Δt can be chosen uniformly for all time steps, but has often to be adjusted to satisfy a stability condition. Each entry of the discrete solution

$$\boldsymbol{U}_i^n \approx \frac{1}{\Delta x} \int_{x_{i-1/2}}^{x_{i+1/2}} \boldsymbol{u}(x, t_n) \, \mathrm{d}x = \frac{1}{\Delta x} \int_{\mathcal{C}_i} \boldsymbol{u}(x, t_n) \, \mathrm{d}x$$

is an approximation to the cell averages at the specific time point. Using the second integral form (2.33) the exact update for the cell average is

$$\frac{1}{\Delta x} \int_{\mathcal{C}_i} \boldsymbol{u}(x, t_{n+1}) \, \mathrm{d}x = \frac{1}{\Delta x} \int_{\mathcal{C}_i} \boldsymbol{u}(x, t_n) \, \mathrm{d}x - \frac{1}{\Delta x} \int_{t_n}^{t_{n+1}} \boldsymbol{f}(\boldsymbol{u}(x_{i+1/2}, t)) - \boldsymbol{f}(\boldsymbol{u}(x_{i-1/2}, t)) \, \mathrm{d}t$$
$$+ \frac{1}{\Delta x} \int_{\mathcal{C}_i} \int_{t_n}^{t_{n+1}} \boldsymbol{s}(\boldsymbol{u}(x, t)) \, \mathrm{d}t \, \mathrm{d}x. \tag{2.75}$$

Concentrating on the homogeneous case ($\boldsymbol{s} \equiv 0$) first, this leads to methods which update the averages by

$$\boldsymbol{U}_i^{n+1} = \boldsymbol{U}_i^n - \frac{\Delta t}{\Delta x} \left(\boldsymbol{F}_{i+1/2}^n - \boldsymbol{F}_{i-1/2}^n \right), \tag{2.76}$$

where $\boldsymbol{F}_{i-1/2}^n$ is an approximation to the mean flux at point $x_{i-1/2}$:

$$\boldsymbol{F}_{i-1/2}^n \approx \frac{1}{\Delta t} \int_{t_n}^{t_{n+1}} \boldsymbol{f}(\boldsymbol{u}(x_{i-1/2}, t)) \, \mathrm{d}t.$$

The value of the solution at the cell boundaries is usually not constant and unknown, so the flux integrals cannot be evaluated exactly in the general case. However, the conservation property represented by the integral form (2.33) (again with $\boldsymbol{s} \equiv 0$) is retained at discrete level:

$$\Delta x \sum_{i=I}^{J} \boldsymbol{U}_i^{n+1} = \Delta x \sum_{i=I}^{J} \boldsymbol{U}_i^n - \Delta t \left(\boldsymbol{F}_{J+1/2}^n - \boldsymbol{F}_{I-1/2}^n \right), \text{ for all } I \leq J \in \mathbb{Z}.$$

If, for example, the numerical fluxes are chosen to depend on the neighboring cell averages only, i.e.

$$\boldsymbol{F}_{i-1/2}^n = \boldsymbol{F}(\boldsymbol{U}_{i-1}^n, \boldsymbol{U}_i^n), \tag{2.77}$$

the resulting update scheme gets

$$\boldsymbol{U}_i^{n+1} = \boldsymbol{U}_i^n - \frac{\Delta t}{\Delta x} \left(\boldsymbol{F}(\boldsymbol{U}_i^n, \boldsymbol{U}_{i+1}^n) - \boldsymbol{F}(\boldsymbol{U}_{i-1}^n, \boldsymbol{U}_i^n) \right).$$

The new approximation only depends on three values of the old time step.

In his book [49] LeVeque names two types of conditions for the convergence of such a method: *consistency* and *stability*. A scheme scheme is consistent if the solution is locally well approximated. For numerical fluxes like in (2.77) this means that

$$\boldsymbol{F}(\bar{\boldsymbol{u}}, \bar{\boldsymbol{u}}) = \boldsymbol{f}(\bar{\boldsymbol{u}}), \text{ for any constant state } \bar{\boldsymbol{u}}.$$

If the solution is constant at the last time step, then the solution over the cell boundary is constant as well and the numerical flux should be just the evaluation of the flux function.

Stability means that small errors do not grow exceedingly. A necessary condition for stability is the famous *Courant-Friedrich-Lewy condition*, usually abbreviated to *CFL* condition [17]. The numerical domain of dependency is given as the support of all numerical approximations at the current time point that influence the numerical approximation for the next time step. The CFL conditions connects stability with the analytic and numerical domains of dependence.

Theorem 2.3 (CFL Condition). *A numerical method can be stable only if the numerical domain of dependency contains the analytic domain of dependency.*

This relation can be measured by the *CFL number*

$$c = \frac{\Delta t}{\Delta x} s_{\max}, \tag{2.78}$$

where $s_{\max}$ is the maximal wave speed at which the information of the true solution moves in x-t-space. Hence, in one time step the influenced domain expands by $\Delta t \, s_{\max}$. For three-point numerical schemes the CFL stability condition can then be expressed by the CFL number: $c \leq 1$.

One famous example of numerical flux functions is the *Lax-Friedrich method*. The associated numerical flux function of type (2.77) is given by

$$\boldsymbol{F}(\boldsymbol{U}_{i-1}^n, \boldsymbol{U}_i^n) = \frac{1}{2} \left(\boldsymbol{f}(\boldsymbol{U}_{i-1}^n) + \boldsymbol{f}(\boldsymbol{U}_i^n) \right) - \frac{\Delta x}{2\Delta t} \left(\boldsymbol{U}_i^n - \boldsymbol{U}_{i-1}^n \right). \tag{2.79}$$

This method is known to add large amount of *numerical diffusion* damping instabilities. This leads to a stable method for CFL numbers up to 1.
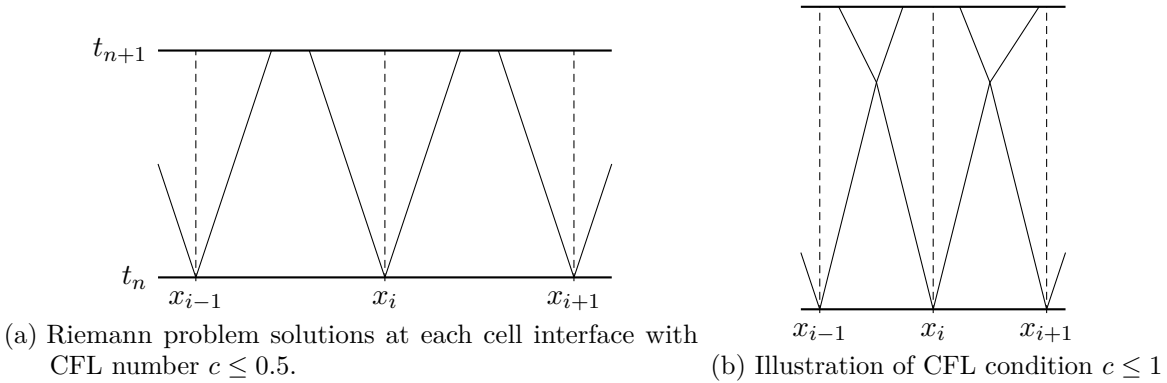
(a) Riemann problem solutions at each cell interface with CFL number $c \leq 0.5$.

(b) Illustration of CFL condition $c \leq 1$

Figure 2.7: Godunov's method [49, Fig 15.1]

Godunov's Method

The idea of Godunov's method is to solve one Riemann problem, as presented in the previous section, for each cell boundary and place their solutions side by side (see Figure 2.7). Using these solutions, the new cell averages can be computed. Choosing time and space discretization with CFL number $c \leq 1/2$ means that the waves of two neighboring Riemann problems will not interact in that time interval. Thus, the solution at the next time step could be explicitly computed and averaged to get the new cell averages. If the exact solution is not required, CFL numbers up to nearly one can be used. This still ensures that the interacting waves of the Riemann problem, that arises when two waves collide inside the cell, do not reach the cell boundary. So the solution at the cell boundary remains constant for every time step. Hence, the associated numerical flux function

$$\boldsymbol{F}^n_{i-1/2} = \boldsymbol{f}(\boldsymbol{u}_G). \tag{2.80}$$

is the exact flow for piecewise linear states. Using this definition, Godunov's method fits to the setting of (2.76). The so called Godunov state $\boldsymbol{u}_G$ here denotes the constant value of the solution of the Riemann problem (2.54) with left initial value $\boldsymbol{U}^n_{i-1}$ and right initial value $\boldsymbol{U}^n_i$ along the ray $x/t = 0$. For the isothermal Euler equation in the subsonic domain the Godunov state is always the unknown middle state connected to the initial values by feasible 1- and 2-waves in the phase space, respectively.

As stated, for Godunov's method not the complete solution structure of the Riemann problem is required. This provides the basis for approximate Riemann solvers computing approximations for the Godunov state or the associated flux. Details and examples can be found in [49] or any other textbooks on numerical solutions for hyperbolic conservation laws. Godunov's method has not been proved to be generally convergent for nonlinear

systems of conservation laws but it and its variations are known to be often successful in practice. However, if the solution sequence for refined grids has a limit function $\boldsymbol{u}(x,t)$ and the Riemann solutions in the Godunov scheme satisfy an entropy condition, then the limit function is a weak solution to the conversation law and satisfies the entropy condition, i.e. the observed shocks are physically correct.

Extension to Networks

The idea of the Godunov method can be directly extended to networks by the ideas already discussed for the theoretical results in the previous section. In addition to the numerical flux at the interior cell interfaces, the only new topic is to define the flux at the coupling junction. Considering for the presentation the same local re-parametrization with coupling at $x = x_{1/2} = 0$ on every coupled edge, the left numerical flux function in the first cells is derived from the solution of the Riemann problem at the junction (2.72). For coupled edge $j \in \{1, \ldots, m\}$ the numerical flux is defined as

$$\boldsymbol{F}_{1/2}^{n,j} = \boldsymbol{f}^j(\boldsymbol{u}_G^j), \tag{2.81}$$

where the $\boldsymbol{u}_G^j$ satisfy the coupling conditions and are connected by feasible waves to the Riemann initial states $\boldsymbol{U}_1^{n,j}$. For the isothermal Euler equations in the subsonic case this again corresponds to

$$\boldsymbol{u}_G^j = \mathcal{L}_2^j(\xi^j, \boldsymbol{U}_1^{n,j})$$

where $\mathcal{L}_2^j$ is the 2-Lax curve and ξ^j the coupling wave strength associated with edge j such that (2.73) is satisfied.

Higher Order Approximation with ADER schemes

The Godunov scheme or any other scheme depending on the cell averages only is bound to be of first order. There are various approaches to derive higher order schemes. We will present the idea of so-called *ADER* schemes (Arbitrary high order using DERivatives). For alternatives and more details we refer again to the text books [66], [49]. The ADER schemes on networks are introduced by a short extract of the ideas presented in the dissertation[43]. For more details, comparisons with other approaches and flavors as well as numerical experiments on different test cases we refer to that thesis and to the related publication [5].

As before, the construction of the ADER method can be motivated starting with the update formula for the cell averages (2.75) deduced from the integral form of the hyperbolic balance law. The question again is how to approximate the flux integral via the numerical

flux

$$\boldsymbol{F}_{i-1/2}^n \approx \frac{1}{\Delta t} \int_{t_n}^{t_n+\Delta t} \boldsymbol{f}(\boldsymbol{u}(x_{i-1/2}, t)) \, \mathrm{d}t, \tag{2.82}$$

and potentially the source by a numerical source

$$S_i^n \approx \frac{1}{\Delta t} \int_{x_{i-1/2}}^{x_{i+1/2}} \int_{t_n}^{t_n+\Delta t} \boldsymbol{s}(\boldsymbol{u}(x, t)) \, \mathrm{d}t \, \mathrm{d}x. \tag{2.83}$$

The basic idea is now to deduce on each cell a polynomial solution of the desired order in time and use it to integrate the flux and source integrals. Having the solution, usually in terms of its Taylor representation in time, flux and source integrals can be evaluated by suitable quadrature rules or again by Taylor expansions of flux and source function. The latter approach requires sufficiently smooth flux and source expressions which are in any case required for the ADER procedure. For the numerical flux, like for the first order Godunov method, we do not need the full solution but only the time evolution of the Godunov state for any cell interface approximated as truncated Taylor series

$$\boldsymbol{u}_{\mathrm{G}}(t) = \sum_{\nu=0}^{k} a_{\mathrm{G}}^\nu \frac{(t)^\nu}{\nu!}. \tag{2.84}$$

There are different procedures to compute the coefficients of the Taylor series. Principal building block of the strategy is the determination and solution of generalized Riemann problems for any cell interface defined as

$$\partial_t \boldsymbol{u} + \partial_x \boldsymbol{f}(\boldsymbol{u}) = \boldsymbol{s}(\boldsymbol{u}), \tag{2.85a}$$

$$\boldsymbol{u}(0, x) = \begin{cases} \boldsymbol{u}_{\mathrm{L}}(x) = \sum_{\nu=0}^{k} a_{\mathrm{L}}^\nu \frac{x^\nu}{\nu!}, & x < 0, \\ \boldsymbol{u}_{\mathrm{R}}(x) = \sum_{\nu=0}^{k} a_{\mathrm{R}}^\nu \frac{x^\nu}{\nu!}, & x > 0. \end{cases} \tag{2.85b}$$

In contrast to the classical Riemann problem, the left and right initial states are in general not constant but polynomial. The polynomials, in more detail the coefficients $a_{\mathrm{L}}^\nu, a_{\mathrm{R}}^\nu$ of its Taylor representation centered in the interface, are obtained by local polynomial reconstructions on cell $\mathcal{C}_i$ of order k using the cell averages on cell $\mathcal{C}_i$ and a certain number of neighbors. There exist different approaches, e.g. the WENO (Weighted Essentially Non Oscillatory) polynomial reconstruction procedure which uses a convex combination of polynomials to avoid large oscillations. The solution to the generalized Riemann problem (2.85) and computation of the coefficient for the representation (2.84) is done by the following steps:

1. Solution of the nonlinear classical homogeneous Riemann problem with initial data of zeroth order.

2. The derivation and solution of linear Riemann problems for each of the k space derivatives.

3. The Cauchy-Kowalewski (CK) procedure to convert the space derivatives into time derivatives.

Both steps 2 and 3 are using the derivatives of the governing system of equations. This procedure requires sufficiently smooth flux functions and possibly source terms. We remark that within the Cauchy-Kowalewski procedure the effect of source terms is incorporated whereas for the determination of the Riemann problems for the derivatives only the homogeneous system is considered. This is usually justified by the argumentation that only the first-instant interaction is needed where source terms are assumed to have only neglectable effect. A slightly different method is obtained changing the order of steps 2 and 3, solving linear Riemann problems for the time derivatives instead of for the spatial derivatives. This procedure provides then directly the coefficients of (2.84).

Source Terms

The ADER procedure can be extended to balance laws with source terms. We have already mentioned that the source term is incorporated in the CK-procedure while the rest of the solution procedure for the generalized Riemann problem is not depending on the source term. The source term has to be considered in the update formula, additionally. To compute the numerical source (2.83) again a Taylor approach is used. From the solution at the interfaces and the polynomial initial data Taylor polynomials are computed and integrated over the time-space cell. Again, Taylor expansion based quadrature rules like for the numerical flux are employed. Choosing different centering points for the Taylor series, result in slightly different methods. Again we refer to the references mentioned before for more details and other approaches to incorporate source terms, like splitting techniques.

ADER on Networks

In this paragraph, we present the extension of the ADER ideas to the network case using the coupling conditions of type (2.47b). Since the nodes are assumed to have no spatial extension, we cannot derive coupling conditions for the spatial derivatives which would be required for an direct extension of the procedure sketched above. Similar to the extension of the Godunov method to networks, only the numerical fluxes at the interfaces connected at junctions have to be defined additionally. Using a quadrature rule given by weights w_μ and quadrature points c_μ, $\mu = 0, \ldots, k$, the numerical flux at the coupled boundary of edge j can

be approximated as

$$\boldsymbol{F}_{1/2}^n = \sum_{\mu=0}^k w_\mu \boldsymbol{f}^j(\boldsymbol{u}_{\mathrm{G}}^j(t_n + c_\mu \Delta t)). \tag{2.86}$$

Instead of the complete time evolution of the Godunov states for each edge, only the values at the quadrature points are required. Therefor, on every edge the reconstructed spatial polynomial centered at the coupling interface is determined and converted into a polynomial $\boldsymbol{u}_{\mathrm{R}}^j(t)$ in time via the CK-procedure of Step 3. For any quadrature point μ the solution of the Riemann problem at junction (2.72) with initial data $\boldsymbol{u}_{\mathrm{R}}^j = \boldsymbol{u}_{\mathrm{R}}^j(t_n + c_\mu \Delta t)$, $j = 1, \ldots, m$ provides the Godunov states $\boldsymbol{u}_{\mathrm{G}}^j(t_n + c_\mu \Delta t)$. For the isothermal Euler equations in the subsonic case on pipe j the required value can be expressed as

$$\boldsymbol{u}_{\mathrm{G}}^j(t_n + c_\mu \Delta t) = \mathcal{L}_2^j(\xi^j, \boldsymbol{u}_{\mathrm{R}}^j(t_n + c_\mu \Delta t)),$$

where ξ^j is the coupling wave strength like in the first order case (2.81). If a suitable quadrature rule is chosen, this procedure yields an approximation to the integral in (2.82) of order k for the boundary flux.

2.3.2 Finite Difference Approximation

The finite volume schemes introduced above are designed to provide high resolution of the solution structure of hyperbolic balance laws. The conservation property and precise capturing of shock and rarefaction effects are to be reproduced by the numerical solution. These features come at the cost of small time steps. To depict that we consider a pipeline of $100\,\mathrm{km}$ length with 200 equal cells of width $\Delta x = 0.5\,\mathrm{km}$. Assuming a typical speed of sound for natural gas of about $s = 300\,\mathrm{m/s}$, CFL number $c \leq 1$ requires time steps $\Delta t \leq 0.6\,\mathrm{s}$. If, for example, the model has to be simulated or optimized over time horizons of a day or even a weak, this requirement implies a very high effort. In this section a simpler discretization strategy is presented based on finite differences, replacing the derivatives in the isothermal Euler equations. The entries of the solution vector $\boldsymbol{U}_i$ are now associated with point evaluations

$$\boldsymbol{U}_i^l \approx \boldsymbol{u}(x_i, t_l) \tag{2.87}$$

corresponding to the time grid $0 = t_0 < t_1 < \cdots < t_M$ and the spatial grid for any pipe $x_0 = 0 < x_1 < \cdots < x_N = L$.

In the publication of Ehrhard and Steinbach [23] the isothermal Euler equation, more precisely the simplification (2.15), is discretized in a comparable context using an implicit

Euler discretization in time, which permits bigger time steps, and one sided finite difference for the spatial derivatives.

In this thesis we use an implicit box scheme proposed by Kolb et al. [45] that yields a similar direct finite difference discretization of the system of isothermal Euler equations using an implicit time step. On the other hand, this scheme also offers properties typical for finite volume scheme. For example, it has been shown that the scheme preserves the conservation property of the balance law (2.33) on the discrete level. For the general balance law (2.31) the scheme reads

$$\frac{\boldsymbol{U}_i^l + \boldsymbol{U}_{i-1}^l}{2} = \frac{\boldsymbol{U}_i^{l-1} + \boldsymbol{U}_{i-1}^{l-1}}{2} - \frac{\Delta t_l}{\Delta x_i} \left(\boldsymbol{f}(\boldsymbol{U}_i^l) - \boldsymbol{f}(\boldsymbol{U}_{i-1}^l) \right) + \Delta t_l \frac{\boldsymbol{s}(\boldsymbol{U}_i^l) + \boldsymbol{s}(\boldsymbol{U}_{i-1}^l)}{2} \qquad (2.88)$$

for any space-time cell $[x_{i-1}, x_i] \times [t_{l-1}, t_l]$ with $\Delta t_l = t_l - t_{l-1}$ and $\Delta x_i = x_i - x_{i-1}$. The scheme can be interpreted based on the integral formulation of the balance law just like the finite volume schemes. Assuming that the state is piecewise constant $\boldsymbol{u}(x,t) = \boldsymbol{u}(x_i, t) =: \boldsymbol{U}_i(t)$ on the shifted cells $x \in [x_i - \frac{1}{2}\Delta x_i, x_i + \frac{1}{2}\Delta x_{i+1}]$, the integral form of the general balance law (2.32) for the test interval $[x_{i-1}, x_i]$ gets

$$\partial_t \frac{\Delta x_i}{2} \left(\boldsymbol{U}_i(t) + \boldsymbol{U}_{i-1}(t) \right) + \boldsymbol{f}(\boldsymbol{U}_i(t)) - \boldsymbol{f}(\boldsymbol{U}_{i-1}(t)) = \frac{\Delta x_i}{2} \left(\boldsymbol{s}(\boldsymbol{U}_i(t)) + \boldsymbol{s}(\boldsymbol{U}_{i-1}(t)) \right). \qquad (2.89)$$

Approximation of the time derivatives by the implicit Euler scheme, i.e. backward finite differences, yields the proposed scheme (2.88). The implicit time discretization implies higher cost for the computation of the new time step but allows to weaken or even drop the upper bound for the time step length implied by the CFL condition. Actually, it has been shown in [45] that the implicit box scheme requires a lower bound on the time step to guarantee that the method is well defined, i.e. that the corresponding system of equations can be uniquely solved for the values at the next time step t_l.

The implicit box scheme applied to the isothermal Euler equations in conservative form (2.6) is then given by

$$\frac{\rho_i^l + \rho_{i-1}^l}{2} = \frac{\rho_i^{l-1} + \rho_{i-1}^{l-1}}{2} - \frac{1}{A}\frac{\Delta t_l}{\Delta x_i}\left(q_i^l - q_{i-1}^l \right), \qquad (2.90)$$

$$\frac{q_i^l + q_{i-1}^l}{2} = \frac{q_i^{l-1} + q_{i-1}^{l-1}}{2} - \frac{1}{A}\frac{\Delta t_l}{\Delta x_i}\left(\left(\frac{q^2}{\rho}\right)_i^l - \left(\frac{q^2}{\rho}\right)_{i-1}^l \right) - A\frac{\Delta t_l}{\Delta x_i}\left(p_i^l - p_{i-1}^l \right)$$

$$- Ags\Delta t_l \frac{\rho_i^l + \rho_{i-1}^l}{2} - \Delta t_l \left(\frac{\phi_i^l}{\rho_i^l} + \frac{\phi_{i-1}^l}{\rho_{i-1}^l} \right), \qquad (2.91)$$

for any space-time cell $[x_{i-1}, x_i] \times [t_{l-1}, t_l]$. We have additionally introduced the abbreviations $\phi_i^l = \phi(q_i^l)$ and $p_i^l = p(\rho_i^l)$ to shorten the notation.

Discretization of other equations

For the finite difference approximation the extension to networks and the other equations modeled in Section 2.1 is more direct. Since the values at the pipe boundaries are explicitly included in the set of unknowns, the coupling relations can be evaluated directly. All quantities not related to pipes can be approximated by one value for each time point defined by the time grid of the PDE discretization because they only depend on time and not on space. We abbreviate the evaluation by

$$\zeta^l \approx \zeta(t_l) \tag{2.92}$$

for all presented quantities. Accordingly, the algebraic relations introduced in Section 2.1 are only considered at the time grid points. This leads to one algebraic relation for each time point and modeling equation. A more detailed summary of the complete model discretized by finite differences is given in Section 4.1 to fix the considered optimization model.

For comparisons and the suitable approximation of integrals, e.g. the operation costs (2.21), we need a reasonable interpretation of the values of the modeling variables between two points of the time grid. Therefor, we take the semidiscretized version of the PDE (2.89) and the associated differential-algebraic system as starting point and deviate the interpretation from the implicit Euler discretization. As commonly accepted for quantities discretized by an implicit Euler scheme, we assume every differential variable, i.e. every variable whose derivative appears in the DAE system, to be piecewise linear on the time subintervals defined by the discretization grid. For this particular model all other variables, sometimes also called algebraic variables in the context of differential-algebraic systems, appear in at least one algebraic equation coupling directly or indirectly the algebraic variable to one of the differential variables. A part of these algebraic relations is nonlinear and a direct interpretation via these couplings is therefore not possible in many cases. Nevertheless, we interpret all algebraic variables to be piecewise linear and use this as a approximation for the intermediate values.

Chapter 3

Optimization Basics and Methods

The search for solutions for optimization problems built on the network model presented in Section 2.1 opens a wide range of areas of investigations although fixing discrete decisions already rules out the wide area of combined continuous and discrete control problems. Clearly at some point of the solution process, a solution or more likely an approximation to the partial differential equations, here the isothermal Euler equations, is required. The level at which the discretization is employed characterizes two approaches for the solution of optimization problems constrained by differential equations.

The *first-optimize* approach uses a function space representation of the model and then investigates the solution in this context. If possible, necessary conditions are stated which are usually not analytically solvable but approximated via discretization techniques. Some basic algorithms for this approach are given in the textbook of Troeltzsch [67]. Herty and Sachers [37] presented an approach for gas networks using a semilinear simplification of the Euler equations, neglecting the advection term in the momentum balance equipped with the ideal gas law.

The other approach, denominated *first-discretize*, as first step replaces all differential equations by finite dimensional discretizations and then employs established algorithms for the finite dimensional problem defined by algebraic relations only. We follow this approach and compute approximate solutions to the original problems using a fully discretized version of the gas network model. In this chapter important theoretical results for this type of nonlinear, restricted, finite dimensional optimization problems are summarized. Finally, we sketch some algorithmic ideas for the numerical solution in Section 3.3. We principally follow the presentation of the textbook of Nocedal and Wright [54]. We refer to this or other textbooks like e.g. [29] for more details and especially for the corresponding proofs which are omitted here.

3.1 Problem Statement and Optimality Conditions

For the theoretical summary we will assume the optimization problem in the following formulation

$$\min_{\boldsymbol{y} \in \mathbb{R}^n} f(\boldsymbol{y}) \quad \text{s.t.} \quad c_i(\boldsymbol{y}) = 0, \quad \forall i \in \mathcal{E}, \tag{3.1a}$$

$$c_i(\boldsymbol{y}) \geq 0, \quad \forall i \in \mathcal{I}, \tag{3.1b}$$

with finite index sets $\mathcal{E}$ and $\mathcal{I}$ denoting equality and inequality constraints, respectively. To shorten the notation, sometimes $\boldsymbol{c}_{\mathcal{E}} = 0$ and $\boldsymbol{c}_{\mathcal{I}} \geq 0$ is used where the "$\geq$" is to be read componentwise. We note that all other types of continuous restrictions like for example simple variable bounds are included or can be equivalently reformulated to this form. All points $\boldsymbol{y} \in \mathbb{R}^n$ satisfying all constraints form the *feasible set*

$$\mathcal{F} = \{\boldsymbol{y} \in \mathbb{R}^n \colon \boldsymbol{c}_{\mathcal{E}}(\boldsymbol{y}) = \boldsymbol{0}, \ \boldsymbol{c}_{\mathcal{I}}(\boldsymbol{y}) \geq \boldsymbol{0}\}. \tag{3.2}$$

We call $\boldsymbol{y}^*$ an *local minimizer* or *local solution* of (3.1) if there exist an open neighborhood $\mathcal{N} \ni \boldsymbol{y}^*$ with

$$f(\boldsymbol{y}^*) \leq f(\boldsymbol{y}), \quad \forall \boldsymbol{y} \in \mathcal{F} \cap \mathcal{N}. \tag{3.3}$$

Accordingly we call $\boldsymbol{y}^*$ an *strict local minimizer* or solution if the inequality (3.3) holds strictly. In the general case it is much more difficult to find *global minimizers*, i.e. feasible points where the inequality (3.3) holds for all $\boldsymbol{y} \in \mathcal{F}$.

A descriptive geometrical necessary condition for a local solution $\boldsymbol{y}^*$ is given by the observation that any feasible step direction must not be a direction of descent. To state this condition in terms of the algebraic relations defining the feasible region, some assumptions are required. First, for the theoretical overview and the numerical algorithms we assume that all model functions are twice continuously differentiable, i.e. f, $\boldsymbol{c}_{\mathcal{E}}$, $\boldsymbol{c}_{\mathcal{I}} \in \mathcal{C}^2$. In addition a so-called *regularity condition* or *constraint qualification* is needed. These ensure that the linearized constraints provide a sufficiently exact description of the feasible directions. To state here the well known *Linear-Independence-Constraint-Qualification* (LICQ), we first need the notion of active constraints:

Definition (Active Set)**.** *A constraint c_i, $i \in \mathcal{E} \cup \mathcal{I}$, is called* active *in $\boldsymbol{y}$ if $c_i(\boldsymbol{y}) = 0$*

The indices of all active constraints in $\boldsymbol{y}$ form the active set *belonging to $\boldsymbol{y}$:*

$$\mathcal{A}(\boldsymbol{y}) = \{j \in \mathcal{E} \cup \mathcal{I} \colon c_j(\boldsymbol{y}) = 0\}$$

Definition (LICQ)**.** *We say that the LICQ holds in a point $\boldsymbol{y}$ if the set of all gradients of constraints active in $\boldsymbol{y}$, $\{\nabla c_j(\boldsymbol{y}) \colon j \in \mathcal{A}(\boldsymbol{y})\}$, is linear independent.*

This is directly equivalent to the Jacobian matrix of active constraints having full row-rank. For an easier statement of the optimality conditions we introduce the *Lagrangian function*

$$\mathcal{L}(\boldsymbol{y}, \boldsymbol{\lambda}) = f(\boldsymbol{y}) - \sum_{i \in \mathcal{E}} \lambda_i c_i - \sum_{i \in \mathcal{I}} \lambda_i c_i \qquad (3.4)$$

As done for the constraints before, we abbreviate by $\boldsymbol{\lambda}_\mathcal{E}$ and $\boldsymbol{\lambda}_\mathcal{I}$ the vectors of *(Lagrange) multipliers* associated with equations and inequalities, respectively. Finally, we have all definitions at hand to state the first-order necessary conditions for optimality for problem (3.1).

Theorem 3.1 (KKT-conditions)**.** *Let a point $\boldsymbol{y}^*$ be a local solution to the minimization problem (3.1) with functions f and c_i, $i \in \mathcal{E} \cup \mathcal{I}$, continuously differentiable. Assume further that the LICQ holds in $\boldsymbol{y}^*$. Then there exist a vector of Lagrange multipliers $\boldsymbol{\lambda}^* \in \mathbb{R}^{|\mathcal{E}| + |\mathcal{I}|}$ satisfying the conditions*

$$\nabla_y \mathcal{L}(\boldsymbol{y}^*, \boldsymbol{\lambda}^*) = 0, \qquad (3.5a)$$

$$\boldsymbol{\lambda}_\mathcal{I}^* \geq 0, \qquad (3.5b)$$

$$\boldsymbol{c}_\mathcal{E}(\boldsymbol{y}^*) = 0, \qquad (3.5c)$$

$$\boldsymbol{c}_\mathcal{I}(\boldsymbol{y}^*) \geq 0, \qquad (3.5d)$$

$$\boldsymbol{\lambda}_i^* c_i(\boldsymbol{y}^*) = 0, \quad \text{for all } i \in \mathcal{I}. \qquad (3.5e)$$

These conditions are also known as *KKT[1]-conditions* and any point $\boldsymbol{y}$ that fulfills them is denominated *KKT-point* or *(KKT-)stationary*. The conditions (3.5a),(3.5b) are usually called dual feasibility or stationarity. The former introduces the concept of dual optimization problems also reflected in the common denomination of the multipliers $\boldsymbol{\lambda}$ as dual variables. We will discuss some aspects of duality later in this chapter. The algebraic description of the (primal) feasible set of the problem description reappears as so-called primal feasibility conditions (3.5c), (3.5d), whereas the *complementarity condition* (3.5e) ensures that only multipliers associated with active constraints may be nonzero. The statement can be proven using weaker constraint qualifications as well. However, the LICQ together with the dual feasibility (3.5a) guarantees uniqueness of the Lagrange multipliers.

Definition (Strict complementarity)**.** *In a primal-dual KKT point $(\boldsymbol{y}, \boldsymbol{\lambda})$ it holds* strict complementarity *if*

$$\lambda_i > 0, \quad \text{for all } i \in \mathcal{I} \cap \mathcal{A}(\boldsymbol{y}).$$

---

[1] honoring their publishers Karush as well as Kuhn and Tucker

In the general case, not every KKT-point is a local minimizer to the NLP. The feasible directions that have to be considered with more attention, are collected as *critical cone* in $(\boldsymbol{y}, \lambda)$.

Definition (Critical cone)**.** *The critical cone in $(\boldsymbol{y}, \lambda)$ is defined as*

$$\mathcal{C}(\boldsymbol{y}, \boldsymbol{\lambda}) = \left\{ d \in \mathbb{R}^n : \begin{array}{l} \nabla c_i^T(\boldsymbol{y})d = 0, \forall i \in \mathcal{E} \cup \{i \in \mathcal{I} : \lambda_i > 0\}, \\ \nabla c_i^T(\boldsymbol{y})d \geq 0, \forall i \in \mathcal{I} \cap \mathcal{A}(\boldsymbol{y}) \end{array} \right\}.$$

Using the dual feasibility conditions we get for the directional derivative

$$\nabla f(\boldsymbol{y})^T \boldsymbol{d} = \sum_{i \in \mathcal{A}(\boldsymbol{y})} \lambda_i \nabla c_i^T(\boldsymbol{y}) \boldsymbol{d} = 0$$

for all $\boldsymbol{d} \in \mathcal{C}$. Thus, these are the linearized feasible direction for which no conclusions about ascent or descend can be made from the first order information.

Proposition 3.2 (Second order conditions)**.** *Let $(\boldsymbol{y}^*, \boldsymbol{\lambda}^*)$ be a primal-dual point satisfying the KKT-conditions* (3.5)*.*

Necessary Condition: *If $\boldsymbol{y}^*$ is a local solution to problem* (3.1) *and LICQ holds in $\boldsymbol{y}^*$, then all $\boldsymbol{d} \in \mathcal{C}(\boldsymbol{y}^*, \boldsymbol{\lambda}^*)$ satisfy*

$$\boldsymbol{d}^T \nabla_{xx}^2 \mathcal{L}(\boldsymbol{y}^*, \boldsymbol{\lambda}^*) \boldsymbol{d} \geq 0.$$

Sufficient Condition: *Assume that for all $\boldsymbol{d} \in \mathcal{C}(\boldsymbol{y}^*, \boldsymbol{\lambda}^*)$ it holds*

$$\boldsymbol{d}^T \nabla_{xx}^2 \mathcal{L}(\boldsymbol{y}^*, \boldsymbol{\lambda}^*) \boldsymbol{d} > 0. \tag{3.6}$$

Then $\boldsymbol{y}^*$ is a strict local minimizer for problem (3.1)*.*

In special cases one can show that the first order conditions (3.5) already characterize global minimizers. We call a problem *convex* if the feasible set $\mathcal{F}$ is a convex set and the objective function f a convex function over $\mathcal{F}$. Thus, a problem as stated in formulation (3.1) is convex if the objective f as well as the inequalities $-c_i$, $i \in \mathcal{I}$, are convex and all equalities c_i, $i \in \mathcal{E}$ are affine functions.

Proposition 3.3 (Convex problems)**.** *Assume the problem* (3.1) *to be convex. Then*

   a) *the set of local solutions is convex,*

   b) *every local solution is already a global solution,*

c) every KKT-point $\boldsymbol{y}^*$, i.e. there is a vector of multipliers $\boldsymbol{\lambda}^*$ such that conditions (3.5) are satisfied, is a global solution.

If additionally the objective f is strictly convex, then the global solution is unique if it exists.

3.2 Lagrangian Duality

To conclude the theoretical base of optimization, in this section we state some well known results on *Lagrangian duality.* These results can be found in almost every textbook on optimization. The following presentation is mainly adapted from [3] and [59].

Interpreting the Lagrangian function (3.4) as function $\mathcal{L} \colon \mathbb{R}^n \times \Lambda \to \mathbb{R}$, with $\Lambda = \mathbb{R}^{|\mathcal{E}|} \times \mathbb{R}_{\geq 0}^{|\mathcal{I}|}$, we can define the basic objects.

Definition (Primal and dual problem). *The primal function $\mathcal{L}_P \colon \mathbb{R}^n \to \bar{\mathbb{R}}$ is defined as*

$$\mathcal{L}_P(\boldsymbol{y}) = \sup_{\boldsymbol{\lambda} \in \Lambda} \mathcal{L}(\boldsymbol{y}, \boldsymbol{\lambda}), \tag{3.7}$$

and the dual function $\mathcal{L}_D \colon \Lambda \to \bar{\mathbb{R}}$ *as*

$$\mathcal{L}_D(\boldsymbol{\lambda}) = \inf_{\boldsymbol{y} \in \mathbb{R}^n} \mathcal{L}(\boldsymbol{y}, \boldsymbol{\lambda}), \tag{3.8}$$

where the functions may take values in the extended real line $\bar{\mathbb{R}} = \mathbb{R} \cup \{\infty\} \cup \{-\infty\}$. The associated primal problem *is defined as*

$$\min_{\boldsymbol{y} \in \mathbb{R}^n} \mathcal{L}_P(\boldsymbol{y}), \tag{3.9}$$

whereas the dual problem *is defined as*

$$\max_{\boldsymbol{\lambda} \in \Lambda} \mathcal{L}_D(\boldsymbol{\lambda}). \tag{3.10}$$

First it has to be noticed that the primal problem (3.9) is equivalent to the original problem (3.1) since from the definition of the primal function it follows immediately

$$\mathcal{L}_P(\boldsymbol{y}) = \begin{cases} \infty, & \boldsymbol{y} \notin \mathcal{F} \\ f(\boldsymbol{y}), & \boldsymbol{y} \in \mathcal{F} \end{cases}.$$

Such a closed form for the dual function can not be derived in the general case. Another basic observation is that the dual function (3.8) is always concave. Hence, all solutions of the dual problem (3.10) are global maximizers.

Next the relations between the original and the dual problem are presented. Without further assumptions it holds the following comparison.

Lemma 3.4 (Weak duality)**.** *For any $\boldsymbol{y} \in \mathcal{F}$ and $\boldsymbol{\lambda} \in \Lambda$ the* weak duality *relation holds:*

$$\mathcal{L}_D(\boldsymbol{\lambda}) \leq f(\boldsymbol{y}). \tag{3.11}$$

The same relation is obviously still correct for solutions $\boldsymbol{y}^*$ of the primal and $\boldsymbol{\lambda}^*$ of the dual problem. The difference $f(\boldsymbol{y}^*) - \mathcal{L}_D(\boldsymbol{\lambda}^*)$ is called the *duality gap*. If there is no duality gap, i.e. the duality gap is zero, it holds *strong duality*. In this case the most useful duality results hold, providing an additional characterization of global optimal solutions to the primal problem.

Proposition 3.5 ([59, Theorem 4.10.])**.** *Assume that there is no duality gap. If $\boldsymbol{\lambda}^* \in \Lambda$ is such that $\mathcal{L}_D(\boldsymbol{\lambda}^*) > -\infty$ then every primal point $\boldsymbol{y}^* \in \mathbb{R}^n$ satisfying*

$$\mathcal{L}(\boldsymbol{y}^*, \boldsymbol{\lambda}^*) = \min_{\boldsymbol{y} \in \mathbb{R}^n} \mathcal{L}(\boldsymbol{y}, \boldsymbol{\lambda}^*),$$

$$\boldsymbol{y}^* \in \mathcal{F},$$

$$\lambda_i^* c_i(\boldsymbol{y}^*) = 0, \quad \text{for all } i \in \mathcal{E} \cup \mathcal{I},$$

is a global solution to the primal problem (3.1).

The conditions clearly implies that $\boldsymbol{\lambda}^*$ is a solution to the dual problem and that in this case we could aim for the primal solution $\boldsymbol{y}^*$ searching for feasible solutions of $\min_{\boldsymbol{y} \in \mathbb{R}^n} \mathcal{L}(\boldsymbol{y}, \boldsymbol{\lambda}^*)$.

It is left to state a situation which guarantees that the duality gap is zero.

Proposition 3.6. *Assume the problem* (3.1) *to be convex. If $\boldsymbol{y}^*$ is a KKT-point satisfying conditions* (3.5) *with multipliers $\boldsymbol{\lambda}^*$, then $\boldsymbol{\lambda}^*$ is a solution to the dual problem* (3.10) *and there is no duality gap.*

Above, we have already stated that $\boldsymbol{y}^*$ is an optimal solution to the primal problem in that case and that all primal solutions where LICQ holds, are also KKT-stationary.

We finish this discussion on duality with some consideration on how to compute derivatives for the dual function. The evaluation of the dual function in general requires to compute a solution $\boldsymbol{y}_{\boldsymbol{\lambda}}$ of the inner problem in the definition of the dual function (3.8). The following result (cf. [3]) shows that the gradient is obtained without extra cost.

Lemma 3.7. *Assume that for every $\boldsymbol{\lambda} \in \mathbb{R}^{|\mathcal{E}|+|\mathcal{I}|}$ the problem $\inf_{\boldsymbol{y} \in \mathbb{R}^n} \mathcal{L}(\boldsymbol{y}, \boldsymbol{\lambda})$ is solved by an unique minimizer $\boldsymbol{y}_{\boldsymbol{\lambda}}$. Then the dual function $\mathcal{L}_D$ is everywhere continuously differentiable with*

$$\boldsymbol{\nabla}\mathcal{L}_D(\boldsymbol{\lambda}) = \boldsymbol{c}(\boldsymbol{y}_{\boldsymbol{\lambda}}), \quad \text{for all } \boldsymbol{\lambda} \in \mathbb{R}^{|\mathcal{E}|+|\mathcal{I}|}.$$

If the problem is convex and its objective in addition strictly convex, then the assumptions of the previous Lemma are satisfied. If the involved functions additionally are, as assumed before, twice continuously differentiable, one can employ the implicit function theorem to compute the Hessian of the dual function

Lemma 3.8. *Let the assumptions of lemma 3.7 hold and assume additionally that the Hessian $\nabla^2_{\boldsymbol{y},\boldsymbol{y}}\mathcal{L}(\boldsymbol{y_\lambda}, \boldsymbol{\lambda})$ is positive definite. Then the second derivative of the dual function is given by*

$$\nabla^2 \mathcal{L}_D(\boldsymbol{\lambda}) = -\nabla\boldsymbol{c}(\boldsymbol{y_\lambda})^T \nabla^2_{\boldsymbol{y},\boldsymbol{y}}\mathcal{L}(\boldsymbol{y_\lambda}, \boldsymbol{\lambda})^{-1} \nabla\boldsymbol{c}(\boldsymbol{y_\lambda}).$$

These results handle all constraints the same way introducing a Lagrange multiplier. Sometimes it is convenient to handle different types of constraints differently. Since we encounter this procedure later in this thesis, we prepare here some of the results for problems of the form

$$\min_{\boldsymbol{y}\in\mathcal{Y}} f(\boldsymbol{y}) \quad \text{s.t.} \quad A\boldsymbol{y} = \boldsymbol{b}. \tag{3.12}$$

We introduce multipliers $\boldsymbol{\lambda}$ for the linear equality constraints and get the corresponding Lagrangian by

$$\bar{\mathcal{L}}(\boldsymbol{y}, \boldsymbol{\lambda}) = f(\boldsymbol{y}) - \boldsymbol{\lambda}^T(A\boldsymbol{y} - \boldsymbol{b}). \tag{3.13}$$

The associated dual function is then defined as

$$\bar{\mathcal{L}}_{\mathrm{D}}(\boldsymbol{\lambda}) = \inf_{\boldsymbol{y}\in\mathcal{Y}} \bar{\mathcal{L}}(\boldsymbol{y}, \boldsymbol{\lambda}). \tag{3.14}$$

For general constraints of the form $\boldsymbol{y} \in \mathcal{Y}$ there also exist necessary conditions as well as constraint qualifications which are both beyond the scope of this thesis. We will assume that the set constraints can be written as solutions to a set of algebraic equations as before

$$\boldsymbol{y} \in \mathcal{Y} \iff \begin{aligned} c_i(\boldsymbol{y}) &= 0, \quad \forall i \in \mathcal{E}, \\ c_i(\boldsymbol{y}) &\geq 0, \quad \forall i \in \mathcal{I}, \end{aligned}$$

and generalize the results of lemmas 3.7 and 3.8 to this case. The Lagrangian function for the inner primal problem of (3.14) is then given by

$$\mathcal{L}(\boldsymbol{y}, \boldsymbol{\lambda}, \boldsymbol{\kappa}) = \bar{\mathcal{L}}(\boldsymbol{y}, \boldsymbol{\lambda}) - \boldsymbol{\kappa}_\mathcal{E}^T \boldsymbol{c}_\mathcal{E}(\boldsymbol{y}) - \boldsymbol{\kappa}_\mathcal{I}^T \boldsymbol{c}_\mathcal{I}(\boldsymbol{y}).$$

We use again favorable assumptions supposing that for any multiplier $\bar{\boldsymbol{\lambda}}$ the inner problem of (3.14) has a unique solution $\boldsymbol{y}^*$. Let the LICQ with respect to the set constraints hold

in $\boldsymbol{y}^*$, assume strict complementarity and the second order sufficient conditions (3.6) to hold. We denote the active constraints by $\boldsymbol{c}_{\mathcal{A}(\boldsymbol{y}^*)}$ and the corresponding multipliers with $\boldsymbol{\kappa}^*$. Note that $\kappa_i^* \neq 0$ for all $i \in \mathcal{A}(\boldsymbol{y}^*)$. Then all constraints that are not active, as well as the corresponding multipliers, can be neglected due to the strict complementarity assumptions. The KKT conditions for the reduced equality constraint problem are

$$\nabla_{\boldsymbol{y}}\mathcal{L}(\boldsymbol{y}^*, \bar{\boldsymbol{\lambda}}, \boldsymbol{\kappa}^*) = \nabla_{\boldsymbol{y}}\bar{\mathcal{L}}(\boldsymbol{y}, \bar{\boldsymbol{\lambda}}) - C^T\boldsymbol{\kappa}^* = 0 \tag{3.15a}$$

$$\boldsymbol{c}_{\mathcal{A}(\boldsymbol{y}^*)}(\boldsymbol{y}^*) = 0, \tag{3.15b}$$

where by $C = \left[\nabla_{\boldsymbol{y}}c_i(\boldsymbol{y}^*)^T \right]_{i \in \mathcal{A}(\boldsymbol{y}^*)}$ we denote the Jacobian matrix of active constraints. Next step is to check if the implicit function theorem can be applied to the system of equations (3.15). Its first derivative w.r.t. $\boldsymbol{y}$ and $\boldsymbol{\kappa}$ in $(\boldsymbol{y}^*, \bar{\boldsymbol{\lambda}}, \boldsymbol{\kappa}^*)$ reads

$$\begin{bmatrix} \nabla_{\boldsymbol{yy}}^2\mathcal{L}(\boldsymbol{y}^*, \bar{\boldsymbol{\lambda}}, \boldsymbol{\kappa}^*) & C(\boldsymbol{y}^*)^T \\ C(\boldsymbol{y}^*) & 0 \end{bmatrix}.$$

The regularity of the derivative follows directly from the LICQ and second order sufficient conditions. Hence, the implicit function theorem can be applied which guarantees the existence of a neighborhood of $\bar{\boldsymbol{\lambda}}$ where $\boldsymbol{y}(\boldsymbol{\lambda})$ and $\boldsymbol{\kappa}(\boldsymbol{\lambda})$ are continuously differentiable functions of $\boldsymbol{\lambda}$ and solutions to (3.15). Note that this neighborhoods have to be possibly restricted to maintain the same active set as for $\boldsymbol{y}(\bar{\boldsymbol{\lambda}})$. Then $\boldsymbol{y}(\boldsymbol{\lambda})$ and $\boldsymbol{\kappa}(\boldsymbol{\lambda})$ are KKT-Points for the inner minimization problem of (3.14).

Using the strict complementarity, the gradient for the dual function can now be computed:

$$\mathcal{L}_{\mathrm{D}}(\bar{\boldsymbol{\lambda}}) = \min_{\boldsymbol{y} \in \mathcal{Y}} \bar{\mathcal{L}}(\boldsymbol{y}, \bar{\boldsymbol{\lambda}}) = \bar{\mathcal{L}}(\boldsymbol{y}^*, \bar{\boldsymbol{\lambda}}) = \mathcal{L}(\boldsymbol{y}^*, \bar{\boldsymbol{\lambda}}, \boldsymbol{\kappa}^*)$$

$$\implies \nabla\mathcal{L}_{\mathrm{D}}(\bar{\boldsymbol{\lambda}}) = \nabla_{\boldsymbol{\lambda}}\boldsymbol{y}^* \underbrace{\nabla_{\boldsymbol{y}}\mathcal{L}(\boldsymbol{y}^*, \bar{\boldsymbol{\lambda}}, \boldsymbol{\kappa}^*)}_{=0} - (A\boldsymbol{y}^* - \boldsymbol{b}) - \nabla_{\boldsymbol{\lambda}}\boldsymbol{\kappa}^* \underbrace{\boldsymbol{c}_{\mathcal{A}(\boldsymbol{y}^*)}(\boldsymbol{y}^*)}_{=0} = \boldsymbol{b} - A\boldsymbol{y}^* \quad (3.16)$$

$$\implies \nabla^2\mathcal{L}_{\mathrm{D}}(\bar{\boldsymbol{\lambda}}) = -\nabla_{\boldsymbol{\lambda}}\boldsymbol{y}^* A^T$$

Thus, to get the Hessian of the dual function, an expression for $\nabla_{\boldsymbol{\lambda}}\boldsymbol{y}^*$ is needed. The fact that for every $\boldsymbol{\lambda}$ in the neighborhood of $\bar{\boldsymbol{\lambda}}$ the parametrized solutions $\boldsymbol{y}(\boldsymbol{\lambda})$ and $\boldsymbol{\kappa}(\boldsymbol{\lambda})$ are KKT-Points with the same active set is exploited:

$$0 = \mathrm{d}_{\boldsymbol{\lambda}}\begin{pmatrix} \nabla_{\boldsymbol{y}}\mathcal{L}(\boldsymbol{y}^*, \bar{\boldsymbol{\lambda}}, \boldsymbol{\kappa}^*) \\ \boldsymbol{c}_{\mathcal{A}(\boldsymbol{y}^*)}(\boldsymbol{y}^*) \end{pmatrix} = \begin{pmatrix} \nabla_{\boldsymbol{\lambda}}\boldsymbol{y}^* \nabla_{\boldsymbol{yy}}^2\mathcal{L}(\boldsymbol{y}^*, \bar{\boldsymbol{\lambda}}, \boldsymbol{\kappa}^*) - A - \nabla_{\boldsymbol{\lambda}}\boldsymbol{\kappa}^* C \\ \nabla_{\boldsymbol{\lambda}}\boldsymbol{y}^* C^T \end{pmatrix}$$

$$\iff \begin{bmatrix} \nabla_{\boldsymbol{yy}}^2\mathcal{L}(\boldsymbol{y}^*, \bar{\boldsymbol{\lambda}}, \boldsymbol{\kappa}^*) & C^T \\ C & 0 \end{bmatrix}\begin{pmatrix} (\nabla_{\boldsymbol{\lambda}}\boldsymbol{y}^*)^T \\ (-\nabla_{\boldsymbol{\lambda}}\boldsymbol{\kappa}^*)^T \end{pmatrix} = \begin{pmatrix} A^T \\ 0 \end{pmatrix}$$

Solution of this linear system by standard Null-Space method gives

$$(\nabla_{\boldsymbol{\lambda}} \boldsymbol{y}^*)^T = Z(Z^T \nabla^2_{\boldsymbol{yy}} \mathcal{L}(\boldsymbol{y}^*, \bar{\boldsymbol{\lambda}}, \boldsymbol{\kappa}^*) Z)^{-1} Z^T A^T$$

and hence

$$\nabla^2 q(\bar{\boldsymbol{\lambda}}) = -AZ(Z^T \nabla^2_{\boldsymbol{yy}} \mathcal{L}(\boldsymbol{y}^*, \bar{\boldsymbol{\lambda}}, \boldsymbol{\kappa}^*) Z)^{-1} Z^T A^T, \tag{3.17}$$

where Z is a matrix whose columns form a basis of $\ker C$. It is clear that $\nabla^2 q(\bar{\boldsymbol{\lambda}}) \leq 0$ since $Z^T \nabla^2_{\boldsymbol{yy}} \mathcal{L}(\boldsymbol{y}^*, \bar{\boldsymbol{\lambda}}, \boldsymbol{\kappa}^*) Z > 0$ because the second order sufficient optimality conditions have been assumed.

3.3 Sketch of Algorithmic Ideas

To conclude this chapter on the basics of nonlinear optimization, a very short review of basic concepts of numerical algorithms for problem (3.1) is given. We concentrate mainly on algorithms for general nonlinear, potentially nonconvex, optimization problems with a smooth objective function and constraints, as assumed before. For an extensive overview of available software and comparisons we refer to the "Decision Tree for Optimization software" [51] that provides information not only about solvers for this problem class. The following paragraphs follow the lines of the textbook [54] again which presents much more details including overviews on existing implementations. Solution techniques for problem (3.1) include *interior-point methods* (IPM) and *sequential quadratic programming* (SQP).

Interior-point methods use an iterative search based on Newton's method for perturbed KKT conditions. General inequalities are reformulated by a vector of slack variables:

$$\min_{\boldsymbol{y} \in \mathbb{R}^n} f(\boldsymbol{y}) \quad \text{s.t.} \quad c_i(\boldsymbol{y}) = 0, \quad \forall i \in \mathcal{E}, \tag{3.18a}$$

$$c_i(\boldsymbol{y}) - s_i = 0, \quad \forall i \in \mathcal{I}, \tag{3.18b}$$

$$s_i \geq 0, \quad \forall i \in \mathcal{I} \tag{3.18c}$$

The search directions are then computed as Newton direction for the nonlinear system of equations given by the KKT conditions (3.5) applied to the *log-barrier* problem:

$$\min_{\boldsymbol{y} \in \mathbb{R}^n} \phi_{\mu}(\boldsymbol{y}) = f(\boldsymbol{y}) + \mu \sum_{i \in \mathcal{I}} \log(s_i) \quad \text{s.t.} \quad c_i(\boldsymbol{y}) = 0, \quad \forall i \in \mathcal{E},$$

$$c_i(\boldsymbol{y}) - s_i = 0, \quad \forall i \in \mathcal{I}$$

This corresponds to a solution of a symmetric linear system with general structure

$$\begin{bmatrix} H & C^T \\ C & -M \end{bmatrix} \begin{pmatrix} \Delta\boldsymbol{y} \\ -\boldsymbol{\lambda} \end{pmatrix} = \begin{pmatrix} \boldsymbol{g} \\ \boldsymbol{h} \end{pmatrix}. \tag{3.19}$$

These systems are often referred to as *KKT-systems* or more generally as saddle-point problems. The matrices H and C are usually approximations or the exact Hessian of the Lagrangian respectively the Jacobian matrix of the constraints. The Matrix M is positive semidefinite and includes the influence of the barrier parameter μ. The system is uniquely solvable if C has full row rank and H is positive definite. Using exact derivatives, this corresponds to the LICQ and the second-order conditions stated above. The update of the iterates has to ensure that these stay in the strict relative interior of the feasible region w.r.t. the slacks, i.e. $s_i > 0$ for $i \in \mathcal{I}$. This procedure is repeated for a sequence of parameters μ that finally converges to zero. If the solutions of the log barrier problems converge for $\mu \searrow 0$, then the limit point satisfies the KKT conditions for the original problem. Using sophisticated update strategies IPMs aim to drive the iterates towards first order stationary points. Popular implementations of interior-point methods include LOQO [68], KNITRO/DIRECT [71], KNITRO/CG [11] as well as the open source code Ipopt [70] and are among the most efficient solvers for nonlinear nonconvex problems.

SQP methods, the other promising approach, are based on the observation that computing a Newton step for the KKT conditions (3.5) for the equality constraint problem, i.e. solving a system of form 3.19 with $M = 0$, is equivalent to the solution of a quadratic problem (QP). This QP arises as minimization of the quadratic approximation of the Lagrangian function subject to the linearized constraints. Generalizing this idea to inequality constrained problems, a SQP method computes new search directions in each iteration as (approximate) solutions to quadratic subproblems of the form

$$\min_{\Delta\boldsymbol{y}} \tfrac{1}{2}\Delta\boldsymbol{y}^T H \Delta\boldsymbol{y} + \boldsymbol{g}^T \Delta\boldsymbol{y} \quad \text{s.t.} \quad C_{\mathcal{E}}\Delta\boldsymbol{y} + \boldsymbol{c}_{\mathcal{E}} = 0,$$

$$C_{\mathcal{I}}\Delta\boldsymbol{y} + \boldsymbol{c}_{\mathcal{I}} \geq 0.$$

SQP methods may differ in terms of the inequality constraints treatment. The inequality constraint problem can be passed to the QP solver directly or, as an alternative, the SQP framework determines an estimate for the current active set, often denominated as *working set* and only passes the corresponding equality constraint problem to a QP solver. Among the most successful implementations of SQP frameworks are SNOPT [31], KNITRO/ACTIVE [10] and CONOPT [20].

Both SQP and IPM frameworks have usually to be complemented by so-called *globalization strategies*. The Newton-type steps are not sufficient for convergence to KKT stationary

points, especially when starting far away from the solution. Such strategies to ensure global convergence, often generalized from unconstrained programming techniques, add additional conditions for the update of the iterate rating if the new step provides an improvement. Whether a step provides sufficient progress, is measured by *penalty or merit functions* as well as by *filter* techniques. All these approaches try to balance the generally competing targets of smaller objective values and smaller infeasibility measures.

As preparation for the following Chapter 5 we also sketch the *Augmented Lagrangian* approach here for problems fitting to the form (3.12). The approach is based on the assumption that the problem is much easier solved without considering the linear constraints $A\boldsymbol{y} = \boldsymbol{b}$. The Augmented Lagrangian iteration then consists of alternating between solving the problem

$$\boldsymbol{y}^+ = \arg\min_{\boldsymbol{y}\in\mathcal{Y}} f(\boldsymbol{y}) - \boldsymbol{\lambda}^T(A\boldsymbol{y} - \boldsymbol{b}) + \frac{\mu}{2}\|A\boldsymbol{y} - \boldsymbol{b}\|_2^2 \tag{3.20}$$

and updating the multiplier estimate according to

$$\boldsymbol{\lambda}^+ = \boldsymbol{\lambda} + \mu(A\boldsymbol{y}^+ - \boldsymbol{b}). \tag{3.21}$$

For more details and more general formulations we refer additionally to the book of Bertsekas [2]. Solver that implement Augmented Lagrangian techniques include MINOS [52] and LANCELOT [16].

If the problem is separable, i.e. has the following special form of constraints

$$\boldsymbol{y} \in \mathcal{Y} \iff (\boldsymbol{y}_1, \boldsymbol{y}_2) \in \mathcal{Y}_1 \times \mathcal{Y}_2$$

and objective $f(\boldsymbol{y}) = f_1(\boldsymbol{y}_1) + f_2(\boldsymbol{y}_2)$, then a slight modification of the Augmented Lagrangian procedure yields the basic *Alternating Direction Method of Multipliers* (ADMM) iteration. In this case, the augmented Lagrangian is given by

$$\mathcal{L}(\boldsymbol{y}_1, \boldsymbol{y}_2, \boldsymbol{\lambda}) = f_1(\boldsymbol{y}_1) + f_2(\boldsymbol{y}_2) - \boldsymbol{\lambda}^T(A_1\boldsymbol{y}_1 + A_2\boldsymbol{y}_2 - \boldsymbol{b}) + \frac{\mu}{2}\|A_1\boldsymbol{y}_1 + A_2\boldsymbol{y}_2 - \boldsymbol{b}\|_2^2.$$

Instead of solving

$$(\boldsymbol{y}_1^+, \boldsymbol{y}_2^+) = \arg\min_{\boldsymbol{y}\in\mathcal{Y}} \mathcal{L}(\boldsymbol{y}_1, \boldsymbol{y}_2, \boldsymbol{\lambda})$$

as it would correspond to an Augmented Lagrangian iteration, the two problems

$$\boldsymbol{y}_1^+ = \arg\min_{\bar{\boldsymbol{y}}_1\in\mathcal{Y}_1} \mathcal{L}(\bar{\boldsymbol{y}}_1, \boldsymbol{y}_2, \boldsymbol{\lambda}),$$
$$\boldsymbol{y}_2^+ = \arg\min_{\bar{\boldsymbol{y}}_2\in\mathcal{Y}_1} \mathcal{L}(\boldsymbol{y}_1^+, \bar{\boldsymbol{y}}_2, \boldsymbol{\lambda})$$

are solved sequentially before the multiplier is updated as before by (3.21). The algorithm alternates between updating the two variable vectors and especially already uses the new result $\boldsymbol{y}_1^+$ for the update of $\boldsymbol{y}_2$. We refer to the survey paper of Boyd et al. [6] for more details on ADMMs and their applications.

Chapter 4

Numerical Results: Gas Pipelines as Storage

This chapter is devoted to numerical results for the optimization of gas transmission networks for the storage of electric energy. Before the numerical results are presented, we state the concrete optimization model such as it will be used for the remainder of this thesis. The principal modeling equations and its discretization with the implicit box scheme have already been explained in Chapter 2 and are summarized in the first section. The second section provides a comparison of the solutions, obtained as optimization results, with a higher order finite volume simulation using an ADER scheme as explained in Section 2.3.1. The finite volume solutions are known to resolve the solution with better accuracy especially in the presence of shock waves. Based on the principal case studies, we compare the solutions to get an indication if for the dynamics on gas transmission pipelines a high resolution approximation is required or if otherwise a coarser discretization covers the principal effect sufficiently well. The third section of this chapter is eventually dedicated to the application of using pipelines as storage as introduced in Section 1.1. The optimal compressor operation to store electric energy in networks is presented for realistic networks. For different scenarios we discuss potential and limitations of this approach.

4.1 Transient Gas Network Optimization

The optimization model is based on the modeling equations stated in Section 2.1 and especially on the implicit box scheme discretization for the isothermal Euler equations posed in Section 2.3.2. We will now state the model using the notation introduced in Chapter 3. Arranging the optimization variables and constraints according to their associated time discretization point and network element, we get an optimization model that preserves these underlying structures. Accordingly, the variable vector is structured globally by the time steps

$$\boldsymbol{y}^T = \begin{pmatrix} \boldsymbol{y}^{1T} & \boldsymbol{y}^{2T} & \dots & \boldsymbol{y}^{MT} \end{pmatrix},\tag{4.1}$$

where the corresponding variable vector for each time point t_l, $l \in \{1, \ldots, M\}$ is composed by variables associated with network elements. By convention, we assume that the model for each node i comprises a variable p_i^l associated with the node pressure while the model for arc $a \in \mathbb{A}$ has variables for (structural) in- and outgoing flow $q_{\text{in},a}^l, q_{\text{out},a}^l$, for each time point $l \in \{1, \ldots, M\}$. The models are first stated for the different edge and arc types and eventually combined in the complete optimization model. We state the constraints only with those variables as function parameters that are required for the presentation. Evaluation of these constraints on the whole variable vector is supposed to include the selection of the corresponding arguments.

Pipe Model

For each pipe $a \in \mathbb{A}_{\text{pi}}$ we have one variable for each evaluation of the modeling unknowns of the Euler equations (2.6) for each point on the discretization time grid and the pipe specific spatial grid $0 = x_{0,a} < \cdots < x_{N,a} = L_a$. As before, we use the abbreviations

$$q_{k,a}^l = q(x_{k,a}, t_l), \quad \rho_{k,a}^l = \rho(x_{k,a}, t_l)$$

for all $l \in \{1, \ldots, M\}$ and $k \in \{0, \ldots, N_a\}$ and additionally introduce the auxiliary variables for pressure and friction terms $p_{k,a}^l$, $\phi_{k,a}^l$. The contribution of pipe $a \in \mathbb{A}_{\text{pi}}$ to the set of variables for time step l is

$$\boldsymbol{y}_a^{l\,T} = \left(q_{0,a}^l, \rho_{0,a}^l, p_{0,a}^l, \phi_{0,a}^l, \ldots, q_{N_a,a}^l, \rho_{N_a,a}^l, p_{N_a,a}^l, \phi_{N_a,a}^l \right). \tag{4.2}$$

To satisfy the convention presented above the flow variables at the boundary are also referred to as $q_{\text{in},a}^l = q_{0,a}^l$ and $q_{\text{out},a}^l = q_{N_a,a}^l$. Choosing the implicit box scheme (2.90), (2.91) for discretization of the Euler equations we get the constraints

$$0 = c_{k,a}^{l,\text{con}} \left(q_{k,a}^l, q_{k-1,a}^l, \rho_{k,a}^l, \rho_{k-1,a}^l, \rho_{k,a}^{l-1}, \rho_{k-1,a}^{l-1} \right)$$

$$= \frac{\rho_{k,a}^l + \rho_{k-1,a}^l}{2} - \frac{\rho_{k,a}^{l-1} + \rho_{k-1,a}^{l-1}}{2} + \frac{1}{A} \frac{\Delta t_l}{\Delta x_k} \left(q_{k,a}^l - q_{k-1,a}^l \right),$$

$$0 = c_{k,a}^{l,\text{mom}} \left(q_{k,a}^l, q_{k-1,a}^l, \rho_{k,a}^l, \rho_{k-1,a}^l, p_{k,a}^l, p_{k-1,a}^l, \phi_{k,a}^l, \phi_{k-1,a}^l q_{k,a}^{l-1}, q_{k-1,a}^{l-1} \right)$$

$$= \frac{q_{k,a}^l + q_{k-1,a}^l}{2} - \frac{q_{k,a}^{l-1} + q_{k-1,a}^{l-1}}{2} + \frac{1}{A} \frac{\Delta t_l}{\Delta x_k} \left(\left(\frac{q^2}{\rho} \right)_{k,a}^l - \left(\frac{q^2}{\rho} \right)_{k-1,a}^l \right)$$

$$+ A \frac{\Delta t_l}{\Delta x_k} \left(p_{k,a}^l - p_{k-1,a}^l \right) + A g s \Delta t_l \frac{\rho_{k,a}^l + \rho_{k-1,a}^l}{2} + \Delta t_l \left(\frac{\phi_{k,a}^l}{\rho_{k,a}^l} + \frac{\phi_{k-1,a}^l}{\rho_{k-1,a}^l} \right),$$

for each time-spatial cell, i.e. for each $l \in \{1, \ldots, M\}$ and $k \in \{1, \ldots, N_a\}$. The introduced auxiliary variables for pressure have to satisfy the constraints

$$0 = c_{k,a}^{l,\mathrm{press}} \left(p_{k,a}^l, \rho_{k,a}^l \right) = p_{k,a}^l - R_{\mathrm{s}} T \rho_{k,a}^l z(p_{k,a}^l, T),$$

for $l \in \{1, \ldots, M\}$ and $k \in \{0, \ldots, N_a\}$. Here T is the given, fixed temperature and the function z one of the three presented choices of compressibility laws, i.e. an ideal gas with $z \equiv 1$, the AGA (2.4) or Papay's equation (2.3). If not stated otherwise, the most exact equation of Papay is used for all computations. The friction variable has to be computed according to the smooth approximation (2.13) for each point $l \in \{1, \ldots, M\}$ and $k \in \{0, \ldots, N_a\}$:

$$0 = c_{k,a}^{l,\mathrm{friction}} \left(\phi_{k,a}^l, q_{k,a}^l \right) = \phi_{k,a}^l - \phi(q_{k,a}^l).$$

Together with additional pressure coupling to head node $j \in \mathbb{V}$ and tail $i \in \mathbb{V}$

$$0 = c_a^{l,\mathrm{p\text{-}cpl,out}}(p_{N_a,a}^l, p_j^l) = p_{N_a,a}^l - p_j^l,$$
$$0 = c_a^{l,\mathrm{p\text{-}cpl,in}}(p_i^l, p_{0,a}^l) = p_{0,a}^l - p_i^l,$$

for each time point $l \in \{1, \ldots, M\}$, the above presented constraints form the set of equality constraints associated to the pipe $a \in \mathbb{A}_{\mathrm{pi}}$ and time point $l \in \{1, \ldots, M\}$. Using the same sorting as for the variables, we get for each time point $l = 1, \ldots, M$:

$$0 = \boldsymbol{c}_a^l \left(p_i^l, \boldsymbol{y}_a^l, p_j^l, \boldsymbol{y}_a^{l-1} \right) = \begin{pmatrix} c_a^{l,\mathrm{p\text{-}cpl,in}}(p_i^l, \boldsymbol{y}_a^l, p_j^l) \\ c_{0,a}^{l,\mathrm{press}}(p_i^l, \boldsymbol{y}_a^l, p_j^l) \\ c_{0,a}^{l,\mathrm{friction}}(p_i^l, \boldsymbol{y}_a^l, p_j^l) \\ c_{1,a}^{l,\mathrm{press}}(p_i^l, \boldsymbol{y}_a^l, p_j^l) \\ c_{1,a}^{l,\mathrm{friction}}(p_i^l, \boldsymbol{y}_a^l, p_j^l) \\ c_{1,a}^{l,\mathrm{con}}(p_i^l, \boldsymbol{y}_a^l, p_j^l, \boldsymbol{y}_a^{l-1}) \\ c_{1,a}^{l,\mathrm{mom}}(p_i^l, \boldsymbol{y}_a^l, p_j^l, \boldsymbol{y}_a^{l-1}) \\ \vdots \\ c_{N_a,a}^{l,\mathrm{press}}(p_i^l, \boldsymbol{y}_a^l, p_j^l) \\ c_{N_a,a}^{l,\mathrm{friction}}(p_i^l, \boldsymbol{y}_a^l, p_j^l) \\ c_{N_a,a}^{l,\mathrm{con}}(p_i^l, \boldsymbol{y}_a^l, p_j^l, \boldsymbol{y}_a^{l-1}) \\ c_{N_a,a}^{l,\mathrm{mom}}(p_i^l, \boldsymbol{y}_a^l, p_j^l, \boldsymbol{y}_a^{l-1}) \\ c_a^{l,\mathrm{p\text{-}cpl,out}}(p_i^l, \boldsymbol{y}_a^l, p_j^l) \end{pmatrix}.$$

Ideal Compressor Model

The modeling equations characterizing an ideal compressor are evaluated at the time points of the PDE discretization. For each active compressor $a \in \mathbb{A}_{\mathrm{cs}}$ and time point $l \in \{1, \dots, M\}$ the associated set of variables is

$$\boldsymbol{y}_a^{l\,T} = \left(q_{\mathrm{in},a}^l, q_{\mathrm{out},a}^l, H_{\mathrm{ad},a}^l, P_a^l \right) \tag{4.3}$$

whereas the set of corresponding constraints (cf. (2.16),(2.18)) is given by

$$0 = \boldsymbol{c}_a^l \left(p_i^l, \boldsymbol{y}_a^l, p_j^l \right) = \begin{pmatrix} c_a^{l,\mathrm{flow}}(q_{\mathrm{in},a}^l, q_{\mathrm{out},a}^l) \\ c_a^{l,\mathrm{ad\text{-}ent}}(H_{\mathrm{ad},a}^l, p_i^l, p_j^l) \\ c_a^{l,\mathrm{power}}(H_{\mathrm{ad},a}^l, P_a^l, q_{\mathrm{out},a}^l) \end{pmatrix} \tag{4.4}$$

$$= \begin{pmatrix} q_{\mathrm{in},a}^l - q_{\mathrm{out},a}^l \\ H_{\mathrm{ad},a}^l - z(p_i^l) T_{\mathrm{in}} R_{\mathrm{s}} \frac{\kappa}{\kappa-1} \left(\left(\frac{p_j^l}{p_i^l} \right)^{\frac{\kappa-1}{\kappa}} - 1 \right) \\ P_a^l - \frac{q_{\mathrm{out},a}^l H_{\mathrm{ad},a}^l}{\eta_{\mathrm{ad},a}} \end{pmatrix}.$$

Here we again denote with p_i^l, p_j^l the pressures at tail node $i \in \mathbb{V}$ and head $j \in \mathbb{V}$. The model for an ideal compressor is completed by simple bounds on flow and power variables

$$q_{\mathrm{in},a}^l, q_{\mathrm{out},a}^l \in [0, q_a^{\max}], \quad P_a^l \in [0, P_a^{\max}].$$

For the more detailed model including the characteristic diagrams more auxiliary variables for compressor and drive as well as the associated constraints have to be included into the set of variables and constraints.

Control Valves Model

Analogously, for each active control valve $a \in \mathbb{A}_{\mathrm{cv}}$ the set of model variables is given by

$$\boldsymbol{y}_a^{l\,T} = \left(q_{\mathrm{in},a}^l, q_{\mathrm{out},a}^l, \Delta p_a^l, \right),$$

for each time point $l \in \{1, \dots, M\}$. Evaluation of the pressure coupling equation (2.22) and mass conservation for every time point gives the set of associated equality constraints

$$0 = \boldsymbol{c}_a^l \left(p_i^l, \boldsymbol{y}_a^l, p_j^l \right) = \begin{pmatrix} c_a^{l,\mathrm{flow}}(q_{\mathrm{in},a}^l, q_{\mathrm{out},a}^l) \\ c_a^{l,\mathrm{press}}(\Delta p_a^l, p_i^l, p_j^l) \end{pmatrix} = \begin{pmatrix} q_{\mathrm{in},a}^l - q_{\mathrm{out},a}^l \\ p_i^l - p_j^l - \Delta p_a^l \end{pmatrix}.$$

In addition, an active control valve is characterized by simple bounds on the pressure drop and the flow direction

$$q_{\text{in},a}^l, q_{\text{out},a}^l \in [0, q_a^{\max}], \quad \Delta p_a^l \in [0, \Delta p_a^{\max}].$$

Short pipe model

The model for short pipes $a \in \mathbb{A}_{\text{sc}}$ has only the minimal set of variables for each time point to satisfy the convention for edges, i.e. one in- and one outflow variable

$$\boldsymbol{y}_a^{l\,T} = \left(q_{\text{in},a}^l, q_{\text{out},a}^l \right),$$

as well as one coupling equation for mass flow and pressure

$$0 = \boldsymbol{c}_a^l \left(p_i^l, \boldsymbol{y}_a^l, p_j^l \right) = \begin{pmatrix} c_a^{l,\text{flow}}(q_{\text{in},a}^l, q_{\text{out},a}^l) \\ c_a^{l,\text{press}}(\Delta p_a^l, p_i^l, p_j^l) \end{pmatrix} = \begin{pmatrix} q_{\text{in},a}^l - q_{\text{out},a}^l \\ p_i^l - p_j^l \end{pmatrix}.$$

The short pipe model is also used to describe compressor stations and control valves in bypass mode.

Node models

For each interior network node $i \in \mathbb{V}_0$ there is one pressure value

$$\boldsymbol{y}_i^l = \left(p_i^l \right)$$

and one evaluation of the mass balance (2.25) without exterior flow

$$0 = \boldsymbol{c}_i^l \left(\boldsymbol{y}_l \right) = \left(c_i^{l,\text{flow-bal}}(\boldsymbol{y}_l) \right) = \sum_{a \in \delta^+} q_{\text{out},a} - \sum_{a \in \delta^-} q_{\text{in},a},$$

for every time point $l \in \{1, \dots, M\}$. The pressure is restricted by simple bounds

$$p_i^l \in [p_i^{\min}, p_i^{\max}],$$

while the pressure equations (2.26) have already been implicitly considered by the choice of the modeling variables and explicitly by the pressure coupling equations for pipes.

For entry or exit node $i \in \mathbb{V}_+ \cup \mathbb{V}_-$ the set of modeling variables is extended by the exterior mass flow

$$\boldsymbol{y}_i^{l\,T} = \left(p_i^l, q_i^{l,\text{ext}} \right).$$

Accordingly, the of mass balance equation is adapted

$$0 = \boldsymbol{c}_i^l\left(\boldsymbol{y}_l\right) = \left(c_i^{l,\text{flow-bal}}(\boldsymbol{y}_l) \right) = q_i^{l,\text{ext}} + \sum_{a \in \delta^+} q_{\text{out},a} - \sum_{a \in \delta^-} q_{\text{in},a},$$

while the simple bounds on the mass flow are distinct for entries $i \in \mathbb{V}_+$

$$q_i^{l,\text{ext}} \geq 0,$$

and exits $i \in \mathbb{V}_-$

$$q_i^{l,\text{ext}} \leq 0.$$

Objective function

In Section 2.3.2 we justified the assumption of piecewise linear compressor powers. According to this interpretation, we approximate the fuel cost integral (2.21) for every compressor station and piecewise constant energy cost functions $e_a(t) = e_a(t_l)$ for $t \in (t_{l-1}, t_l]$ by the trapezoidal rule:

$$f^{\text{cost}}(\boldsymbol{y}) = \sum_{a \in \mathbb{A}_{\text{cs}}} \sum_{l=1}^{M} \frac{\Delta t_l e_a(t_l)}{2} \left(P_a^{l-1} + P_a^l \right). \tag{4.5}$$

Initial and boundary values

Initial values for the mass flow and the density have to be given for each spatial discretization points on the pipes. To make the presentation simpler, we aggregate these in the vector $\boldsymbol{y}^0$ and note that it is not part of the optimization variable vector but has to be considered as externally prescribed parameters. On the other hand, boundary values are explicitly included as additional equality constraints fixing the mass flow or pressure variable of the corresponding boundary vertex.

Operation cost optimization

All the constraints together form the vector of equality constraints

$$\boldsymbol{c}^T(\boldsymbol{y}) = \left(\boldsymbol{c}^1(\boldsymbol{y}^0, \boldsymbol{y}^1)^T \quad \boldsymbol{c}^2(\boldsymbol{y}^1, \boldsymbol{y}^2)^T \quad \dots \quad \boldsymbol{c}^M(\boldsymbol{y}^{M-1}, \boldsymbol{y}^M)^T \right),$$

where

$$\boldsymbol{c}^l(\boldsymbol{y}^{l-1}, \boldsymbol{y}^l) = \left(\boldsymbol{c}_e^l\left(\boldsymbol{y}^{l-1}, \boldsymbol{y}^l \right) \right)_{e \in \mathbb{V} \cup \mathbb{A}}.$$

Only the equations from the discretized isothermal Euler system couple variables associated with consecutive time points while all other constraints only depend on a subset of variables associated to the same time point as the equation.

The complete optimization problem then formally reads

$$\min_{\boldsymbol{y}} f^{\text{cost}}(\boldsymbol{y}) \quad \text{s.t.} \quad \boldsymbol{c}(\boldsymbol{y}) = 0 \tag{4.6a}$$

$$\boldsymbol{y} \in [\boldsymbol{y}^{\min}, \boldsymbol{y}^{\max}] \tag{4.6b}$$

with the simple bounds introduced above. As usual, nonexistent bounds are set to $\pm\infty$ to unify the notation.

Solvers and implementation

The model, in the form stated above, is a standard NLP that can be solved by established solvers. The model has been implemented in C++ and is coupled to the interfaces of the interior-point solvers Ipopt (cf. [70]) and Clean::IPM (cf. [61]). Both solvers are configured to use the sparse linear solver MA57 (cf. [21, 41]) from the HSL Mathematical Software Library [40] for the solution of the primal-dual systems. All optimization solutions given in the remainder of this chapter have been computed with Ipopt in version 3.11 on a single core of a Fujitsu Primergy RX4770 M2 with Intel Xeon e7-8867 v3 CPU @ 2.50 GHz (4 socket x 16 cores x 2 smt) and 512 GB RAM. The operating system is CentOS 7. The C++ code is compiled using g++ of GCC in version 7.1.0. Ipopt is configured using the basic monotone barrier term update strategy. The optimization code has been compiled without any optimization flags.

4.2 Comparison with High Order Finite Volume Simulation

This section is devoted to numerical experiments for a comparison of the two depicted discretization strategies. The ADER schemes are constructed to resolve the dynamics of hyperbolic balance laws also in the presence of shocks. The question is whether these specialized techniques are required for the typical dynamics present in gas transmission networks or if the simpler implicit box scheme leads to similar approximate solutions.

Simulation software and implementation

We compare the optimization solution with simulation results computed with the Matlab code of J. Kall and R. Borsche from TU Kaiserslautern. It implements the ADER solution strategies depicted in Section 2.3.1 in different variants and flavors. Some parts of the code

have been adapted to the present problem for the gas transport. The simulations for the fourth order approximation are computed using the following solver choices for subproblems. The interior interfaces on each edge are handled by the basic ADER solution procedure for generalized Riemann problems where the nonlinear Riemann problems of zeroth order are solved using the approximate Riemann solver EVILIN (cf. [65]). The linear Riemann problems for the higher spatial derivatives in Step 2 are solved exactly using the transformation to the basis of eigenvectors (cf. Section 2.2.1). The fluxes at the boundary are evaluated numerically by the described extension using a numerical quadrature rule with suitable Gauß-Lobatto quadrature nodes. The nonlinear algebraic systems (2.47b) at the coupling junctions for each of these nodes are solved by a Newton method with approximated derivatives. The numerical integration of the rarefaction part of the used 2-Lax curves are computed with the Matlab internal numerical integrator. For more details we once more refer to the dissertation of J. Kall [43] and the references therein.

While the optimization solver can be used to compute an optimal compressor operation under the present conditions, the simulation has to be fed with the control values. The optimization solution provides the optimal control as one value for each time point on the discretization time grid while the simulation requires one control value for every time step of the simulation procedure which result to be much smaller. Following the last paragraph of Section 2.3.2 we assume a piecewise linear control profile. Hence, the control values can be obtained by linear interpolation from the optimization solution.

The simulations have been obtained in single core computations on the same hardware and software setting used for the optimization runs. The used Matlab version is R2016b. Since both codes are not optimized with respect to computation speed, the real computation times do not suffice for a rigorous comparison but give an idea on the different effort for the computations, anyway.

4.2.1 Comparison for Pipeline

The first test case for the optimization solution is the 'OPAL'-pipeline („Ostsee-Pipeline-Anbindungs-Leitung", German for "Baltic Sea Pipeline Link", cf. [55]) which is one of the biggest gas transmission pipelines in Germany. The pipeline which has a length of about 475 km and a diameter of 1.4 m connects the sub sea pipeline for Russian gas with the south and middle European gas transmission pipelines. It starts at the Baltic Sea coast and goes south through eastern Germany where it ends at the Czech boarder. The basic network structure consists of two pipeline segments with an intermediate compressor station at about 2/3 of the pipeline length. A schematic overview and some essential data are given in Figure 4.1. The optimization solution is computed for a constant outflow of $3 \times 10^6 \, \mathrm{m^3/h}$

- Length: $476.2\,\mathrm{km}$
  ($= 285.4\,\mathrm{km} + 190.8\,\mathrm{km}$)

- Diameter $1400\,\mathrm{mm}$.

- Maximal pressure: $100\,\mathrm{bar}$.

- Maximal compressor power $\approx 3 \times 32\,\mathrm{MW}$
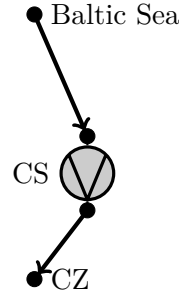
(a) Illustration of OPAL pipeline

Figure 4.1: OPAL: Basic structure of the OPAL network

under normal conditions which corresponds to about 85% of the maximal flow capacity. This mass flow is fixed as boundary value at the exit point at the Czech boarder where additionally a contractual minimal pressure level of $74\,\mathrm{bar}$ is imposed. At the entry a fixed pressure level of the maximal $100\,\mathrm{bar}$ is given. The optimal control is computed for a varying electricity price profile with hourly data for a week in October 2013. In [23] an additional terminal constraint for the optimization problem has been introduced to ensure a reasonable state at the end of the computation horizon. We avoid this by adding six hours with constant energy price to the end of the considered time horizon. As initial state of the network we set a stationary solution that satisfies the boundary values prescribed for the initial time point.

For the spatial discretization a grid length of about $10\,\mathrm{km}$ is chosen. We use smaller cell sizes near the ends of a pipeline anticipating more dynamics in these parts of the pipe. The time step is fixed to $900\,\mathrm{s}$, i.e. the time horizon of seven days and six hours is divided in 696 intervals. The resulting optimization problem has $456\,576$ variables and $455\,184$ equation constraints. Using the stationary solution as starting value, which is feasible in this case, the problem is solved by Ipopt 3.11 with linear solver MA57 as described above in 28 iterations requiring about $350\,\mathrm{s}$. The optimal control for the compressor station and the corresponding pressure profile inside the two pipelines are visualized in Figures 4.2 and 4.4a, respectively. In the compressor power profile there appear some smaller and three major variations from the constant base line of a stationary solution. The pressure profile visualization shows the associated pressure increase in the second pipeline segment that moves with the time towards the exit node. Conversely, sectors with lower pressure appear in the first pipe. In Section 4.3 the optimization solution is examined in more detail from the application's point of view. Here we concentrate on the comparison with the simulation.

The high order simulation procedure is fed with the same boundary values and additionally with the computed optimal power profile for the compressor station. In this case the compressor station indeed couples only two pipelines. Hence, the network model presented
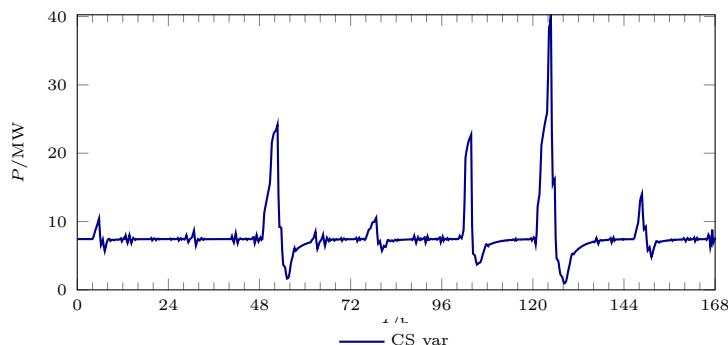
Figure 4.2: OPAL: Control profiles of compressor

in Section 2.2 can be applied directly without modifications. For the first pipeline segment we choose 200 spatial cells with resulting cell width of about 1.4 km. Using a similar cell width for the second pipe we need another 134 cells giving a total of 334 spatial cells. We compute a fourth order approximation using the CFL number $c = 0.8$ which leads to more than 175 000 time steps with 3.5 s average step size. The computation time with `Matlab` on a single core has been almost 2 days.

To compare the solutions, we first concentrate on the boundary values, especially on the not fixed external flow at the entry and the pressure at the exit node. Because the simulation solution is given as cell averages for every time point of the simulation, we have to reconstruct the corresponding boundary values. We choose the same approach that is also included in the simulation procedure. Assuming only outgoing edges from the nodes, this means to find the state that satisfies the coupling conditions and lies on the 2-Lax curve connected to the reconstructed value at the boundary interface. Figures 4.3a and 4.3c illustrate that the results for the boundary flow at the entry and for the pressure level at exit are very close. To get a better impression of the differences, the distances between the two solutions are computed explicitly. Since the discretized solutions correspond to different grids in time, we have to choose a way to transfer the solutions from one grid to the other. For the boundary

Table 4.1: OPAL: Computing statistics

	Optimization	Simulation
average time step size	900 s	3.5 s
# time steps	696	177 449
cell size	≤10 km	≈1.4 km
# spatial cells	105	334
computation time	350 s	47.36 h

(a) Comparison of boundary flows at the entry

(b) Distance of boundary flows at the entry

(c) Comparison of boundary pressures at the exit
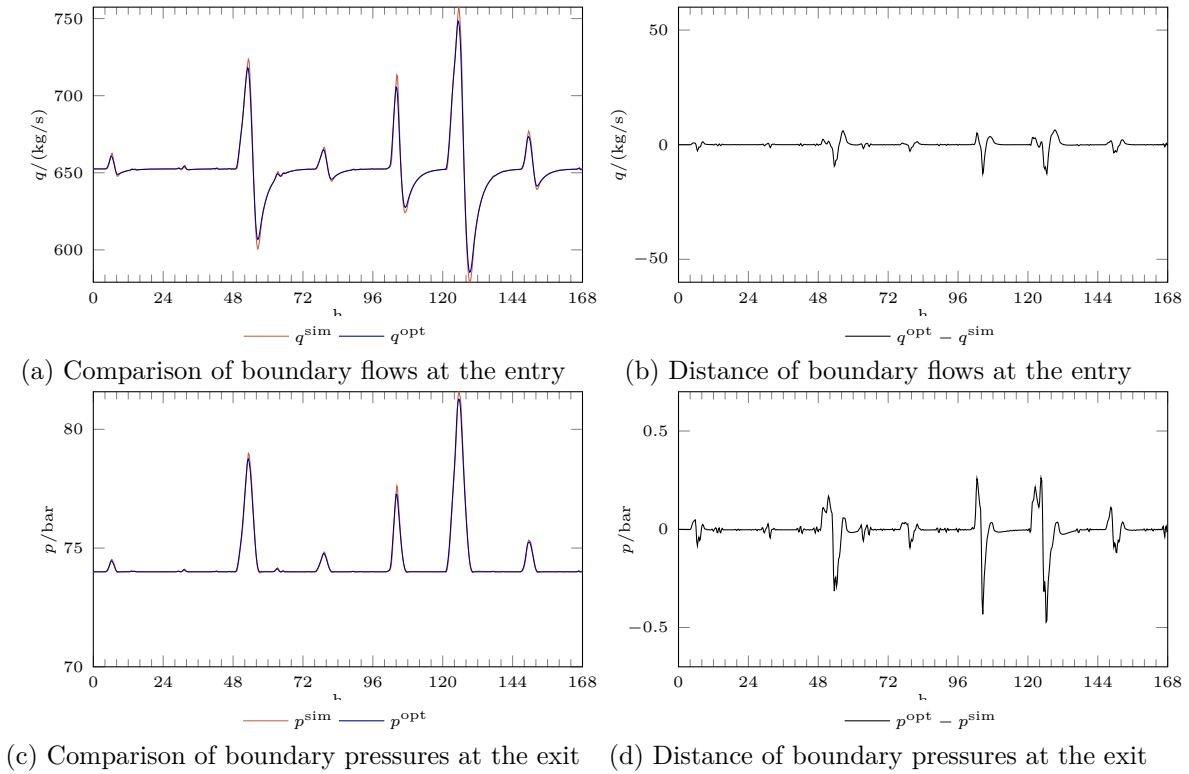
(d) Distance of boundary pressures at the exit

Figure 4.3: OPAL: Comparison of uncontrolled boundary values

values we compare the values of an optimization time point t_{opt} with the simulation data of the last time point t_{sim} of the simulation time grid that is smaller then t_{opt}. This strategy is consistent with the determination of the boundary values, described above.

The Figures 4.3b and 4.3d illustrate the differences of the uncontrolled boundary values obtained by the procedures stated above. The vertical axes of the difference plots are scaled to about 1% of the minimum flow or pressure, respectively, to get an idea of the relative errors as well. Not surprisingly, the distances between the two solutions is larger for time points around the greater variations in the compressor power. All peaks for the pressure at the exit node seem to have a characteristic profile. First there are some time points with higher value of the optimization solution which are followed by some times points with significantly higher value of the simulation. Finally, again there follow some time points with a slightly higher value of the optimization solution. The pressure changes at the exit node are induced by a higher compressor operation. Hence, the increased pressure that is transported through the second pipeline, at the exit is represented as a sharper pressure peak by the simulation solution.

(a) Pressure profile of optimization solution   (b) Pressure profile of simulation
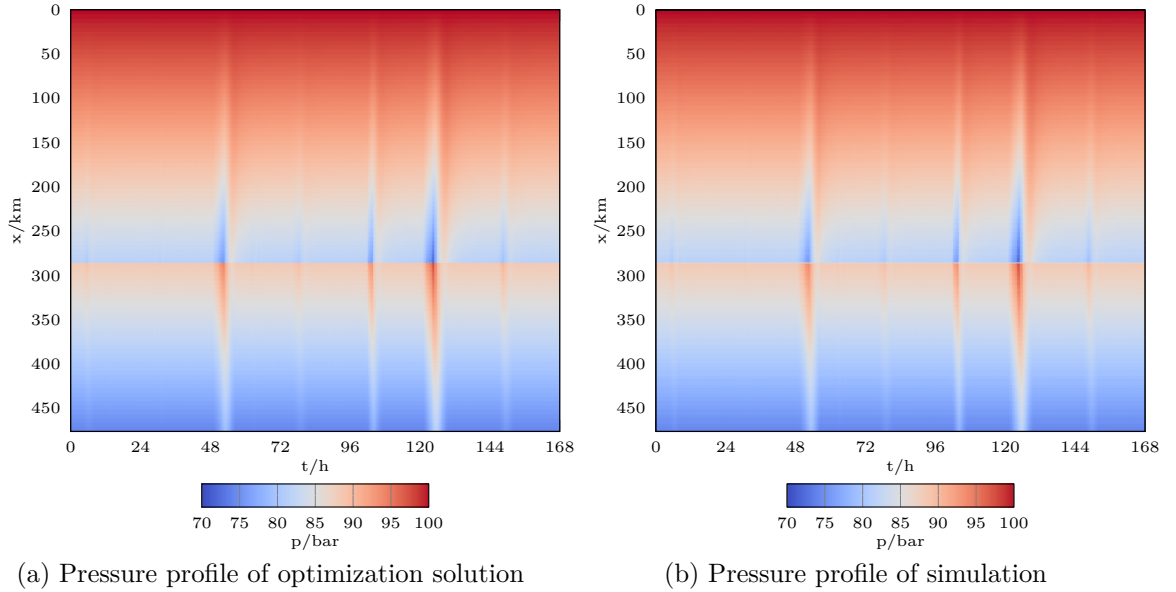
Figure 4.4: OPAL: Pressure profiles

For a comparison of the complete time-spatial profiles we additionally need to map the spatial points. This is done by simply choosing the spatial cell C_j that contains the grid point x_k of the finite difference approximation. The value of the box-scheme approximation at time-space point (t_{opt}, x_k) is then compared with cell average $\boldsymbol{U}_j^{t_{\mathrm{sim}}}$ for the time point t_{sim} of the simulation time grid that has smallest distance to the t_{opt}. The pressure profile of the simulation mapped to the optimization grid is shown in Figure 4.4b. The absolute differences in pressure and flow profiles, mapped as indicated above, are given in Figure 4.5.

Like for the boundary values the biggest differences are observed in the areas of the transported perturbation of the stationary solution due to the increase of the compressor power. Even if their absolute difference is not that small it stays beyond 1% of the actual value. Like for the boundary values the pressure peak is steeper than its representation in the optimization solution. In the pressure profile plots the shortcoming of the grid mapping approach is visible. A regular pattern in space is caused by the different step widths. The used cell average is often commonly associated with the point value at the cell midpoint. Since the coarser discretization grid size is not an integer multiple of the simulation grid size the relative positions of the cell midpoints and the finite difference discretization points vary and result in this particular pattern which could be probably avoided by a more sophisticated comparison procedure. However, the results already show, that the differences are small, even if the solutions show large variations.
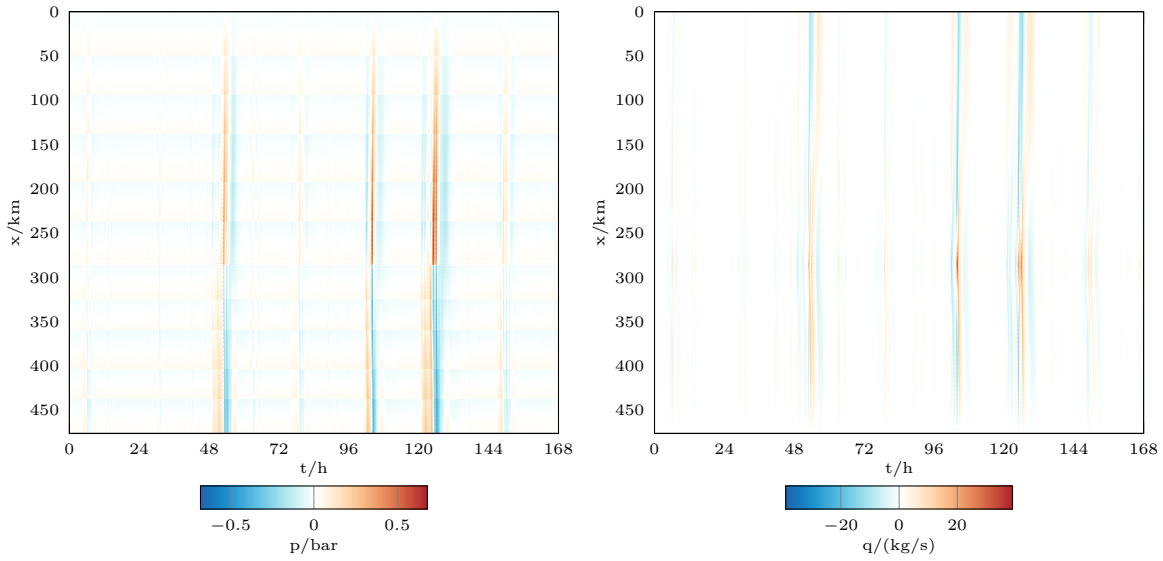
(a) Differences between pressure profiles $p^{\mathrm{opt}} - p^{\mathrm{sim}}$ (b) Differences of flow profiles $q^{\mathrm{opt}} - q^{\mathrm{sim}}$

Figure 4.5: OPAL: Differences for optimization and simulation.

4.2.2 Comparison for Networks

In this section we compare the two discretization approaches for a slightly more complicated gas transmission network that has been used for the illustrations in the article of Ehrhardt and Steinbach [23]. An overview of the structure is given in Figure 4.6 which does not represent correctly the pipe lengths. The network comprises three compressor stations and one control valve as controllable elements. The gas is mainly transported from entry `I1` to the exit node `O3`. At entry node `I2` as well as at exits `O1` and `O2` only much smaller amounts of gas are passed to or taken from the network. The pipe segments have different diameters and lengths in the range of $0.5\,\mathrm{m}$ to $1.1\,\mathrm{m}$ and $50\,\mathrm{km}$ to $120\,\mathrm{km}$, respectively. Constant external flows for entry `I1` and exits `O1`, `O2` are set as boundary values while at the principal exit `O3` a sinusoidal flow profile is prescribed. For the left entry `I2` the optimization problem contains
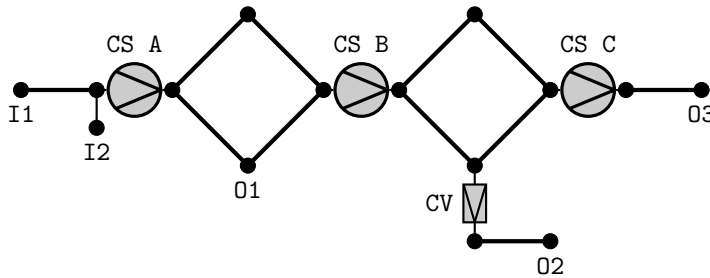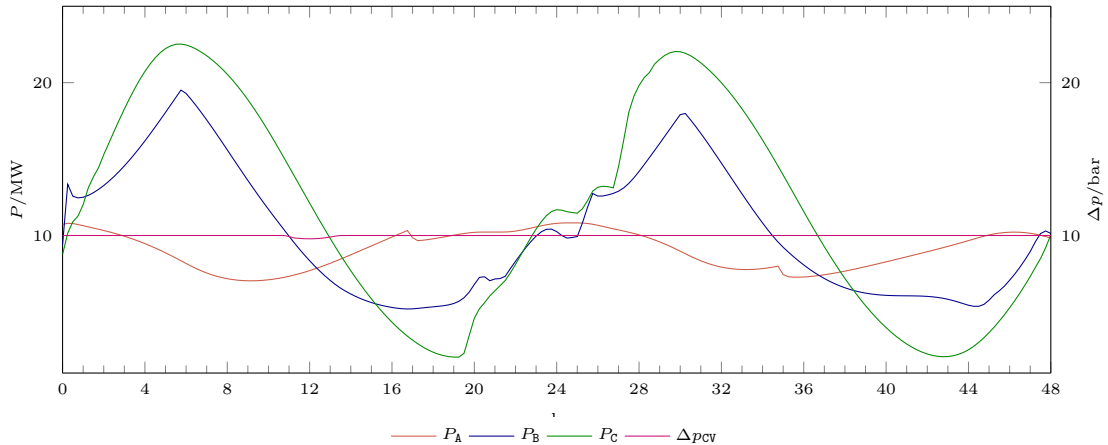

Figure 4.6: Test network

Figure 4.7: Network: Control profiles of active elements

only bounds on pressure and external flow. Again the network is set to be at a stationary state at time $t = 0$ that satisfies all boundary values. We use a constant price profile for the compressor fuel costs and do not consider operation costs for the control valve. Like in the original article the time horizon is chosen as 48 hours which we extend again by another 6 hours with constant outflow to diminish end effects of the optimization solution.

The optimization problem is assembled using the same fixed time step size of 900 s and spatial grid size of about 10 km. This results in a total number of 216 time steps and 218 spatial cells and eventually an optimization problem of 320328 variables and 319248 equality constraints. The solution with the described model implementation and Ipopt as solver requires 61 iterations and around 340 s of run time. As before we used the stationary solution as starting vector, which is not feasible for this problem because of the varying prescribed boundary values. The optimal controls of the compressor stations A– C and the control valve for the minimal operation cost optimization with time constant energy prices are visualized in Figure 4.7. The control valve almost all the time operates at its upper bounds of 10 bar while the compressor powers follow the varying profiles of the main exit O3. The upper bounds for powers are not active for any of the compressors. This result corresponds roughly to the test case a) presented in the article [23].

For the simulation of this network operation we have to extend the already presented node models to cover the nodes of this network. The edge set of the model for finite volume simulations only consists of pipes. As before compressor stations have to be modeled as coupling nodes. We have stated the model for compressor stations in this context only for one in- and one outgoing pipe connected to the compressor. For this network the compressors and the control valve have more than two connected pipes and hence, the present model cannot be applied directly. The new coupling conditions of type (2.47b) are required to

comprise all equations corresponding to the compressor station or control valve as well as its tail and head node. We have to distinguish the edges that are connected to the tail and those connected to the head node. The pipes are therefore enumerated such that the first l of the m coupling pipes are connected to the tail while the last $m - l$ pipes are connected to the head of the compressor station or control valve. The coupling conditions suitable for compressors B and C can then be stated as

$$\Psi^{\mathrm{CS}}(\boldsymbol{u}) = \begin{pmatrix} \sum_{i=1}^{m} q^i \\ p(\rho^2) - p(\rho^1) \\ \vdots \\ p(\rho^l) - p(\rho^1) \\ p(\rho^{l+2}) - p(\rho^{l+1}) \\ \vdots \\ p(\rho^m) - p(\rho^{l+1}) \\ \frac{\sum_{i=l+1}^{m} q^i}{\eta_{\mathrm{ad}}} H_{\mathrm{ad}} \left(p(\rho^{l+1}), p(\rho^1) \right) \end{pmatrix}.$$

Analogously, the coupling for the control valve is extended. The compressor station A has to be treated individually because we have to include the model associated with the entry point I2 to the compressor model, too. This entry node is coupled by a simple short pipe to the compressor entry node and thus has the same pressure value as the input node of compressor A. For the optimization the boundary pressure and external flow at I2 are not fixed. Nevertheless, one of these values has to be included as external control profile to the simulation. For the simulation we fix the pressure at the compressor input because the optimization solution for this node pressure is constant at the upper variable bound. The coupling conditions for the compressor A and its neighboring nodes with that choice are given by

$$\Psi^{\mathrm{CSA}}(\boldsymbol{u}^1, \boldsymbol{u}^2, \boldsymbol{u}^3) = \begin{pmatrix} p(\rho^{I2}) - p(\rho^1) \\ p(\rho^2) - p(\rho^3) \\ \frac{q^2 + q^3}{\eta_{\mathrm{ad}}} H_{\mathrm{ad}} \left(p(\rho^2), p(\rho^{I2}) \right) \end{pmatrix},$$

where $\boldsymbol{u}^1$ corresponds to the ingoing pipe while $\boldsymbol{u}^2, \boldsymbol{u}^3$ are associated with the two outgoing pipes. These additional coupling conditions are implemented as part of the ADER simulation software. As before, these systems have to be solved for each time step and for each quadrature point at every coupling node. A basic Newton method with approximated derivatives is used for the numerical solution of these nonlinear systems. The extended software is then capable to compute solutions for the small test network incorporating the compressor power of the three compressors and the computed pressure drop in the control valve as additional input.

Table 4.2: Network: Computing Statistics

	Optimization	Simulation
average time step size	$900\,\mathrm{s}$	$2.6805\,\mathrm{s}$
# time steps	216	$72\,523$
cell size	$<10\,\mathrm{km}$	$\approx 1\,\mathrm{km}$
# spatial cells	218	920
computation time	$340\,\mathrm{s}$	$53.9\,\mathrm{h}$

For the pipelines we choose a cell width of about $1\,\mathrm{km}$. We use CFL number $c = 0.8$ for the computation of the simulation of approximation order four. This leads to more than $72\,500$ time steps with $2.68\,\mathrm{s}$ average time step size. The computation time with `Matlab` has been greater than 2 days.

The pressure profiles for the boundary nodes with uncontrolled pressure variables are visualized in Figure 4.8. On a first glance the differences between the solution from the optimization model and the simulation are quite small. However, there are some visible differences that should be visualized more clearly. As example, we take a closer look on the pressure profile in exit `O3` and on the also uncontrolled flow profile for the input `I2`. Figures 4.9a and 4.9b show that indeed the boundary pressures have some visible differences but that these stay within a relative distance of 1%. The inflow values for the entry `I2` show slightly bigger differences with up to 2% relative errors. The boundary flow in the simulation solution seems to vary much more and faster than the boundary pressures. In particular, the external flow in `I2` leaves the feasible range for some time points.
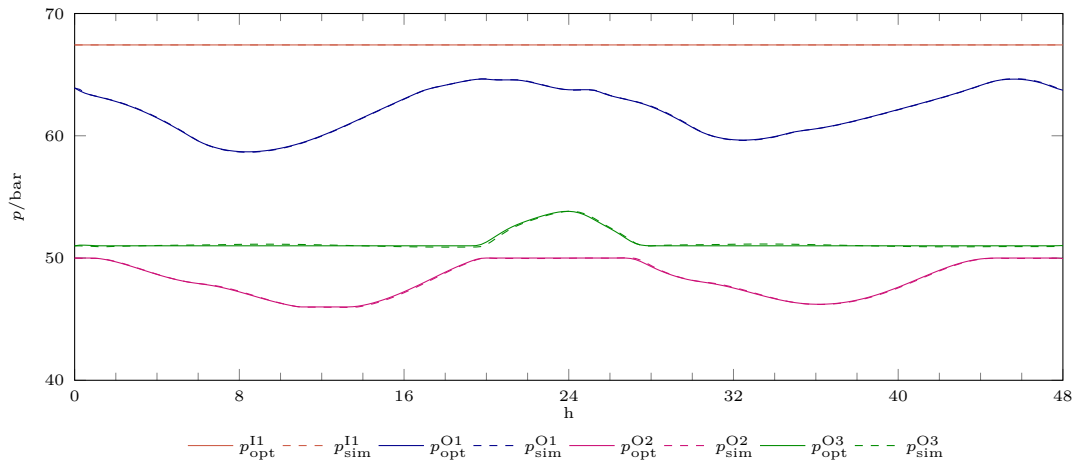

Figure 4.8: Network: Comparison of boundary pressures

(a) Comparison of boundary pressures at exit O3

(b) Distance of boundary pressures at exit O3

(c) Comparison of flow profile at entry I2

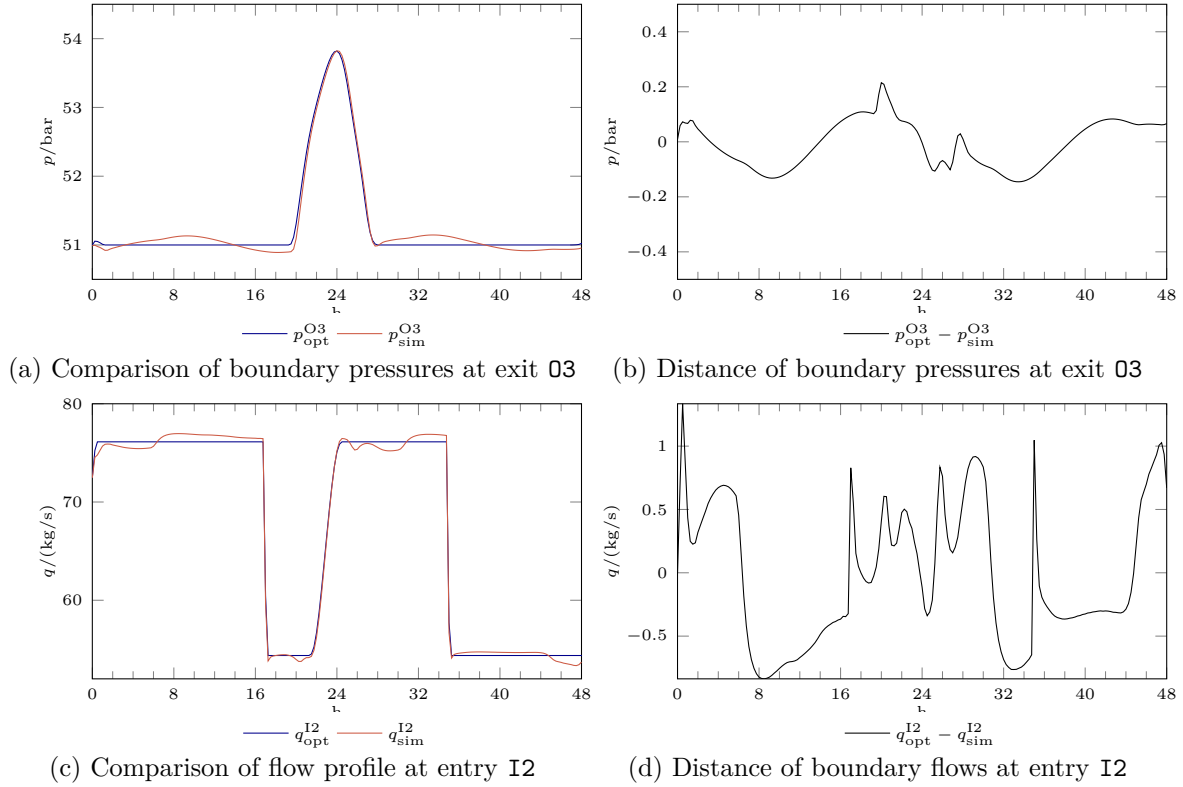(d) Distance of boundary flows at entry I2

Figure 4.9: Network: Comparison of uncontrolled boundary values

A comparison of the other boundary flows is not necessary because these have been included as boundary values to the simulation and are therefore equal (up to the precision of the included nonlinear solver for the couplings). Despite of the visible deviations, the differences between the optimization solution and the fine simulation are remarkably small for this network as well.

4.2.3 Comparison for simplified Euler Equations

As already mentioned before in Section 2.1 the isothermal Euler equations are often further simplified by neglecting the advection term $\partial_x \frac{q^2}{\rho}$. For the usual state of the flow in pipelines it is commonly accepted that this term has a very small contribution to the momentum equation. However, because of this term and the nonlinear pressure function the equation obtains its nonlinear hyperbolic nature.

In this section we compare the optimization solution obtained for this simplified Euler equations with the high order simulation of the full Euler equations. The simplified Euler equations are discretized by the implicit box discretization scheme as applied for the full Euler equations. Hence, we solve almost the model stated in Section 4.1 except the discretized

Table 4.3: OPAL v2: Computing statistics

	Optimization	Simulation
average time step size	$900\,\mathrm{s}$	$3.53\,\mathrm{s}$
# time steps	696	177 452
cell size	$\leq 10\,\mathrm{km}$	$\approx 1.4\,\mathrm{km}$
# spatial cells	105	334
computation time	$360\,\mathrm{s}$	$45.08\,\mathrm{h}$

version of the advection term is missing in the momentum equations. We apply this model on the already introduced OPAL transmission pipeline using the same spatial discretization grid as in the previous section. The model is again assembled for the fixed time step size of $900\,\mathrm{s}$ and finally is made of 456 576 variables and 455 184 equality constraints, which are exactly the same as for the complete momentum equation. However, the system has less nonlinearities which is reflected by the smaller number of nonzero entries in the Hessian matrix of the Lagrangian (376 536 vs. 451 008). The model is solved by Ipopt in 28 iterations using around $350\,\mathrm{s}$.

Because the optimal optimization solution with this simplified version of the Euler equations is slightly different from the basic case, we have to recompute the simulation as well. We use, as before, the boundary values and the computed optimal compressor power profile as input for the simulation. The simulation computes a fourth order approximation with CFL number $c = 0.8$. Using the same spatial discretization again, this yields to more than 177 000 time steps of average size $3.53\,\mathrm{s}$. The Matlab computation requires almost 2 days.

Figure 4.10 shows the uncontrolled boundary profiles and the differences for this simplification. As for the basic case, we can also compare the complete pressure and flow profiles for the complete time and space domain by the depicted mapping. The results are given in Figure 4.11. There are no big differences visible w.r.t. the experiments with the complete model. The differences are again more significant around the areas of the large variation. Just as remarked for the previous test case, the pressure difference for the boundary values again changes its sign showing the above described characteristic profile. This can be interpreted as better resolution of the pressure increase moving through the pipe in the finite volume simulation. The small differences confirm the known hypothesis that the advection term can be neglected without producing a big error as well for this test case. However, there is no great difference in the solution statistics for the optimization neither. Hence, the advantage of using the simplified version is not very big for this test case and the used discretization.

(a) Comparison of boundary flows at the entry

(b) Distance of boundary flows at the entry

(c) Comparison of boundary pressures at the exit

(d) Distance of boundary pressures at the exit
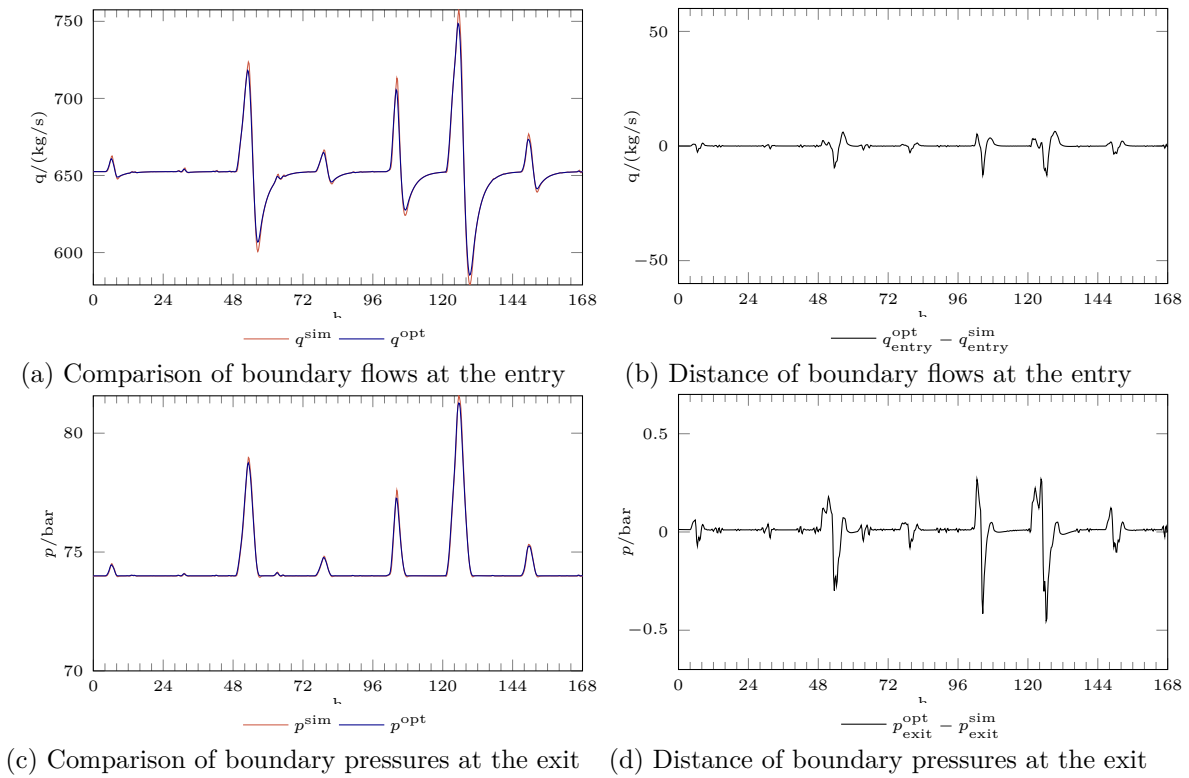
Figure 4.10: OPAL v2: Comparison of uncontrolled boundary values

(a) Differences between pressure profiles $p^{\mathrm{opt}} - p^{\mathrm{sim}}$

(b) Differences between flow profiles $q^{\mathrm{opt}} - q^{\mathrm{sim}}$
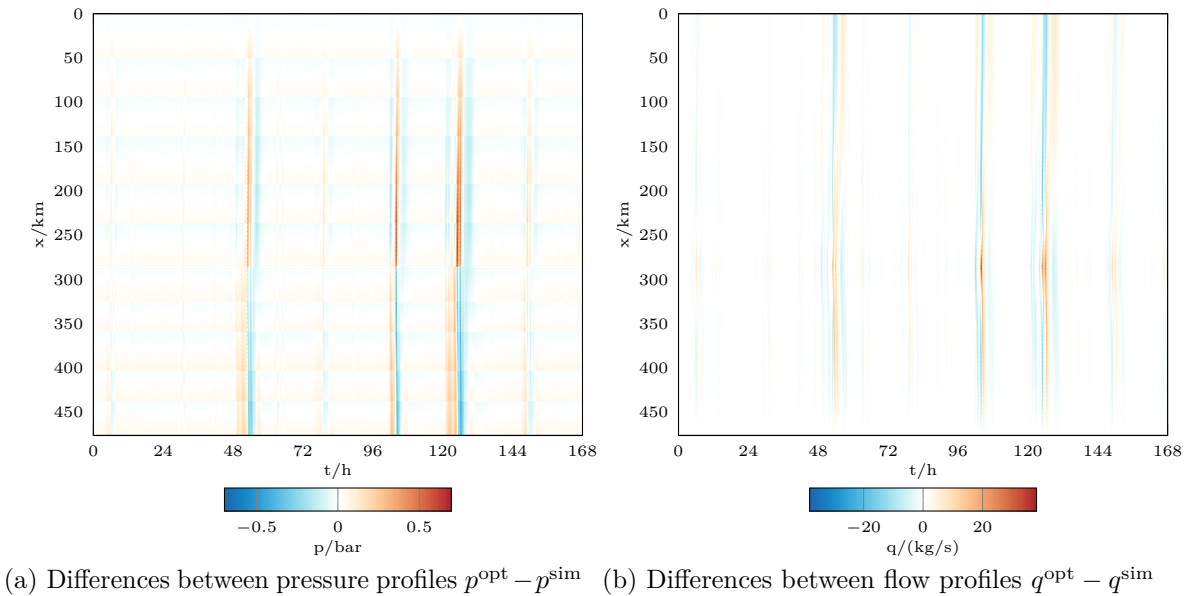
Figure 4.11: Opal v2: Differences for optimization and simulation.

Summary

All three test cases have shown that the finite box scheme is able to resolve the typical dynamics in gas transmission pipelines. Only if there are large variations induced by the compressor operation, there appear visible differences between the two solutions though staying within a 1% margin. The used implicit box scheme can therefore be considered suitable for the present flow regimes in gas transmission pipelines of this type.

For some time points the simulation solution shows the violation of simple variable bounds only included in the optimization model. Even if these violations are not big, they can be problematic for the real implementation. However, this problem is not only related to the used discretization scheme, i.e. the quality of approximation. A solution to an optimization problem will not include any safety margin, except the modeler includes it. Additionally, a numerical algorithm provides solutions that satisfy the constraints up to a selected numerical tolerance. Hence, constraints are possibly violated up to that tolerance if this helps to decrease the objective.

All in all, the extensively higher effort using the finite volume discretization of higher order is not reflected in a significantly higher solution quality for the present cases. The computation times differ by orders of magnitude. Even if the computation times are not comparable and there possibly is a lot of potential to accelerate the simulations, the difference will remain significant. The simulation for the network requires more computation time then the actual time horizon considered by the model. It is important to note here that we compare the computational effort of two different tasks. Whereas the optimization provides an optimal control for the compressor station, the simulation requires the control values to be externally given. Hence, applying optimization methods, that usually require an evaluation of the constraint system repeatedly, to the model assembled using the finite volume discretization, the already excessive effort would be even larger.

The results using the simplified model without the advection term of the isothermal Euler equations give similar results. For the simple setting of two pipelines there also appear only very small differences compared to the finite volume simulation. But since the solution of the corresponding optimization problem is not significantly faster, there is no advantage to use the simplified model for our cases. Hence, we will use the complete optimization model as presented in Section 4.1 for the remainder of this thesis.

4.3 Storage of Electric Energy

In this section we present and discuss results on the "power-to-compression" application introduced initially in Section 1.1. We will inspect the computations of the last section
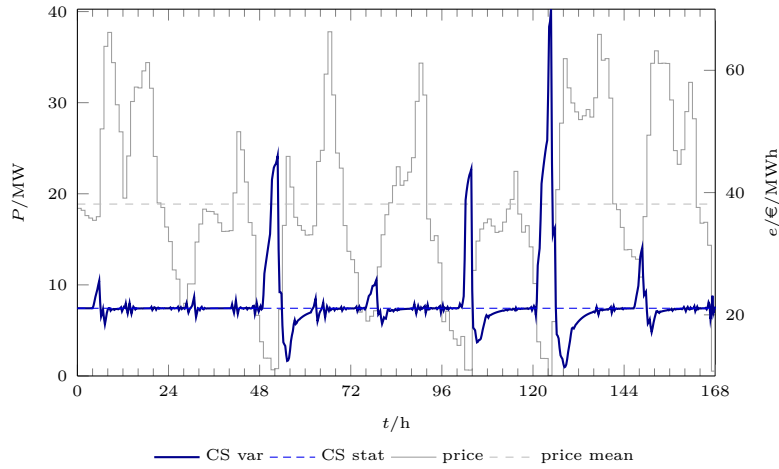
Figure 4.12: OPAL: Control profiles of compressor for varying and constant electricity price

from an application point of view, starting with the previously discussed simple network representing the OPAL pipelines (cf., Figure 4.1, [55]) of two subsequent pipelines and an intermediate compressor station. It has been already stated in Section 1.1 that a strong correlation between the availability of renewable energy in the electricity network and the electricity market price is assumed for the discussions. Therefore, the optimal control for the storage of electric energy in the pipeline is computed as cost optimization problem using the above presented optimization model.

In Figure 4.12, which shows the same compressor control profile as Figure 4.2, it is illustrated how the optimal compressor power profile fits as expected to the varying electricity price profile sketched in the background. For a comparison we also compute the optimal stationary operation of the compressor which is optimal assuming a constant electricity price and represented by a thinner dashed blue line in the graphic. This control profile represents the necessary operation to satisfy the boundary conditions without taking variations of the price into account. There are three to four bigger variations in the compressor power. All these events correspond to some time periods of low energy prices followed by a strong ascent of the price. As expected in the times of lower energy prices the compressor operation is increased significantly from the necessary. During the first period of ascended price the compressor power is below the stationary case. Part of the stored energy is regained in these periods. For this particular price profile of one week the energy consumption is about 107 % of the stationary case but the operation cost are only 96 % compared to the constant operation.

The same computations for other weekly profiles of electric energy market prices are presented in Table 4.4 and show similar results with savings between 0.5 % and 32 %. The results

Table 4.4: OPAL: Results for different price profiles

Profile	Energy/MW h	Energy rel.	Costs/€	Costs stat./€	Costs rel.
1	1388.1	1.073	52 437.0	54 756.0	0.957
2	1337.0	1.034	74 189.0	75 368.0	0.984
3	1297.6	1.003	53 022.0	53 205.0	0.996
4	1693.5	1.309	43 417.0	50 964.0	0.851
5	1308.2	1.011	70 802.0	71 131.0	0.995
6	2058.4	1.592	21 893.0	32 147.0	0.681

for the fourth and especially the sixth price profile show much higher energy consumption and very high savings. These profiles contain periods with even negative market prices. For this optimization model this means that one actually gains money consuming energy by higher compression powers. Hence, the compressor power is at its upper bound during these time periods resulting in these significant savings or better earnings. In contrast, the third profile offers only very small potential for savings which is reflected in the compressor energy consumption that is at almost the same amount as in the stationary case. These test cases only differ in the electricity profile while all other parameters are selected as described before for the first profile. Hence, these results show the different financial benefit from storing electric energy and regaining it by using less compression power afterwards. The present state of the network, that is only fixed by the boundary values, should provide the same capacity for all cases to store electric energy in the pipeline but the results driven by the financial benefit differ a lot.

Considering subsequent pipes

Already for this very simple setting there is a potential saving. However, another view on the pressure profile at the exit node at the Czech border shown in Figure 4.3c gives an indication for further improvement. The pressure plot shows that the increased pressure in the pipe, i.e. the stored energy, to a large extend is transported to the boundary and thus out of the observed pipe segment. This is not too surprising but means that a large part of the stored energy cannot be regained at the same location it has been stored. The effect of an extension of the network and a hypothetical cooperation of two gas transmission operators is addressed by the following example. Of course, the OPAL pipeline does not actually end at the border but is connected to a subsequent pipeline of another 170 km which is operated by a different company and transports the gas through the Czech republic. At its end another compressor station is located which increases the pressure to the level of the subsequent network. The structure of the extended network is sketched in Figure 4.13a. Considering this network,
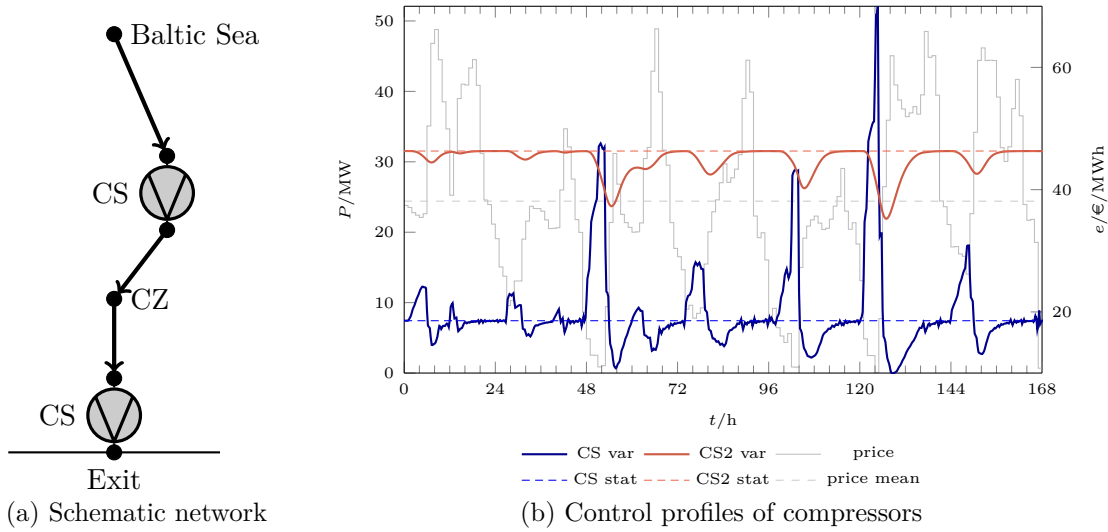
(a) Schematic network

(b) Control profiles of compressors

Figure 4.13: Extended OPAL network

the boundary values at the intermediate point at the Czech boarder are also relaxed. The fixed outflow is now located at the connection point with the subsequent network behind the second compressor station while the lower pressure bound at the border point is kept at 74 bar. To get a comparable effect of this extension, we only include the operation costs of the first compressor station to the objective function.

The resulting optimal compressor controls are visualized in Figure 4.13b. The relaxation of the flow value at the intermediate node at the Czech boarder enables a more efficient operation. The events with higher and following lower compressor operation are of larger time extend and also of bigger amplitude. Additionally, price variations that for the basic case only produced a small change in the compressor operation, like, e.g. the one observed after approximately the 76th hour of the considered time horizon, cause here a significant event. This is reflected by the numbers for the first price profile as well. While the energy consumption is about 114% w.r.t. the stationary case the operation cost is at only 92.5% compared to the costs for the stationary operation.

For this extended view there is another possible benefit considering the second compressor station. In the stationary case this station is required to increase the incoming pressure from less than 60 bar to the assumed 80 bar of the subsequent network. For the varying price profile the higher pressures, induced by the compressor operation, are transported to the second compressor. The power plot shows the resulting periods where the compressor operation in the second station required less power. The second station consumes only 0.96% compared to the energy consumption in the stationary case. This can be interpreted as regaining stored energy, now at the second compressor station. Summing up the energy consumption for the
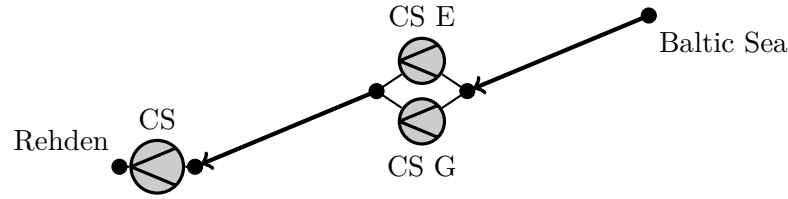
Figure 4.14: NEL pipeline

two stations, the nonconstant operation requires only 99.5 % of the energy consumption in the stationary operation. This is surprising on a first glance since in this case there seems to be no energy loss storing and regaining the energy in terms of pressure. However, this effect can be explained, because the relative pressure loss is lower at higher pressures which provides a third saving effect in this setting.

4.3.1 Parallel Operation of Gas and Electric Drives

The previous example provides an idea of the additional potential using electric driven compressors for gas transmission. We already remarked in Section 1.1 that the majority of the compressors in Germany is driven by gas turbines. Planning a new compressor station, different criteria influence the decision whether to build electric motors or gas turbines as drives. To benefit from the advantages of both choices, it might be reasonable to build a station using electric drives as well as gas turbines. The effects on the optimal control of such a station is illustrated based on a possible extension of the flow through a pipeline in northern Germany. Just like the OPAL pipeline, the here discussed 'NEL' ([53], „Nordeuropäische Erdgas-Leitung", German for "North European Natural Gas Pipeline") starts at the same transfer station at the coast of the Baltic sea in north eastern Germany but then runs westwards through northern Germany. It ends near to one of the biggest gas storage facilities near Rehden, located south of Bremen, where the transported gas is stored or passed to the subsequent transmission network.

   We consider an extension to the real pipeline assuming an additional compressor station after around 200 km. A compressor station had already been planned along the NEL but the process is currently frozen. The network consists of two pipelines of diameter of 1.4 m that are connected by a compressor station. At the end of the NEL a second compressor station increases the pressure of the incoming gas to the pressure level of the subsequent networks. Figure 4.14 shows the coarse structure of the pipeline under investigation. The main purpose of this numerical experiment is to model the possible combination of electric motors and gas turbines as drives in one compressor station. Since again the model of an ideal compressor

(a) Pure market price

(b) Including full taxes and charges
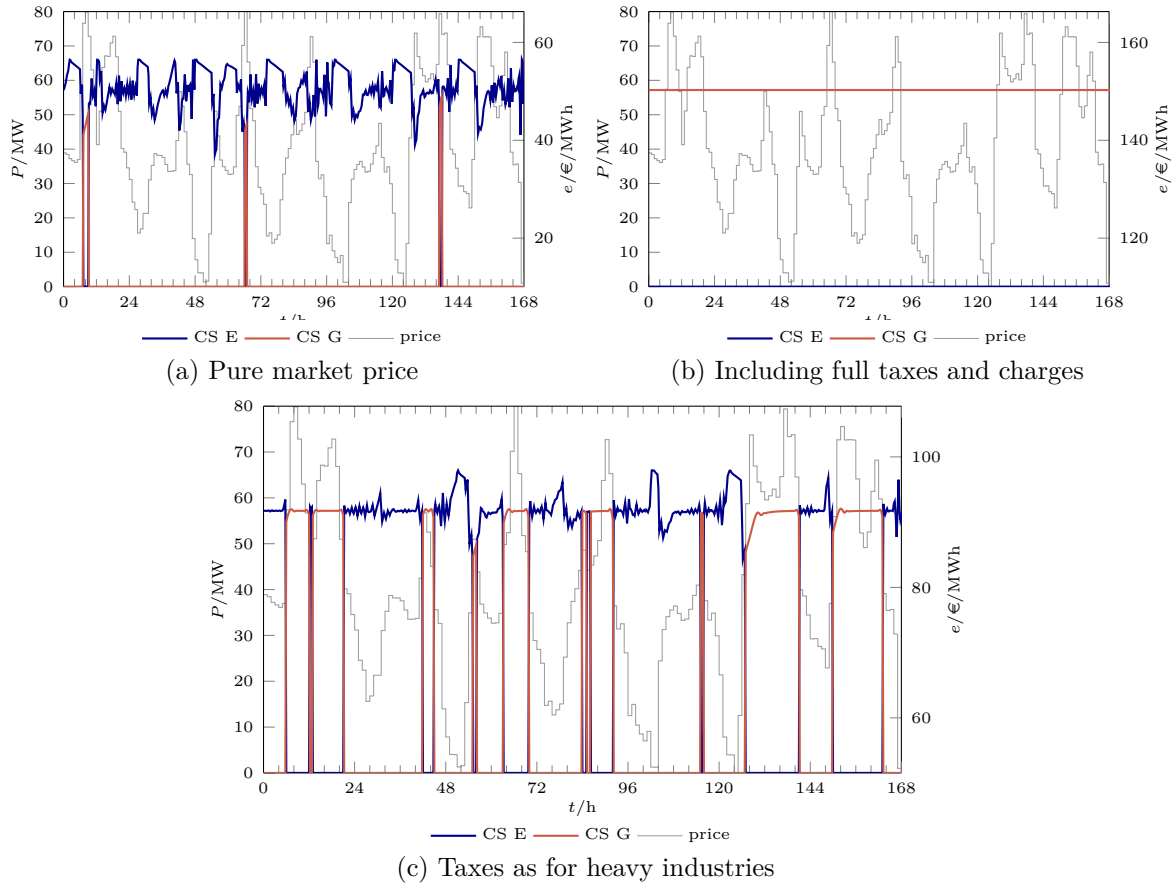

(c) Taxes as for heavy industries

Figure 4.15: NEL: Optimal compressor control

for both stations is used, this can be achieved splitting the central station into two stations arranged in parallel, where one is driven by gas and the other by electricity.

The test scenario assumes a constant gas outflow at the exit point at a minimal pressure level of 80 bar of the subsequent network. The input pressure at the transfer station at the Baltic sea is fixed to the maximum pressure of 100 bar. As energy cost we assume a constant gas price for the gas turbine and use the varying electricity price already discussed for the OPAL test cases for the electric motor. In the previous test cases only the pure electricity market price has been considered. Here we add taxes and network charges to get a more comprehensive comparison of the two drive types. The operation costs of the second station in Rehden are not included in the objective function because this would hide the effects at the central compressor station.

In Figure 4.15 the optimal controls for the central compressor station are visualized for different charge policies applied to the electricity market price. The first subfigure 4.15a is obtained for the pure market price. We can observe that in almost the complete time horizon
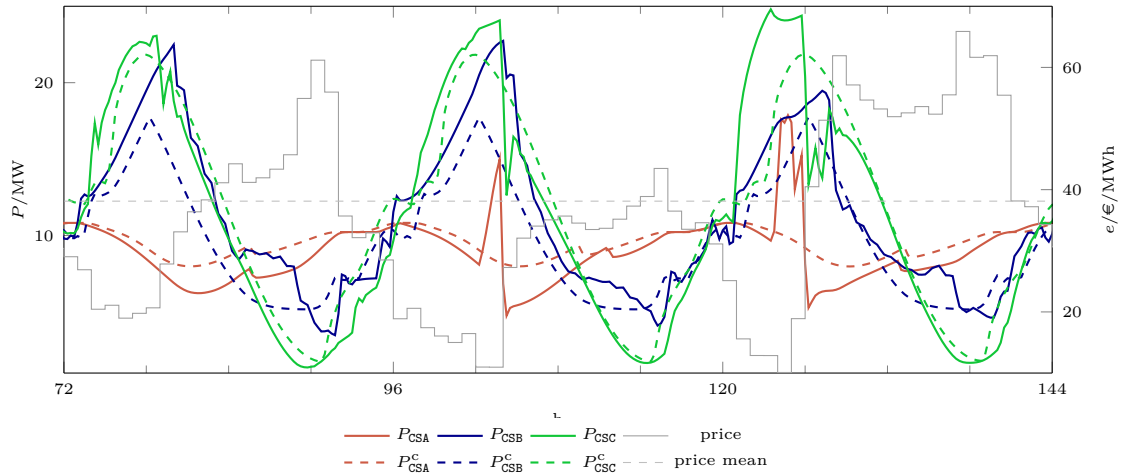
Figure 4.16: Network: Control profiles of compressors

the electric drive is used. Additionally, the load shift we have seen before in the OPAL test case, is visible since the optimal control is anti cyclic w.r.t. the electricity price. The second subfigure 4.15b shows the result for an electricity price containing full taxes and charges like for a private household. In this case the cost for the gas driven compressor is always lower than the varying electricity price and the electric motor is not even used. The third graphic 4.15c visualizes the solution for a market price profile increased by reduced taxes and charges as they are applied to heavy or energy-intensive industries. For this cost profile there are more changes between gas and electricity driven compression. In periods with electricity price peaks the compression power is provided by the gas drive. If the electricity price is very low the used compression energy is higher than for the stationary case followed by a period of lower compression. Here some of the energy is regained. However, in comparison to the solution for the pure market price fewer of these load shifting events can be observed. For all cases there are no time points where the compressor power of both compressors is nonzero. Hence, the results can be interpreted as switching between two compressor or drive types.

4.3.2 Network Test Cases

Finally, we apply the cost optimization to the test network presented for the comparison in Section 4.2.2 using the same electricity price profiles already tested with the OPAL pipeline. The optimal compressor controls for the days 4 to 6 of the first weekly profile and the constant price are plotted in Figure 4.16. The compressor powers show similar profiles as for the constant price case and principally follow the periodical outflow profile but there are also significant differences induced by the variations in the electricity price. As expected in time periods with higher price the compression is lower while in the presence of lower prices the

Table 4.5: Network: Results for single stations

CS	E/MW h	E^{base}/MW h	E/E^{base}	Costs/€	Costs base/€	Costs rel.
A	1548.2	1633.9	0.948	61 875.4	66 343.6	0.933
B	1886.8	1704.5	1.107	70 932.8	66 351.1	1.069
C	2071.3	2070.4	1.000	74 357.4	77 269.3	0.962
Sum	5506.3	5408.8	1.018	207 165.5	209 964.0	0.987

Table 4.6: Network: Results for different price profiles

Profile	Energy/MW h	Energy rel.	Costs/€	Costs base/€	Costs rel.
1	5506.3	1.018	207 165.5	209 964.0	0.987
2	5456.4	1.009	292 276.4	294 538.9	0.992
3	5427.7	1.003	214 384.6	215 347.0	0.996
4	5718.2	1.057	201 643.5	211 799.4	0.952
5	5437.3	1.005	281 367.2	282 995.6	0.994
6	5979.4	1.105	114 443.6	121 768.0	0.940

compression is increased compared to the basic case. The summed results for the single compressor presented in Table 4.5 as well as the visualization show that the compressor operations are adapted in a different way to the varying electricity price. The general load balance between the three stations is changed. The first compressor A is operated at a lower level and its power is increased above the basic level only in time periods of very low prices. While the first station thus only requires 95 % of the energy, the second station B on the other hand is operated on a higher level all the time using about 110 % of the energy used for the basic operation. There are only very few visible adaptions of the power of station B to the variation in the electricity price. Most variations can be observed for station C. Following the profile of the outflow at exit O3, the operation is adapted to the varying price as already known from the OPAL tests. A rapid increase of the price from rather low to high prices is used for a load-shift increasing the pressure in subsequent pipes first to be able to lower the compression in the presence of higher prices. Summing up the results for the three stations the total numbers do not differ much from the basic operation. The computed control requires about 2 % of extra energy which results in the saving of only slightly more than 1 %.

Like for the simple pipeline case, similar computations have been made for different price profiles. The results are shown in Table 4.6. The freedom for additional operation as storage appears to be smaller for this network compared to the simple OPAL pipeline since the potential relative savings for all tested price profiles are lower than for the OPAL tests. This

observation is especially backed by the fact that the two profiles 4 and 6, which showed excessive savings for the OPAL case study, here fit much better with the other price profiles and only results in savings of 5 resp. 6 %.

Summary and outlook

The results of this section provide indications to consider electric drives for compressors in gas transmission networks. The computations even for very simple network configurations have shown that it is possible to use gas pipelines in its normal operation as short term storage for electric energy. But it has also been visible that the potential benefit depends on the present state of operation. For the simple OPAL case an extended view on the subsequent network showed much more potential for storage and saving because this relaxed the constraints for the operation. On the other hand, the network test case is an examples for a gas transmission system whose capacity is almost completely required for the basic operation. For this network and flow scenario a smaller storage potential is visible.

There are different open points left to continue these investigations. To get nearer towards a possible incorporation into the compressor operation the tests have to be done on a better and more detailed data basis. Especially for the compressor stations, better models should be used to validate the obtained results. So far only ideal compressors are considered for the optimization which cannot represent all restrictions to the feasible operation range of compressors. To get reliable data for test cases, has again proved to be a big challenge and obstacle for the related project.

The tests were all executed in terms of operation costs optimization using the electricity prices as indicator for the availability of energy to store. This led to extreme results for energy prices with negative electricity prices as well as to case studies with almost no potential, whose electricity price profiles do not exhibit exploitable variations. The first problem could be fixed using additional constraints for the compressor or network. However, if storage of electricity in gas transmission pipelines is required, then different incentives may be considered and incorporated in the optimization model as alternative indicator for the availability of renewable energy. This possibly requires a more sophisticated coupling of electricity and gas networks than only utilizing electric driven compressors.

The computations so far have shown only the potential for short term storage. Regaining energy at the same compressor station used for storage is only possible in a small time period after storing the energy since the increased pressure has shown to move away from the compressor station. To overcome this problem, we have considered different stations for storage and withdrawal of energy. In this case this would imply cooperation of different compressor operators. Another approach might be to introduce gas storage facilities into the

setting. For example the presented NEL pipeline ends near one of the largest gas storage in Germany. Here the increased pressure, i.e. the stored energy, will not move outside the region where it can be regained. Again on a good data basis computations could investigate on the potential of this approach and show if there exist enough freedom for storage of electric energy additionally to the normal operation of the network.

Embedding economical investigations are required to extend and complement the presented results. The influence of taxes and charges, visible in the NEL test case, is only one example of the strong influence of exterior factors to be included. Regulatory rules on the gas market (see [36] for a comprehensive overview) require the unbundling of functions like transport and storage of gas. These rules are disadvantageous for the operation of gas transmission pipelines in general and for the usage as storage as well. A review of these rules w.r.t. the coupling of gas and electricity networks should therefore be part of further investigations. The results so far can only give new incentives to consider electric drives for compressor stations and ideas to exploit the potential of varying compressor operation in the presence of varying prices and the need for short term storage.

Mathematical supplement to Section 4.3.1

Before closing this chapter on the numerical results, we take another point of view on the results in Section 4.3.1. We point out that although we modeled the central station by two parallel compressors, there is no point of the time horizon for which the two compressors share the compression load. The first point to note here is, that this type of switching is only possible for the ideal compressor model since a closed compressor has to be feasible w.r.t. the set of constraints associated with active compressors. In the following we will show that this complementarity in the operation is a direct consequence of the KKT conditions applied to this model. Hence, it is necessary condition for a local solution for any time point where the actual costs per power value are not equal for the two drive types. Reorganization of the fuel cost objective (4.5) yields

$$f^{\mathrm{cost}}(\boldsymbol{y}) = \sum_{l=1}^{M} \sum_{a \in \mathbb{A}_{\mathrm{cs}}} c_a^l P_a^l,$$

where the coefficients c_a^l comprise the operation cost and the time discretization step size as well. Using this representation, we get for the gradient of the objective function:

$$\partial_i f^{\mathrm{cost}}(\boldsymbol{y}) = \begin{cases} c_a^l, & \text{if } y_i = P_a^l, \\ 0, & \text{else.} \end{cases}$$

The observed complementarity is now shown using selected components of the KKT conditions. The dual feasibility conditions (3.5a) for the derivatives w.r.t. the model variables of the central compressor stations (cf. (4.3),(4.4)) with head j and tail i are:

$$0 = \partial_{q^l_{\text{in,CsE}}} \mathcal{L}(\boldsymbol{y}^*, \boldsymbol{\lambda}^*) = \lambda^{l,\text{flow-bal}}_i - \lambda^{l,\text{flow}}_{\text{CsE}},$$

$$0 = \partial_{q^l_{\text{in,CsG}}} \mathcal{L}(\boldsymbol{y}^*, \boldsymbol{\lambda}^*) = \lambda^{l,\text{flow-bal}}_i - \lambda^{l,\text{flow}}_{\text{CsG}},$$

$$0 = \partial_{q^l_{\text{out,CsE}}} \mathcal{L}(\boldsymbol{y}^*, \boldsymbol{\lambda}^*) = \lambda^{l,\text{flow}}_{\text{CsE}} + \lambda^{l,\text{power}}_{\text{CsE}} \frac{H^l_{\text{ad,CsE}}}{\eta_{\text{ad,CsE}}} - \lambda^{l,\text{flow-bal}}_j,$$

$$0 = \partial_{q^l_{\text{out,CsG}}} \mathcal{L}(\boldsymbol{y}^*, \boldsymbol{\lambda}^*) = \lambda^{l,\text{flow}}_{\text{CsG}} + \lambda^{l,\text{power}}_{\text{CsG}} \frac{H^l_{\text{ad,CsG}}}{\eta_{\text{ad,CsG}}} - \lambda^{l,\text{flow-bal}}_j.$$

Since the increase in adiabatic enthalpy depends only on input and output pressure as variables, it holds $H^l_{\text{ad,CsG}} = H^l_{\text{ad,CsE}}$. Assuming the case $H^l_{\text{ad,CsG}} > 0$ we get from the previous system:

$$\frac{\lambda^{l,\text{power}}_{\text{CsE}}}{\eta_{\text{ad,CsE}}} = \frac{\lambda^{l,\text{power}}_{\text{CsG}}}{\eta_{\text{ad,CsG}}}.$$

Only for simplicity we further assume $\eta_{\text{ad,CsE}} = \eta_{\text{ad,CsG}}$ and obtain

$$\lambda^{l,\text{power}}_{\text{CsE}} = \lambda^{l,\text{power}}_{\text{CsG}} =: \lambda^{l,\text{power}}_{\text{Cs}}.$$

The dual feasibility w.r.t. the power variables in the two compressors is then

$$0 = \partial_{P^l_{\text{CsE}}} \mathcal{L}(\boldsymbol{y}^*, \boldsymbol{\lambda}^*) = c^l_{\text{CsE}} - \lambda^{l,\text{power}}_{\text{Cs}} - (\lambda^{l,\text{low}}_{\text{Pow,Cs}} - \lambda^{l,\text{up}}_{\text{Pow,CsE}}), \tag{4.7}$$

$$0 = \partial_{P^l_{\text{CsG}}} \mathcal{L}(\boldsymbol{y}^*, \boldsymbol{\lambda}^*) = c^l_{\text{CsG}} - \lambda^{l,\text{power}}_{\text{Cs}} - (\lambda^{l,\text{low}}_{\text{Pow,Cs}} - \lambda^{l,\text{up}}_{\text{Pow,CsG}}), \tag{4.8}$$

where the previous results are already included. We assume, for example, that in time point l for the cost coefficients $c^l_{\text{CsE}} < c^l_{\text{CsG}}$ holds and suppose that the power of the gas driven compressor is strictly positive $P^l_{\text{CsG}} > 0$. By complementarity (3.5e), for the multiplier associated with the lower bounds it must hold $\lambda^{l,\text{low}}_{\text{Pow,Cs}} = 0$. We then deduce from condition (4.8) and the nonnegativity condition (3.5b) that

$$c^l_{\text{CsG}} - \lambda^{l,\text{power}}_{\text{Cs}} = -\lambda^{l,\text{up}}_{\text{Pow,CsG}} \leq 0.$$

Insertion in equation (4.7) yields

$$\lambda^{l,\text{low}}_{\text{Pow,CsE}} - \lambda^{l,\text{up}}_{\text{Pow,CsE}} \leq c^l_{\text{CsE}} - c^l_{\text{CsG}} \overset{\text{assump.}}{<} 0.$$

It follows from the KKT condition (3.5b) that the multiplier for the upper bound $\lambda^{l,\text{up}}_{\text{Pow},\text{CsE}}$ must be strictly positive and hence by complementarity that

$$P^{l}_{\text{CsE}} = P^{l,\text{max}}_{\text{CsE}}.$$

In general the optimality conditions show that the more expensive compressor is used only if the cheaper one is at its upper operation bound. Conversely if non of both are at its upper bounds then no combined operation appears if the prices are always distinct. This simple computations show that for this setup the switching between the two compressors can be modeled without explicitly incorporating the discrete decision. However, this is restricted to the case of ideal compressors where the case of no flow through a compressor is feasible. For active compressors described by characteristic diagrams this is usually not the case since real compressor machines have a characteristic minimal throughput and compression ratio.

Chapter 5

Using a Distributed Nonconvex Optimization Method for Gas Networks

The theory in Chapter 3 and the algorithms used for solving the optimization problems as presented in Chapter 4 do not rely on more problem structure than given by the problem formulation (3.1). Structure exploitation is a very important point of departure for the efficient solution of difficult but structured problems. There are numerous examples that can be quite general up to algorithms for complete problem subclasses as linear or quadratic programming as well as fundamental properties of the problem as convexity with consequences as presented before.

We concentrate on a more specific structure that in the gas model case is inherited from the time discretization. In sections 5.1 and 5.2 we present the algorithm ALADIN ("Augmented Lagrangian based Alternating Direction Inexact Newton") proposed by Houska et al. [39] and our experiences applying it to the cost optimization problem on gas transmission pipelines. However, first we have to show that the optimization problem introduced in Section 4.1 can be rewritten in the special form required by the algorithm:

$$\min_{\boldsymbol{x}} \sum_{i=0}^{N} f_i(\boldsymbol{x}_i) \quad \text{s.t.} \quad \sum_{i=0}^{N} A_i \boldsymbol{x}_i = \boldsymbol{b}, \tag{5.1a}$$

$$\left. \begin{aligned} \boldsymbol{h}_i(\boldsymbol{x}_i) &= 0, \\ \boldsymbol{r}_i(\boldsymbol{x}_i) &\in [\boldsymbol{r}_i^{\mathrm{l}}, \boldsymbol{r}_i^{\mathrm{u}}], \\ \boldsymbol{x}_i &\in [\boldsymbol{b}_i^{\mathrm{l}}, \boldsymbol{b}_i^{\mathrm{u}}], \end{aligned} \right\} \quad i \in \{1, \ldots, N\}, \tag{5.1b}$$

For every stage $i \in \{1, \ldots, N\}$ a vector of variables $\boldsymbol{x}_i \in \mathbb{R}^{\tilde{n}_i}$, vectors of equality and range constraints $\boldsymbol{h}_i \in \mathbb{R}^{m_{\mathrm{eq},i}}, \boldsymbol{r}_i \in \mathbb{R}^{m_{\mathrm{r},i}}$ and corresponding ranges $\boldsymbol{r}_i^{\mathrm{l}}, \boldsymbol{r}_i^{\mathrm{u}} \in \mathbb{R}^{m_{\mathrm{r},i}}$ as well as upper and lower bounds $\boldsymbol{b}_i^{\mathrm{l}}, \boldsymbol{b}_i^{\mathrm{u}} \in \mathbb{R}^{\tilde{n}_i}$ are introduced associated to the stage.

We refer to the partial problems associated with one stage as *stage problems* or *local NLPs*

in the remainder of this thesis:

$$\min_{\boldsymbol{x}_i} \quad f(\boldsymbol{x}_i) \tag{5.2a}$$

$$\text{s.t.} \quad \boldsymbol{h}_i(\boldsymbol{x}_i) = 0 \tag{5.2b}$$

$$\boldsymbol{r}_i(\boldsymbol{x}_i) \in [\boldsymbol{r}_i^{\mathrm{l}}, \boldsymbol{r}_i^{\mathrm{u}}] \tag{5.2c}$$

$$\boldsymbol{x}_i \in [\boldsymbol{b}_i^{\mathrm{l}}, \boldsymbol{b}_i^{\mathrm{u}}]. \tag{5.2d}$$

To shorten the notation, we sometimes denote the feasible set of the stage problem with

$$\mathcal{F}_i = \{\boldsymbol{x}_i \in \mathbb{R}^{\tilde{n}_i} : \boldsymbol{h}_i(\boldsymbol{x}_i) = 0, \boldsymbol{r}_i(\boldsymbol{x}_i) \in [\boldsymbol{r}_i^{\mathrm{l}}, \boldsymbol{r}_i^{\mathrm{u}}], \boldsymbol{x}_i \in [\boldsymbol{b}_i^{\mathrm{l}}, \boldsymbol{b}_i^{\mathrm{u}}]\}$$

and its Cartesian product by $\tilde{\mathcal{F}} = \mathcal{F}_1 \times \cdots \times \mathcal{F}_N$.

Time Structure of Optimization Problem

Each variable or constraint of the optimization model for the gas transmission networks has been introduced in Section 4.1 associated with one time point t_l of the discretization grid. Associating each of the M discretization time steps of the used finite differences discretization with one stage, the optimization problem (4.6) can almost be written in the form (5.1). The equations resulting from the discretized Euler equations, are the only constraints coupling two successive time point, i.e. stages. Unfortunately, these equations are nonlinear and therefore do not fit into the form (5.1) which only covers linear coupling between variables of different stages. However, this is not an actual limitation since it can be remediated by a simple reformulation. As introduced in (4.1) the vector $\boldsymbol{y}^l$ contains all model variables associated with time point l of the time grid. For the reformulation, we introduce for any time step $l \in \{1, \ldots, M\}$ a vector of auxiliary variables $\boldsymbol{y}^{l,-} \in \mathbb{R}^{n_l^-}$ containing one component for any entry of $\boldsymbol{y}^{l-1}$ that appears in any of the constraints collected in $\boldsymbol{c}^l$. For our optimization problem (4.6) this means exactly one entry for mass flow and density for every point on the spatial discretization grids of the pipes:

$$\boldsymbol{y}^{l,-} = \left(\boldsymbol{y}_a^{l,-}\right)_{a \in \mathbb{A}_{\mathrm{pi}}} \quad \text{with} \quad \boldsymbol{y}_a^{l,-} = \left(q_{0,a}^{l,-}, \rho_{0,a}^{l,-}, \ldots, q_{N_a,a}^{l,-}, \rho_{N_a,a}^{l,-}\right), \quad \text{for all } a \in \mathbb{A}_{\mathrm{pi}}. \tag{5.3}$$

We extend the variable vector $\boldsymbol{y}^l$ by the auxiliary variables and define the new stage vector $\boldsymbol{x}_l = \left(\boldsymbol{y}^{l,-T}, \boldsymbol{y}^{lT}\right)^T$. The equations $\boldsymbol{c}^l(\boldsymbol{y}^{l-1}, \boldsymbol{y}^l) = 0$ for every $l \in \{1, \ldots, M\}$ are then equivalently replaced by

$$\boldsymbol{c}^l(\boldsymbol{x}_l) = 0,$$

$$\begin{bmatrix} 0 & \hat{I} \end{bmatrix} \boldsymbol{x}_{l-1} + \begin{bmatrix} -I & 0 \end{bmatrix} \boldsymbol{x}_l = 0,$$

where $I \in^{n_l^- \times n_l^-}$ is the identity matrix and $\hat{I} \in^{n_l^- \times n_{l-1}}$ is the matrix with only one entry of value 1 in each row selecting the corresponding representative from the complete vector of the previous time point as described above. With this reformulation the problem has the desired structure (5.1):

$$f_i(\boldsymbol{x}_i) = f_i^{\text{cost}}(\boldsymbol{y}_i) = \sum_{a \in \mathbb{A}_{\text{cs}}} \frac{\Delta t_i e_a(t_i) + \Delta t_{i+1} e_a(t_{i+1})}{2} P_a^i$$

$$\boldsymbol{h}_i(\boldsymbol{x}_i) = \boldsymbol{c}^i(\boldsymbol{x}_i)$$

$$\boldsymbol{b}_i^{\text{l}} = \left(\boldsymbol{y}_i^{\text{low},-T}, \boldsymbol{y}_i^{\text{low}T} \right)^T, \quad \boldsymbol{b}_i^{\text{u}} = \left(\boldsymbol{y}_i^{\text{up},-T}, \boldsymbol{y}_i^{\text{up}T} \right)^T$$

$$A_i = \begin{bmatrix} 0 \\ \vdots \\ 0 \\ -I \quad 0 \\ 0 \quad \hat{I} \\ 0 \\ \vdots \\ 0 \end{bmatrix}, \text{ for all } i = 1, \ldots, M, \qquad \boldsymbol{b} = \begin{pmatrix} 0 \\ \vdots \\ 0 \end{pmatrix}$$

The optimization model used through this thesis has no further range constraints, hence $m_{\text{r},i} = 0$ for all $i = 1, \ldots, M$. To simplify the notation in the remainder of this thesis, we will focus on this reformulated model and therefore use $\boldsymbol{x}_i$ as well as $\boldsymbol{y}_i$ for the complete vector of variables associated to stage i, $i = 1, \ldots, N$.

5.1 ALADIN - An Augmented Lagrangian based Decomposition Method

In this section we present the algorithm ALADIN as it has been introduced by Houska et al. [39] for problems of structure (5.1). Following the lines of original article, we present the algorithm, discuss some of the features and summarize the global convergence proof for the algorithm. More details on the algorithm and its motivation as well as a promising numerical result can be found in the mentioned article [39].

The proposed algorithm is a distributed and parallelizable method that combines ideas from different algorithmic frameworks like SQP and Augmented Lagrangian methods. Additionally, it is inspired by ADMMs and dual decomposition methods (see [6] for a survey). Similar to ADMM, ALADIN uses a primal-dual iterate but tries to extend its idea for nonconvex problems for each stage. The authors motivate the new algorithm by the observation that

for problems where the stage problems (5.2) are only weakly coupled, an unnecessary large number of SQP iterations would be required. Even if for the function evaluations and the solution to the QP subproblems distributed methods are used, every iteration would contain potentially expensive communication points. The abstract statement of the ALADIN algorithm is given in Algorithm 1. This presentation assumes the existence of suitable algorithms for the solution of the augmented stage NLPs and the coupling QP (5.7). We will address our choices later in the upcoming subsection 5.1.2 and comment first on some aspects at the abstract level.

For the primal dual iterate $\boldsymbol{x}, \boldsymbol{\lambda}$ in Step 1 the augmented stage problems (5.4) have to be solved. Because the set of constraints is a subset of the original problem, the problem admits a feasible solution if the original does. Choosing the parameters ρ and the positive definite scaling matrices Σ_i makes it possible to weight the different terms with the original objective. Both augmenting terms are required to ensure global convergence of the algorithm. Their role becomes more obvious from the later presented globalization results.

We denote by $\boldsymbol{\kappa}_i^{\text{eq}}, \boldsymbol{\kappa}_i^{\text{ru}}, \boldsymbol{\kappa}_i^{\text{rl}}, \boldsymbol{\kappa}_i^{\text{bu}}, \boldsymbol{\kappa}_i^{\text{bl}}$ the Lagrange multipliers associated with equality, upper and lower range as well as upper and lower bound constraints, respectively. We assume that all minimizers to the problems (5.4) satisfy the LICQ and inspect the optimality conditions (3.5) first. The Lagrangian for the original problem (5.1) is given by:

$$
\begin{aligned}
\mathcal{L}(\boldsymbol{x}, \boldsymbol{\lambda}, \boldsymbol{\kappa}) = &\sum_{i=0}^{N} f_i(\boldsymbol{x}_i) - \boldsymbol{\lambda}^T (\sum_{i=0}^{N} A_i \boldsymbol{x}_i - \boldsymbol{b}) - \sum_{i=0}^{N} (\boldsymbol{\kappa}_i^{\text{eq}})^T \boldsymbol{h}_i(\boldsymbol{x}_i) \\
&- \sum_{i=0}^{N} (\boldsymbol{\kappa}_i^{\text{rl}})^T (\boldsymbol{r}_i(\boldsymbol{x}_i) - \boldsymbol{r}_i^{\text{l}}) - \sum_{i=0}^{N} (\boldsymbol{\kappa}_i^{\text{ru}})^T (\boldsymbol{r}_i^{\text{u}} - \boldsymbol{r}_i(\boldsymbol{x}_i)) \\
&- \sum_{i=0}^{N} (\boldsymbol{\kappa}_i^{\text{bl}})^T (\boldsymbol{x}_i - \boldsymbol{b}_i^{\text{l}}) - \sum_{i=0}^{N} (\boldsymbol{\kappa}_i^{\text{bu}})^T (\boldsymbol{b}_i^{\text{u}} - \boldsymbol{x}_i).
\end{aligned}
\tag{5.8}
$$

Comparing the corresponding dual feasibility condition (3.5a)

$$
\begin{aligned}
\nabla_{\boldsymbol{x}_i} \mathcal{L}(\boldsymbol{x}, \boldsymbol{\lambda}, \boldsymbol{\kappa}) = &\nabla_{\boldsymbol{x}_i} f_i(\boldsymbol{x}_i) - A_i^T \boldsymbol{\lambda} - \nabla_{\boldsymbol{x}_i} \boldsymbol{h}_i(\boldsymbol{x}_i)^T \boldsymbol{\kappa}_i^{\text{eq}} \\
&- \nabla_{\boldsymbol{x}_i} \boldsymbol{r}_i(\boldsymbol{x}_i)^T (\boldsymbol{\kappa}_i^{\text{rl}} - \boldsymbol{\kappa}_i^{\text{ru}}) - (\boldsymbol{\kappa}_i^{\text{bl}} - \boldsymbol{\kappa}_i^{\text{bu}}),
\end{aligned}
\tag{5.9}
$$

with its counterpart for the augmented decoupled NLPs (5.4)

$$
\begin{aligned}
\mathcal{L}(\boldsymbol{y}_i, \boldsymbol{\kappa}_i) := &f(\boldsymbol{y}_i) - \boldsymbol{\lambda}^T A_i \boldsymbol{y}_i + \frac{\rho}{2} \|\boldsymbol{y}_i - \boldsymbol{x}_i\|_{\Sigma_i}^2 \\
&- (\boldsymbol{\kappa}_i^{\text{eq}})^T \boldsymbol{h}_i(\boldsymbol{y}_i) - (\boldsymbol{\kappa}_i^{\text{rl}})^T (\boldsymbol{r}_i(\boldsymbol{y}_i) - \boldsymbol{r}_i^{\text{l}}) - (\boldsymbol{\kappa}_i^{\text{ru}})^T (\boldsymbol{r}_i^{\text{u}} - \boldsymbol{r}_i(\boldsymbol{y}_i)) \\
&- (\boldsymbol{\kappa}_i^{\text{bl}})^T (\boldsymbol{y}_i - \boldsymbol{b}_i^{\text{l}}) - (\boldsymbol{\kappa}_i^{\text{bu}})^T (\boldsymbol{b}_i^{\text{u}} - \boldsymbol{y}_i),
\end{aligned}
\tag{5.10}
$$

Algorithm 1 ALADIN

Input: Initial guess $\boldsymbol{x}, \boldsymbol{\lambda}$
Repeat:
1: Choose tuning parameter $\rho > 0$ and solve for all $i \in \{1, \ldots, N\}$ the decoupled NLPs

$$\min_{\boldsymbol{y}_i} \quad f_i(\boldsymbol{y}_i) - \boldsymbol{\lambda}^T A_i \boldsymbol{y}_i + \frac{\rho}{2} \|\boldsymbol{y}_i - \boldsymbol{x}_i\|_{\Sigma_i}^2 \tag{5.4a}$$

$$\text{s.t.} \qquad \boldsymbol{h}_i(\boldsymbol{y}_i) = 0, \tag{5.4b}$$

$$\boldsymbol{r}_i(\boldsymbol{y}_i) \in [\boldsymbol{r}_i^{\text{l}}, \boldsymbol{r}_i^{\text{u}}], \tag{5.4c}$$

$$\boldsymbol{y}_i \in [\boldsymbol{b}_i^{\text{l}}, \boldsymbol{b}_i^{\text{u}}], \tag{5.4d}$$

with $\Sigma_i \geq 0$.
2: If $\left\| \sum_{i=0}^{N} A_i \boldsymbol{y}_i - \boldsymbol{b} \right\|_1 \leq \epsilon$ and $\rho\|\Sigma_i(\boldsymbol{y}_i - \boldsymbol{x}_i)\| \leq \epsilon$, terminate with solution $\boldsymbol{x}^* := \boldsymbol{y}$.
3: Choose constraint Jacobian approximations $C_i \approx C_i^*$ of the Jacobians of active constraints and bounds. Compute modified gradient

$$\begin{aligned} \boldsymbol{g}_i := \nabla_{\boldsymbol{y}_i} f_i(\boldsymbol{y}_i) &- (C_i^{\text{eq}^*} - C_i^{\text{eq}})^T \boldsymbol{\kappa}_i^{\text{eq}} \\ &- (C_i^{\text{ar}^*} - C_i^{\text{ar}})^T (\boldsymbol{\kappa}_i^{\text{rl}} - \boldsymbol{\kappa}_i^{\text{ru}}) - (\tilde{I} - C_i^{\text{ab}})(\boldsymbol{\kappa}_i^{\text{bl}} - \boldsymbol{\kappa}_i^{\text{bu}}) \end{aligned} \tag{5.5}$$

and choose symmetric Hessian approximations

$$H_i \approx H_i^* = \nabla_{ii}^2 \left(f_i(\boldsymbol{y}_i) - (\boldsymbol{\kappa}_i^{\text{eq}})^T \boldsymbol{h}_i(\boldsymbol{y}_i) - (\boldsymbol{\kappa}_i^{\text{rl}} - \boldsymbol{\kappa}_i^{\text{ru}})^T \boldsymbol{r}_i(\boldsymbol{y}_i) \right). \tag{5.6}$$

4: Choose tuning parameter $\mu > 0$ and solve the coupled equality constraint QP

$$\begin{aligned} \min_{\Delta \boldsymbol{y}, \boldsymbol{s}} \quad & \sum_{i=0}^{N} \tfrac{1}{2} \Delta \boldsymbol{y}_i^T H_i \Delta \boldsymbol{y}_i + \boldsymbol{g}_i^T \Delta \boldsymbol{y}_i - \boldsymbol{\lambda}^T \boldsymbol{s} + \frac{\mu}{2} \|\boldsymbol{s}\|_2^2 \\ \text{s.t.} \quad & \sum_{i=0}^{N} A_i(\boldsymbol{y}_i + \Delta \boldsymbol{y}_i) = \boldsymbol{b} + \boldsymbol{s}, \\ & C_i \Delta \boldsymbol{y}_i = 0, \quad i \in \{1, \ldots, N\}. \end{aligned} \tag{5.7}$$

5: Choose step sizes $\alpha_1, \alpha_2, \alpha_3 \in \mathbb{R}_+$ with $\alpha_1 + \alpha_2 + \alpha_3 > 0$ and define new iterates

$$\boldsymbol{x}^+ := \boldsymbol{x} + \alpha_1(\boldsymbol{y} - \boldsymbol{x}) + \alpha_2 \Delta \boldsymbol{y},$$
$$\boldsymbol{\lambda}^+ := \boldsymbol{\lambda} + \alpha_3(\boldsymbol{\lambda}_{\text{QP}} - \boldsymbol{\lambda})$$

6: Update iterates $\boldsymbol{x} \leftarrow \boldsymbol{x}^*, \boldsymbol{\lambda} \leftarrow \boldsymbol{\lambda}^+$ and continue with Step 1.

$$0 \stackrel{!}{=} \nabla_{\boldsymbol{y}_i} \mathcal{L}(\boldsymbol{y}_i, \boldsymbol{\kappa}) = \nabla_{\boldsymbol{y}_i} f_i(\boldsymbol{y}_i) - A_i^T \boldsymbol{\lambda} + \rho \Sigma (\boldsymbol{y}_i - \boldsymbol{x}_i) - \nabla_{\boldsymbol{y}_i} \boldsymbol{h}_i(\boldsymbol{y}_i)^T \boldsymbol{\kappa}_i^{\mathrm{eq}}$$
$$- \nabla_{\boldsymbol{y}_i} \boldsymbol{r}_i(\boldsymbol{y}_i)^T (\boldsymbol{\kappa}_i^{\mathrm{rl}} - \boldsymbol{\kappa}_i^{\mathrm{ru}}) - (\boldsymbol{\kappa}_i^{\mathrm{bl}} - \boldsymbol{\kappa}_i^{\mathrm{bu}}), \tag{5.11}$$

the termination criterion of Step 2 is explained. If the composition $\boldsymbol{y}$ solves the augmented stage problems, then it satisfies the dual feasibility condition for the original problem up to the term $\rho \Sigma_i (\boldsymbol{y}_i - \boldsymbol{x}_i)$. Clearly, the NLP solutions are feasible w.r.t. the stage constraints $\boldsymbol{y}_i \in \mathcal{F}_i$, for all stages $i = 1, \ldots, N$. For primal feasibility, considering the complete set of constraints, therefore only the coupling conditions $\sum_{i=0}^{N} A_i \boldsymbol{y}_i - \boldsymbol{b}$ are left to check. Hence, the conditions in Step 2 check if the solutions to the decoupled stage problems are primal and dual feasible and thus a solution candidate for the complete problem (5.1). If both infeasibilities, measured in the 1-norm, are sufficiently small, i.e. smaller than the chosen tolerance ϵ, the current vector of solutions to the stage problems is returned as solution.

If the NLP solutions do not suffice these conditions, a quadratic problem is assembled and solved to compute a primal dual update for the iterates. The quadratic subproblem (5.7) uses a positive definite approximation on the Hessian of the Lagrangian evaluated in $\boldsymbol{y}$ and is only equality constraint. It incorporates explicitly an approximation to the linearized active NLP constraints and the stage coupling conditions by an Augmented Lagrangian relaxation. Like for inexact SQP methods the approximated Jacobian matrices to the active NLP constraints are compensated by the modified gradient (5.5).

Eventually, the iterates are updated using a globalization strategy presented in the next section. For the primal update a combination of the two steps computed from the solution of the decoupled stage problems and the coupling quadratic problem are considered. The dual iterate is usually updated with a step computed from the Lagrange multiplier $\boldsymbol{\lambda}_{\mathrm{QP}}$, associated with the relaxed coupling constraints of the QP.

From one point of view, Algorithm 1 can be seen as an equality constraint SQP method for the partial augmented Lagrangian with respect to the coupling constraints. The authors of [39] showed that the ALADIN algorithm is roughly obtained, if for the Augmented Lagrangian method (cf. Section 3.3) the subproblem for current $\boldsymbol{\lambda}$

$$\min_{\Delta \boldsymbol{y}} \quad \sum_{i=0}^{N} f_i(\boldsymbol{y}_i + \Delta \boldsymbol{y}_i) + \boldsymbol{\lambda}^T \left(\sum_{i=0}^{N} A_i(\boldsymbol{y}_i + \Delta \boldsymbol{y}_i) - \boldsymbol{b} \right) + \frac{\mu}{2} \left\| \sum_{i=0}^{N} A_i(\boldsymbol{y}_i + \Delta \boldsymbol{y}_i) - \boldsymbol{b} \right\|_2^2$$
$$\text{s.t.} \quad \boldsymbol{y}_i + \Delta \boldsymbol{y}_i \in \mathcal{F}_i, \quad \text{for all } i = 1, \ldots, N$$

is only approximately solved by a single SQP step. The corresponding original subproblem would contain inequality constraints while the quadratic subproblem in Step 4 only comprises equality constraints. This corresponds to an equality-constrained QP method (EQP, see [54]) where the information on the active set is handled at SQP level and only equality-constrained

QPs are solved for each iteration. The main difference to common methods of this type is, how the approximation on the active set is computed. Usually, the working set is updated adding or removing inequalities depending on the last primal and dual step. In the ALADIN iteration additionally the decoupled stage problems are solved to determine a new estimate for the active set. Compared with the solution of inequality constraint QPs, the solution with only equality constraints is much simpler and thus normally faster. Comparing with other EQP methods, the more sophisticated procedure to determine a good working set gives hope for lower total numbers of iterations.

On the other hand, in the original ALADIN article the authors mention the ADMM as additional inspiration. With the special choice $\Sigma_i = A_i^T A_i$, approximations $C_i = 0$ and $H_i = \rho A_i^T A_i$ for $\mu \to \infty$ the ALADIN iteration is shown to be very similar to the ADMM applied the original problem (5.1) in a consensus reformulation. These rather coarse choices for the approximations indicate the potential of ALADIN in comparison with ADMMs. However, for any parameter choice ALADIN shares the structure with ADMMs and solves decoupled small NLPs first and then a large coupling problem. In that sense the algorithm alternates between solving two parts of the problem.

5.1.1 Step Size Computation and Global Convergence

In this subsection we summarize the steps to guarantee global convergence of the ALADIN algorithm as presented in [39] and review some of its parts. The issue of global convergence is mainly hidden in the step size choice of Algorithm 1. Houska et al. propose the following procedure of three steps to compute the step sizes α_1, α_2, α_3.

a) Try to take full step $\alpha_1 = \alpha_2 = \alpha_3 = 1$ and check if the trial $x^+ = \boldsymbol{y} + \Delta\boldsymbol{y}$ yields sufficient progress.

b) If the full step is not accepted, check if the NLP solutions $x^+ = \boldsymbol{y}$, i.e. $\alpha_1 = 1$, $\alpha_2 = \alpha_3 = 0$ yield sufficient progress.

c) If none of the previous trials is accepted, set $x^+ = x$ and update only the dual variable, i.e. set $\alpha_1 = \alpha_2 = 0$. Choose $\alpha_3 \in (0, 1]$ such that $V_\rho(x, \boldsymbol{\lambda} + \alpha_3(\boldsymbol{\lambda}_{\mathrm{QP}} - \boldsymbol{\lambda}))$ is globally maximized, where V_ρ denotes the optimal objective of the problem

$$V_\rho(\bar{\boldsymbol{x}}, \boldsymbol{\lambda}) := \min_{\boldsymbol{y} \in \tilde{\mathcal{F}}} \tilde{f}(\boldsymbol{y}; \boldsymbol{\lambda}, \bar{x}) := \min_{\boldsymbol{y} \in \tilde{\mathcal{F}}} \sum_{i=0}^{N} \left[f_i(\boldsymbol{y}_i) - \boldsymbol{\lambda}^T A_i \boldsymbol{y}_i + \frac{\rho}{2} \|\boldsymbol{y}_i - \bar{\boldsymbol{x}}_i\|_{\Sigma_i}^2 \right] + \boldsymbol{\lambda}^T b.$$

(5.12)

First, we concentrate on Steps a) and b) with a primal update. The progress of the algorithm is measured using a classical L_1-penalty function

$$\Phi(x) := \sum_{i=0}^{N} f_i(\boldsymbol{x}_i) + \bar{\lambda} \left\| \sum_{i=0}^{N} A_i \boldsymbol{x}_i - \boldsymbol{b} \right\|_1 \tag{5.13}$$

$$+ \bar{\kappa} \sum_{i=0}^{N} \Big[\|\boldsymbol{h}_i(\boldsymbol{x}_i)\|_1 + \sum_{k} \max(0, \boldsymbol{r}_i^{\mathrm{l}} - \boldsymbol{r}_i(\boldsymbol{x}_i))_k + \max(0, \boldsymbol{r}_i(\boldsymbol{x}_i) - \boldsymbol{r}_i^{\mathrm{u}})_k$$

$$+ \sum_{j} \max(0, \boldsymbol{b}_i^{\mathrm{l}} - \boldsymbol{x}_i)_j + \max(0, \boldsymbol{x}_i - \boldsymbol{b}_i^{\mathrm{u}})_j \Big].$$

Trials x^+ are accepted if the condition

$$\Phi(x) - \Phi(x^+) \geq \gamma \left(\sum_{i=0}^{N} \frac{\rho}{2} \|\boldsymbol{y}_i - \boldsymbol{x}_i\|_{\Sigma_i}^2 + \bar{\lambda} \left\| \sum_{i=0}^{N} A_i \boldsymbol{y}_i - \boldsymbol{b} \right\|_1 \right) \tag{5.14}$$

is satisfied for $0 < \gamma \ll 1$ where $\boldsymbol{y}_i$ are the solutions of last decoupled NLPs. If Algorithm 1 is not stopped by the termination criteria in step 2, then the right-hand side of (5.14) is bounded away from 0. It is clear then, that the algorithm stops after a finite number of iterations with steps sizes computed in steps a) or b) if Φ is bounded from below. For penalty parameters $\bar{\lambda}$ and $\bar{\kappa}$ sufficiently large this means that the original objective f of the optimization problem (5.1) is bounded from below on the feasible set $\tilde{\mathcal{F}}$. The original globalization strategy only considers the choices $\alpha_1 = \alpha_2 = 1$ and $\alpha_1 = 0$, $\alpha_2 = 1$, which could sometimes be improved by considering partial primal steps as well. These could be obtained using common line-search or planar search procedures. If the resulting primal trial yields sufficient progress (5.14), the argumentation sketched above still holds.

The third step of the globalization procedure is more involved. We start with some remarks and observations and give a short summary of the resting part of the globalization proof afterwards. First, we cite the remark made in [39] that the exact line-search, used for the presentation, is numerically not viable in practice. It can be replaced by practical inexact line-search algorithms based on Wolfe or Goldstein conditions for sufficient increase with respect to the objective function V_ρ.

The idea of Step c) is to make dual progress towards a multiplier $\boldsymbol{\lambda}$ that maximizes the dual objective $V_\rho(\bar{\boldsymbol{x}}, \boldsymbol{\lambda})$ for fixed $\bar{\boldsymbol{x}}$. Of course, this implies that the dual line-search in Step c), independently of being exact or inexact, has to be along a direction of sufficient increase to ensure the existence of a positive step length α_3. For the upcoming we consider a general dual search direction $\Delta\boldsymbol{\lambda}$ and the more general line-search subproblem to solve (approximately):

$$\tilde{V}(\alpha_3) := V_\rho(x, \boldsymbol{\lambda} + \alpha_3 \Delta\boldsymbol{\lambda}) = \min_{\boldsymbol{y} \in \Omega} \tilde{f}(\boldsymbol{y}; \boldsymbol{\lambda} + \alpha_3 \Delta\boldsymbol{\lambda}, \bar{\boldsymbol{x}}) \tag{5.15}$$

If the minimizer of the inner problem in (5.15) at $\alpha_3 = 0$ is unique and satisfies the second order necessary condition, LICQ and strong complementarity then we get from implicit function theorem that $\tilde{V}(\alpha_3)$ is continuously differentiable in a neighborhood of zero with

$$\mathrm{d}_{\alpha_3}\tilde{V}(\alpha_3) = \nabla_{\alpha_3}\tilde{f}(\boldsymbol{y}; \boldsymbol{\lambda} + \alpha_3\Delta\boldsymbol{\lambda}, \bar{\boldsymbol{x}}) = -\Delta\boldsymbol{\lambda}^T(\sum_{i=0}^{N} A_i\boldsymbol{y}_i(\alpha_3) - \boldsymbol{b}) \qquad (5.16)$$

$$\implies \mathrm{d}_{\alpha_3}\tilde{V}(0) = -\Delta\boldsymbol{\lambda}^T(\sum_{i=0}^{N} A_i\boldsymbol{y}_i - \boldsymbol{b}), \qquad (5.17)$$

where $\boldsymbol{y}$ is the solution of the inner problem (5.15) for $\alpha_3 = 0$. This corresponds to the solution of the augmented decoupled NLPs in Step 1 of the current ALADIN iteration. We note that this coincides with the results presented in Section 3.2. The search direction $\Delta\boldsymbol{\lambda}$ is thus an ascent direction if

$$\Delta\boldsymbol{\lambda}^T \left(\boldsymbol{b} - \sum_{i=0}^{N} A_i\boldsymbol{y}_i\right) > 0. \qquad (5.18)$$

The ALADIN algorithm is stated using $\Delta\boldsymbol{\lambda} = \boldsymbol{\lambda}_{\mathrm{QP}} - \boldsymbol{\lambda}$ as step for the dual update and the line-search of Step c) as well. We assume that the approximations H_i for Hessian are positive definite and the approximate Jacobian matrices C_i have full rank. Analogous computations as in [39, Appendix A] show then that this dual step satisfies

$$\boldsymbol{\lambda}_{\mathrm{QP}} - \boldsymbol{\lambda} = -(M - \frac{1}{\mu}I)^{-1}(\,\mathrm{d}_{\boldsymbol{\lambda}}V - \rho\sum_{i=0}^{N} A_i\tilde{M}_i\Sigma_i(\boldsymbol{y}_i - \boldsymbol{x}_i)), \qquad (5.19)$$

with

$$\mathrm{d}_{\boldsymbol{\lambda}}V = b - \sum_{i=0}^{N} A_i\boldsymbol{y}_i,$$

$$M = -\sum_{i=0}^{N} A_i\tilde{M}_iA_i^T \quad \text{with} \quad \tilde{M}_i = Z_i(Z_i^TH_iZ_i)^{-1}Z_i^T.$$

Here with Z_i we denote matrices whose columns form a basis for the Null space of C_i. The matrix M is negative semidefinite and hence $(M - \frac{1}{\mu}I) < 0$. We note that this corresponds to the results presented in Section 3.2 with the choices $A = [A_1 \dots A_n]$, $\mathcal{Y} = \tilde{\mathcal{F}}$ and the quadratic objective of the QP in Step 4. For the special choice $\rho = 0$ it is therefore clear that $\Delta\boldsymbol{\lambda} = \boldsymbol{\lambda}_{\mathrm{QP}} - \boldsymbol{\lambda}$ is indeed an ascent direction. Houska et al. remarked that in this case the dual search direction corresponds to a regularized dual Newton direction for a dual decomposition method.

Since $\rho = 0$ cannot be expected to hold during the iteration, it may be necessary to compute an ascent direction before accessing the Step c) of the globalization procedure. In order to avoid unnecessary computations, it is first checked whether the already computed direction $\boldsymbol{\lambda}_{\mathrm{QP}} - \boldsymbol{\lambda}$ is an ascent direction, anyway. If not, the most simple choice for an ascent direction would be to select the gradient direction

$$\Delta\boldsymbol{\lambda} = \mathrm{d}_{\boldsymbol{\lambda}}V = b - \sum_{i=0}^{N} A_i \boldsymbol{y}_i. \tag{5.20}$$

Inserting in (5.17) shows that this is clearly an ascent direction but it is well known that gradient methods may lead to slow convergence rates. We can solve another QP, similar to that in Step 4 of ALADIN, to get a search direction that can be interpreted as Newton-like direction, too. The only difference is to set the linear terms of the objective function directly as $\boldsymbol{g}_i = -A_i^T \boldsymbol{\lambda}$. For the QP multiplier $\tilde{\boldsymbol{\lambda}}_{\mathrm{QP}}$ computed with this slight variation we obtain the result (5.19) with $\rho = 0$. Hence, we get an ascent direction from $\tilde{\boldsymbol{\lambda}}_{\mathrm{QP}} - \boldsymbol{\lambda}$.

To come back to the global convergence of ALADIN, we note that $V_\rho(\bar{\boldsymbol{x}}, \boldsymbol{\lambda})$ for fixed $\bar{\boldsymbol{x}}$ is the partial dual function of the optimization problem

$$Z_\rho(\bar{\boldsymbol{x}}) := \min_{\boldsymbol{y} \in \tilde{\mathcal{F}}} \quad \sum_{i=0}^{N} \left[f_i(\boldsymbol{y}_i) + \frac{\rho}{2} \|\boldsymbol{y}_i - \bar{\boldsymbol{x}}_i\|_{\Sigma_i}^2 \right] \tag{5.21a}$$

$$\text{s.t.} \quad \sum_{i=0}^{N} A_i \boldsymbol{y}_i = \boldsymbol{b} \tag{5.21b}$$

with optimal objective value $Z_\rho(\bar{\boldsymbol{x}})$. Solving the decoupled stage problems in Step 1 thus corresponds to the evaluation of V_ρ in $\bar{\boldsymbol{x}}, \boldsymbol{\lambda}$. The solution of the central QP can then be interpreted as computation of an approximated Newton step for V_ρ followed by a line-search procedure to determine the optimal step length α_3. Now we are ready to cite the global convergence statement for Algorithm 1.

Theorem 5.1 ([39, Theorem 1]). *Let the optimization problem* (5.1) *be feasible and bounded from below. Assume that all functions* $f_i, \boldsymbol{h}_i, \boldsymbol{r}_i$ *are twice continuously differentiable with bounded second derivative. If the matrices* Σ_i *are chosen positive definite and* ρ, $\bar{\lambda}$, $\bar{\kappa}$ *are chosen sufficiently large, then Algorithm 1 using the presented procedure for computing the step sizes terminates after a finite number of steps.*

The global convergence proof given in [39] is split in two parts: First, it is supposed that Algorithm 1 runs infinitely often with Step c) of the globalization procedure and thus the primal iterate $\boldsymbol{x}$ is never updated. If in every iteration a dual ascent direction is computed, then the algorithm behaves like a dual ascent method for $V_\rho(\bar{\boldsymbol{x}}, \boldsymbol{\lambda})$ for fixed $\bar{\boldsymbol{x}}$. This means that the dual iterates $\boldsymbol{\lambda}$ converge to a maximizer of $V_\rho(\bar{\boldsymbol{x}}, \boldsymbol{\lambda})$ if it exists. In [39] it has been

shown that for a sufficiently large parameter ρ the maximum exists and that there is no duality gap:

$$\sup_{\boldsymbol{\lambda}} V_\rho(\bar{\boldsymbol{x}}, \boldsymbol{\lambda}) = Z_\rho(\bar{\boldsymbol{x}})$$

This means that the primal variables, i.e. the solutions of the augmented decoupled NLPs, converge to a limit $\boldsymbol{y}^*$ which is the solution of problem (5.21). On the other hand, it has been shown that every solution to this auxiliary problem satisfies the primal descent condition (5.14) if the penalty parameters $\bar{\lambda}$, $\bar{\kappa}$ are chosen sufficiently large. All together, this shows that after a finite number of steps at least the primal trial $\boldsymbol{x}^+ = \boldsymbol{y}$ corresponding to $\alpha_1 = 0$ is accepted in Step b). This contradicts the assumption that the algorithm uses Step c) infinitely often.

Hence, if the algorithm does not stop after a finite number of steps the primal trial has to be accepted in Steps a) or b) in an infinite number of iterations. As already mentioned before this is impossible if the optimization problem (5.1) is bounded from below and the penalty parameters $\bar{\lambda}$, $\bar{\kappa}$ are chosen sufficiently large because the progress in every iteration with accepted primal trial w.r.t. the L_1-penalty function (5.13) is bounded from below. Eventually, this contradicts the assumption of an infinite number of iterations.

5.1.2 Implementation

In this subsection we describe in more detail the methods used in the steps of Algorithm 1. We will present algorithmic choices as well as the actual selection of solvers for the subproblems that are incorporated in our concrete implementation utilized for the numerical experiments in Section 5.2.

Our experimental implementation of Algorithm 1 is done in C++ which offers a wide variety of programming paradigms. This choice also enables us to couple the algorithm directly to the model implementation briefly introduced before and to parts of the software framework Clean. This library is described best by citing the authors partly former colleagues M. Schmidt [61], J. Hübner [42] and D. Rose [58] who implemented numerical algorithms as part of their dissertations: "[The implementation] is part of the software framework Clean, which is an acronym for A *C++ Library of Efficient Algorithms in Numerics*. Clean is a generic library that is developed in the working group *Algorithmic Optimization* of Marc Steinbach at the Leibniz Universität Hannover. It is intended to become public domain when it is considered to be sufficiently mature."[1] The implementation of ALADIN follows the ideas of Clean and extensively uses C++ templates to get a generic implementation which permits a clearer separation of algorithm and data structures. For a more detailed description of the

---

[1][61, Chap. 5.2]

ideas of Clean and for examples of their realization in numerical algorithms we refer to the above mentioned references.

Initialization

We assume that the initial primal estimate $\boldsymbol{x}$ is passed to the algorithm by the user. This value is used unchanged to start the iterations. Special attention should be paid to the initial choice of the dual iterate $\boldsymbol{\lambda}$. If the primal start vector is already optimal, Algorithm 1 is not able to detect this in the first step if the dual starting vector is badly chosen. This would require costly ALADIN iterations with step size computation of type c) including the dual line-search. We spent an extra KKT solution to compute the dual multipliers $\boldsymbol{\lambda}$ that minimizes the violation of the dual feasibility condition (5.9) w.r.t. to the Euclidean norm. A similar procedure is described in [61] and used in the related interior-point method Clean::IPM.

Solution of the decoupled NLPs

The first subalgorithm of ALADIN to be chosen is the numerical solver for the decoupled problems (5.4) for each stage. Because we aim to apply the algorithm for example to the cost optimization problem for gas networks, this subsolver must be able to solve nonconvex optimization problems. There exist a variety of solvers that are able to handle this problem class. We use the interior-point solver Ipopt for the solution of these subproblems using its C++ interface for the coupling with the model implementation.

For Step 1 a penalty parameter ρ and the scaling matrices Σ_i have to be chosen. We implemented different strategies to set and adapt these during the iteration. For the norm inducing matrices we have implemented the identity matrix $\Sigma_i = I$, the positive definite Hessian approximation of the last iteration $H_i \approx H_i^*$ or the ADMM inspired choice $A_i^T A_i + \delta_c I$ that has to be convexified using the parameter $\delta_c > 0$ as possible selections. For the penalty parameter ρ an initial choice has to be provided to the algorithm. It is then adapted during the iteration following the simple procedure cited in the survey of Boyd et al. [6]. The parameter is increased or decreased if the primal and dual infeasibility of the solutions of the decoupled subproblems differ too much. In detail, the new penalty parameter is chosen according to

$$\rho = \begin{cases} \tau^{\text{incr}}\rho, & \text{if } \|\Sigma_i(\boldsymbol{y}_i - \boldsymbol{x}_i)\| > \mu^{\text{incr}}\|\sum_{i=0}^{N} A_i\boldsymbol{y}_i - \boldsymbol{b}\| \\ \rho/\tau^{\text{decr}}, & \text{if } \|\sum_{i=0}^{N} A_i\boldsymbol{y}_i - \boldsymbol{b}\| > \mu^{\text{decr}}\|\Sigma_i(\boldsymbol{y}_i - \boldsymbol{x}_i)\| \\ \rho, & \text{otherwise,} \end{cases} \tag{5.22}$$

with parameters $\tau^{\text{incr}}, \tau^{\text{decr}}, \mu^{\text{incr}}, \mu^{\text{decr}} > 1$. A slightly weakened variant of this procedure is also available that only updates the parameter if the conditions implying a change are satisfied in k successive iterations.

The coupling QP

For Step 3 we have to select the approximation to the Jacobian matrices of the active constraints as well as for the Hessian of the Lagrangian. We decide to take the exactly evaluated derivatives here. Of course, the use of approximations makes the algorithm more flexible and may accelerate the solution of the coupling QP. However, in the current state we aim to test the performance of the algorithm fed with the best available data.

Additionally, this step includes the determination of the active set corresponding to the current $\boldsymbol{y}$. Since the solver of the decoupled NLPs is not guaranteed to explicitly hold information on the active set of the solutions $\boldsymbol{y}_i$, we select the numerically active constraints based on the primal and dual solution of the decoupled problems (5.4). This is in line with the usage of Ipopt as solver for the stage NLPs since it provides access to the multipliers associated with the returned solution.

We solve the assembled quadratic problem (5.7) by solving the associated KKT-system for the primal and dual variables. The system is obtained as KKT conditions (3.5) for the coupling QP. Its Lagrangian function and the corresponding stationarity conditions are

$$\mathcal{L}(\Delta \boldsymbol{y}_i, \boldsymbol{s}, \boldsymbol{\lambda}_{\text{QP}}, \boldsymbol{\kappa}_{\text{QP}}) := \sum_{i=0}^{N} \{ \tfrac{1}{2} \Delta \boldsymbol{y}_i^T H_i \Delta \boldsymbol{y}_i + \boldsymbol{g}_i^T \Delta \boldsymbol{y}_i - \boldsymbol{\kappa}_{\text{QP},i}^T (C_i \Delta \boldsymbol{y}_i) \}$$

$$- \boldsymbol{\lambda}^T \boldsymbol{s} + \frac{\mu}{2} \|\boldsymbol{s}\|_2^2 - \boldsymbol{\lambda}_{\text{QP}}^T \left(\sum_{i=0}^{N} A_i(\boldsymbol{y}_i + \Delta \boldsymbol{y}_i) - \boldsymbol{b} - \boldsymbol{s} \right)$$

$$(5.23)$$

$$0 \overset{!}{=} \nabla_{\Delta \boldsymbol{y}_i} \mathcal{L}(\Delta \boldsymbol{y}_i, \boldsymbol{s}, \boldsymbol{\lambda}_{\text{QP}}, \boldsymbol{\kappa}_{\text{QP}}) = H_i \Delta \boldsymbol{y}_i + \boldsymbol{g}_i - A_i^T \boldsymbol{\lambda}_{\text{QP}} - C_i^T \boldsymbol{\kappa}_{\text{QP},i}, \quad \forall i \in \{1, \dots, N\}$$

$$(5.24)$$

$$0 \overset{!}{=} \nabla_{\boldsymbol{s}} \mathcal{L}(\Delta \boldsymbol{y}_i, \boldsymbol{s}, \boldsymbol{\lambda}_{\text{QP}}, \boldsymbol{\kappa}_{\text{QP}}) = -\boldsymbol{\lambda} + \boldsymbol{\lambda}_{\text{QP}} + \mu \boldsymbol{s}.$$

$$(5.25)$$

These conditions rewritten in matrix-vector form complemented with the primal conditions

yield the KKT-System:

$$
\begin{bmatrix}
H_1 & & & A_1^T & C_1^T & & \\
& \ddots & & \vdots & & \ddots & \\
& & H_N & A_N^T & & & C_N^T \\
& & & \mu I & -I & & \\
A_1 & \dots & A_N & -I & & & \\
C_1 & & & & & & \\
& \ddots & & & & & \\
& & C_N & & & & \\
\end{bmatrix}
\begin{pmatrix}
\Delta \boldsymbol{y}_1 \\
\vdots \\
\Delta \boldsymbol{y}_N \\
\boldsymbol{s} \\
-\boldsymbol{\lambda}_{\mathrm{QP}} \\
-\boldsymbol{\kappa}_{\mathrm{QP},1} \\
\vdots \\
-\boldsymbol{\kappa}_{\mathrm{QP},N}
\end{pmatrix}
=
\begin{pmatrix}
-\boldsymbol{g}_1 \\
\vdots \\
-\boldsymbol{g}_N \\
+\boldsymbol{\lambda} \\
\boldsymbol{b} - \sum_{i=0}^N A_i \boldsymbol{y}_i \\
0 \\
\vdots \\
0
\end{pmatrix}
\tag{5.26}
$$

It is well known that if the approximations to the Hessian (5.6) are positive definite on the Null space of full rank Jacobian matrices C_i, then the solution of the coupling QP (5.7) is equivalent to the solution of the linear system. Using (5.25) we get

$$
\boldsymbol{s} = \frac{\boldsymbol{\lambda} - \boldsymbol{\lambda}_{\mathrm{QP}}}{\mu}.
$$

That can be exploited to eliminate the *slack* $\boldsymbol{s}$ from the linear system:

$$
\sum_{i=0}^N A_i(\boldsymbol{y}_i + \Delta \boldsymbol{y}_i) - b = \boldsymbol{s} = \frac{\boldsymbol{\lambda} - \boldsymbol{\lambda}_{\mathrm{QP}}}{\mu}
\tag{5.27}
$$

$$
\iff \sum_{i=0}^N A_i \Delta \boldsymbol{y}_i + \frac{1}{\mu}\boldsymbol{\lambda}_{\mathrm{QP}} = \boldsymbol{b} - \sum_{i=0}^N A_i \boldsymbol{y}_i + \frac{1}{\mu}\boldsymbol{\lambda}
\tag{5.28}
$$

This corresponds to the reduced linear system

$$
\begin{bmatrix}
H_1 & & & A_1^T & C_1^T & & \\
& \ddots & & \vdots & & \ddots & \\
& & H_N & A_N^T & & & C_N^T \\
A_1 & \dots & A_N & -\frac{1}{\mu}I & & & \\
C_1 & & & & & & \\
& \ddots & & & & & \\
& & C_N & & & & \\
\end{bmatrix}
\begin{pmatrix}
\Delta \boldsymbol{y}_1 \\
\vdots \\
\Delta \boldsymbol{y}_N \\
-\boldsymbol{\lambda}_{\mathrm{QP}} \\
-\boldsymbol{\kappa}_{\mathrm{QP},1} \\
\vdots \\
-\boldsymbol{\kappa}_{\mathrm{QP},N}
\end{pmatrix}
=
\begin{pmatrix}
-\boldsymbol{g}_1 \\
\vdots \\
-\boldsymbol{g}_N \\
\boldsymbol{b} - \sum_{i=0}^N A_i \boldsymbol{y}_i + \frac{1}{\mu}\boldsymbol{\lambda} \\
0 \\
\vdots \\
0
\end{pmatrix},
\tag{5.29}
$$

which can be solved by any linear solver. We require an additional feature of the used linear solver. Since we want to use the exact Hessian matrices whenever possible, there is no guarantee in general that all are positive definite. We therefore apply an adaptive convexification scheme, like it is used for example in Ipopt (cf. [70]), that uses information obtained during the factorization of system (5.29). A convexification parameter δ_c is increased

repeatedly yielding a Hessian approximation $H = H^* + \delta_c I$ if necessary to obtain a unique solution of the linear system. These strategies are usually based on the so-called *inertia* of the matrix, i.e. the number of positive, negative and zero eigenvalues. We refer for example to the survey of Forsgreen [25] for more details. The sparse linear solver MA57 [41],[21] that we has been selected as linear solver for Ipopt, too, provides this information during the factorization and is therefore a viable choice as linear solver.

Another point related to the coupling QP is the update of the augmented Lagrangian penalty parameter μ. We start with a rather small parameter and adapt it depending on the progress of the algorithm with respect to the relaxed coupling conditions. The strategy stated for example in the textbook of Nocedal and Wright [54, Alg. 17.4] for the present case is given in Algorithm 2. It is called after each QP solution to determine the new parameter μ for the upcoming iteration and checks if the relaxed coupling constraints are satisfied sufficiently well compared to a threshold that is diminished in the course of iterations.

Algorithm 2 Update of Augmented Lagrangian penalty parameter μ

Input: μ^{old}, $\eta > 0$
1: **if** $\|\sum_{i=0}^{N} A_i(\boldsymbol{y}_i + \Delta\boldsymbol{y}_i) - \boldsymbol{b}\|_1 < \eta$ **then**
2: $\quad \mu = \mu^{\text{old}}$
3: $\quad \eta = \eta/\mu^{0.9}$
4: **else**
5: $\quad \mu = 100\,\mu^{\text{old}}$
6: $\quad \eta = 1/\mu^{0.1}$
7: **end if**

Step length computation

Our implementation of the step length computation in Step 5 basically follows the procedure presented in the previous section. The first difficulty is to determine the penalty parameters $\bar{\lambda}$ and $\bar{\kappa}$ for the primal descent condition (5.14). It is commonly accepted that the determination of optimal penalty parameters for merit functions is in general a hard task that motivated for example the development of alternative globalization frameworks (cf. [24]). However, we use a strategy presented in [54] for SQP methods that aims to choose sufficiently large penalty parameters that do not interfere with the progress of the algorithm. As extension of the basic search in globalization Steps a) and b), we employ a basic backtracking search along the whole line segment for $\alpha_1 = 1$ and $\alpha_2 \in [0, 1]$ for an acceptable trial, starting with the full step $\alpha_1 = \alpha_2 = 1$.

If no primal acceptable point is found, we have to invoke the dual line-search of globalization step c) and follow the remarks made above. We select an ascent direction for V_ρ by checking

first if the already existing dual direction $\boldsymbol{\lambda}_{\mathrm{QP}} - \boldsymbol{\lambda}$ satisfies condition (5.18). If this is not the case, we compute a new Newton-like condition by solving the QP (5.7) or the equivalent KKT matrix again with modified right-hand-side:

$$
\begin{bmatrix} H & A^T & C^T \\ A & -\frac{1}{\mu}I & 0 \\ C & 0 & 0 \end{bmatrix} \begin{pmatrix} \bar{\boldsymbol{y}} \\ \bar{\boldsymbol{\lambda}}_{\mathrm{QP}} \\ \bar{\boldsymbol{\kappa}} \end{pmatrix} = \begin{pmatrix} -A^T \boldsymbol{\lambda} \\ \boldsymbol{b} - A\boldsymbol{y} + \frac{1}{\mu}\boldsymbol{\lambda} \\ 0 \end{pmatrix}
$$

Here we used the compact notation combining the matrices $H = \mathrm{diag}(H_1, \ldots, H_N)$, $C = \mathrm{diag}(C_1, \ldots, C_N)$ and $A = [A_1, \ldots, A_n]$. As already stated above, then the analog choice $\Delta\boldsymbol{\lambda} = \bar{\boldsymbol{\lambda}}_{\mathrm{QP}} - \boldsymbol{\lambda}$ yields an ascent direction if all Hessian approximations are positive definite. We want to remark here that this procedure provides a Newton-like ascent direction without an additional factorization of the KKT matrix. This strategy may lead to problems if we use the exact Hessian as described above. The Hessian are augmented by the convexifications if necessary but only to ensure that the Hessian H is positive definite on the Null space of $\begin{bmatrix} A \\ C \end{bmatrix}$. From the computations for the Hessian of the dual (3.17) we can see that we at least need the Hessian H to be positive definite on the Null space of C to guarantee that $\Delta\boldsymbol{\lambda} = \bar{\boldsymbol{\lambda}}_{\mathrm{QP}} - \boldsymbol{\lambda}$ is an ascent direction. Hence, an additional factorization may be required. Alternatively, we could just select the gradient direction (5.20). As last comment on the step computation we remark on the denomination "Newton-like" for the dual steps. To get, the still regularized, dual Newton direction for V_ρ, the scaling matrices Σ_i have to be considered when assembling the H_i. Thus, the computation would require a new matrix factorization for the case $\rho \neq 0$. Once we have a dual ascent direction, we determine the step size α_3 by a common backtracking line-search. The evaluation at every trial step size comprises the solution of the decoupled stage problems.

5.2 Numerical Experiences

In this section we present our numerical experiences using the ALADIN algorithm for the solution of the energy cost optimization problems stated and discussed in the previous chapters. As principal test case for the computations the OPAL pipeline (see sec. 4.2.1) is used. For the presented optimization model we compare the performance of the implementation of ALADIN with the solution progress obtained by the interior-point method Ipopt which has been used before to compute the numerical results in Chapter 4.

As mentioned in the previous section, the ALADIN algorithm is run using Ipopt as solver for the decoupled stage NLPs. Exact Hessian and Jacobian matrices are computed for the QP which is solved by the sparse solver HSL MA57 that is also used by Ipopt. The focus at

implementing the algorithm and the model evaluation has not been set on the performance. Hence, a comparison of CPU times would not provide meaningful results, yet. There is clearly lot of potential for further improvement in the implementation, e.g. parallelization. One point that definitely should be parallelized is the solution of the local NLPs for every stage. In our experimental implementation the whole algorithm runs sequentially, hence solves the decoupled problems in sequence as well. However, it is reasonable to compare the total number of iterations which corresponds directly to the number primal-dual KKT systems, i.e. equality constraint QPs, to solve. Since the linear systems to be solved in each iteration of ALADIN or Ipopt, do not differ significantly in structure, size and sparsity, the iteration number characterizes if the ALADIN algorithm has the potential to perform better on these instances. To do so, the number of ALADIN iterations should be significantly lower than the number of Ipopt iterations.

Comparison for basic pipeline test

We start with a simple example that shows promising performance of the implementation of ALADIN. The optimization model is set up for the first weekly energy price profile and a coarse time discretization grid of only one time step per hour, i.e. $\Delta t = 3600\,\text{s}$, for the time horizon of the complete week (and additional 6 hours). The resulting structured NLP then has 174 stages with 656 variables and 440 equations each. Together with the 37 236 coupling constraints this sums up to a total of 114 144 variables and 113 796 equations.

We select the ADMM inspired choice for the scaling matrices $\Sigma_i = A_i^T A_i + 0.01I$ and the penalty parameters are initially chosen as $\rho = 5$ and $\mu = 10^5$. With the chosen parameter choice the ALADIN algorithm performs well on this test problem and solves it in only 6 iterations which requires almost 2 minutes of computing time.

In Figure 5.1 the relevant feasibility measures are plotted. For better readability we use the notation

$$\boldsymbol{\theta}(\boldsymbol{x}) = \begin{pmatrix} \theta_1(\boldsymbol{x}_1) \\ \vdots \\ \theta_N(\boldsymbol{x}_N) \end{pmatrix} \quad \text{with} \quad \boldsymbol{\theta}_i(\boldsymbol{x}_i) = \begin{pmatrix} \boldsymbol{h}_i(\boldsymbol{x}) \\ \max(0, \boldsymbol{r}_i(\boldsymbol{x}_i) - \boldsymbol{r}_i^{\text{u}}) - \max(0, \boldsymbol{r}_i^{\text{l}} - \boldsymbol{r}_i(\boldsymbol{x}_i)) \\ \max(0, \boldsymbol{x}_i - \boldsymbol{b}_i^{\text{u}}) - \max(0, \boldsymbol{b}_i^{\text{l}} - \boldsymbol{x}_i) \end{pmatrix},$$

for the violation of the constraints associated with the stage NLPs, where the max is to be understood componentwise. The plot shows a favorable behavior of the ALADIN implementation. First, the initial vector corresponds to the stationary solution of the problem and is hence feasible for this problem with constant boundary data. The linear coupling conditions are exactly satisfied while the nonlinear equations are fulfilled only up to a tolerance since the initial is obtained as result of an antecedent numerical computation for the stationary
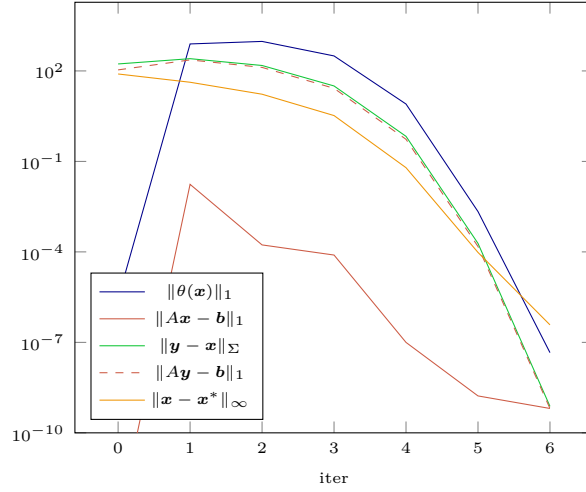
Figure 5.1: ALADIN: Infeasibilities vs Iterations

state. For this particular problem the algorithm is making only full steps. This means that in this case for every iteration we have $\boldsymbol{x} = \boldsymbol{y} + \Delta\boldsymbol{y}$ and the coupling error $\|A\boldsymbol{x} - \boldsymbol{b}\|_1$ is the same as for the QP-solution. The varying convergence rate for the coupling error can be explained by the update procedure for the Augmented Lagrangian penalty term μ which is increased before iteration 2 and 4. We have also plotted the distance $\|\boldsymbol{x} - \boldsymbol{x}^*\|_\infty$ of the iterates from the optimal solution as computed by lpopt. The final distance is 3.8×10^{-7} which is not decreased in further iterations. lpopt uses a heuristic relaxing simple bounds during the run to avoid numerical difficulties. The lpopt solution is finally computed with slightly different bounds and thus serves as reference solution only up to a certain tolerance. However, the iterates seem to converge with superlinear rate towards the solution. The infeasibility with respect to the constraints associated to the stage NLPs $\|\theta(\boldsymbol{x})\|_1$ shows a similar behavior. Additionally, the primal infeasibility $\|A\boldsymbol{y} - \boldsymbol{b}\|_1$ and dual infeasibility $\|\boldsymbol{y} - \boldsymbol{x}\|_\Sigma$ corresponding to the NLP solutions are plotted. The penalty parameter ρ is updated according to (5.22) with the objective that these two infeasibility measures converge at similar rate. As desired, both terms converge with the same rate for this instance, keeping ρ constant at its initial choice. The same model instance is solved by lpopt in 21 iterations.

The performance of the ALADIN implementation is now compared with lpopt for the cost optimization problem for different time discretizations. We consider the first two days of the first energy price profile as well as the complete weekly (again with additional 6 hours at the end) profile for time step length of one to five time steps per hour, i.e. time step lengths of 3600 s, 1800 s, 1200 s, 900 s and 720 s. Since it is not clear a-priori how to parametrize the ALADIN code we have made tests for a range of parameters for the penalty parameter ρ, its update strategy parameters (cf. Equation 5.22) and the selection of the scaling matrices Σ_i.

Table 5.1: Comparison of iteration numbers: ALADIN vs. lpopt

Prob.	Δt/s	#Stages	#Iter. lpopt	#Iter. ALADIN (Configuration)	solved
048.1	3600	48	17	4 (e.g. $\rho = 5$, $\Sigma_i = A_i^T A_i + 10^{-2}I$)	80
048.2	1800	96	18	5 (e.g. $\rho = 5$, $\Sigma_i = A_i^T A_i + 10^{-2}I$)	80
048.3	1200	144	20	8 (e.g. $\rho = 5$, $\Sigma_i = A_i^T A_i + 10^{-2}I$)	79
048.4	900	192	24	11 (e.g. $\rho = 5$, $\Sigma_i = A_i^T A_i + 10^{-2}I$)	78
048.5	720	240	24	16 (e.g. $\rho = 100$, $\Sigma_i = I$)	11

The results for adaptively changed ρ have not shown any improvements in our tests compared to the constant parameter choice. This includes that in most of the runs the update formula (5.22) does not change the parameter. Hence, we concentrate on constant penalty parameters for the discussion, which yields 80 parametrizations of our ALADIN implementation then used to solve the cost optimization problem. Table 5.1 shows the results for the comparison of the lpopt iteration number and the best ALADIN run for the first test with 48 h time horizon. The parametrization for one of the runs of Algorithm 1 with smallest iteration number is given as well as the total number of parametrizations that have been able to solve the problem within the time limit of 2 hours and at most 100 iterations. The failures also include collapsing solution procedures for the subproblems, i.e. the augmented stage problems, the QP as well as the dual line-search. The results show that the implementation is able to solve the instances for time discretizations with up to four time steps per hour quite well and especially in significantly less iterations than required by lpopt. The problem's difficulty is increasing with the number of stages which is reflected in moderately increasing iteration numbers of both implementations. Except for the results for the time step size of 720 s, the results are as expected. As a first observation we remark that for this case only 11 parametrizations of ALADIN solve the problem whereas the instances for bigger time steps are solved by almost all parametrizations. Additionally, the minimal iteration number increases significantly and in particular is not obtained by the parametrizations that are among the fastest for the smaller instances. All successful runs are characterized by a greater convexification of the augmented objectives of the stage problems achieved by bigger values for the parameter ρ or the convexification of $A^T A$. We remark additionally that all the ALADIN runs presented above always select the full step, i.e. $\boldsymbol{x}^+ = \boldsymbol{y} + \Delta \boldsymbol{y}$, in Step 5 of Algorithm 1.

The same test runs have also been done for the same OPAL network using the complete weekly energy profile. The results are given in Table 5.2. As for the smaller time horizon there can be found parametrizations for our implementation of Algorithm 1 that beat lpopt in the number of total iterations. For the coarser time grids for one and two time steps per

Table 5.2: Comparison of iteration numbers: ALADIN vs. lpopt

Prob.	Δt/s	#Stages	#Iter. lpopt	#Iter. ALADIN (Configuration)	solved
0174.1	3600	174	21	6 (e.g. $\rho = 5$, $\Sigma_i = A_i^T A_i + 10^{-2}I$)	80
0174.2	1800	348	23	10 (e.g. $\rho = 5$, $\Sigma_i = A_i^T A_i + 10^{-2}I$)	74
0174.3	1200	522	25	16 (e.g. $\rho = 5$, $\Sigma_i = A_i^T A_i + 10^{-2}I$)	72
0174.4	900	696	28	21 (e.g. $\rho = 5$, $\Sigma_i = A_i^T A_i + 10^{-2}I$)	49
0174.5	720	870	29	26 ($\rho = 25$, $\Sigma_i = A_i^T A_i + 5 \times 10^{-2}I$)	11

hour the iteration number is below the half of the number of iterations required by lpopt. Hence, for these cases a considerably number of KKT system solutions can be avoided.

For the time step size of 1800 s a comparison of the iteration of lpopt and the ALADIN implementation with parameters $\rho = 5$, $\Sigma_i = A_i^T A_i + 10^{-2}I$ is illustrated in Figure 5.2. As before, we take the lpopt solution as reference point and plot its distance to the iterates measured by the maximum norm. The plot shows the expected advantage of the ALADIN algorithm since the iterates seem to reach much faster the local convergence region where the Newton type convergence comes into effect. The final distance to the reference should again be attributed to the lpopt strategy of relaxing the bounds by small amounts.

For finer time discretizations the problems seem to be much more difficult to solve for our implementation. This is expressed by the total number of parametrizations that are able to solve the problem instance. Like for the smaller time horizon this number decreases especially for the finest time discretization. Clearly, this is also related to the constant choice of the time limit which is more likely to be violated for large problems that naturally require longer run times. But even the best parametrization beats the result of lpopt in the number of iterations only by a few iterations. For these cases the effort of solving the decoupled NLPs in each iterations is not refunded in the number of total iterations.
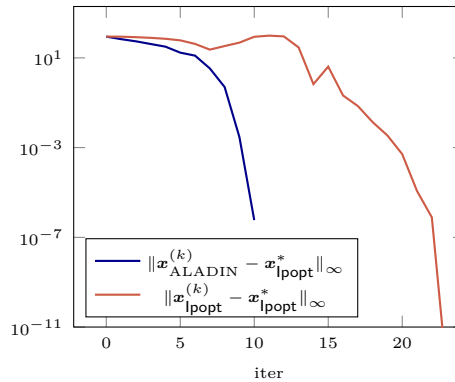

Figure 5.2: ALADIN vs. lpopt: Comparison for runs for Problem `0174.2`

Table 5.3: Comparison of ALADIN iteration numbers for different constant penalty parameters ρ and scaling matrices Σ_i for Problem `0174.4`.

Σ_i	$\rho = 1$	$\rho = 5$	$\rho = 10$	$\rho = 20$	$\rho = 25$	$\rho = 35$	$\rho = 50$	$\rho = 100$	$\rho = 150$
$H_i + \delta_c I$	–	32	24	–	–	–	–	–	–
$B_i(0.01)$	–	21	21	21	23	25	25	–	26
$B_i(0.05)$	36	24	22	24	28	–	–	–	–
$B_i(0.1)$	–	22	22	25	26	25	25	27	28
$B_i(0.5)$	23	24	31	31	29	34	–	39	31
$B_i(1)$	23	21	32	–	34	30	28	29	33
$B_i(5)$	21	–	27	–	–	30	35	–	–
I	23	25	–	–	–	27	–	–	–

Note that the increasing difficulty seems to be related to the discretization step size and not purely to the problem size. The number of stages which is directly associated with the total problem size, for problem `048.5`, i.e. the first 48 hours with five time steps per hour, is much smaller then problem `0174.2` for the complete time horizon and two time steps per hour. The former smaller problem is only solved by 11 parametrizations whereas the latter is solved by almost all parametrizations (74 of 80).

To show the strong dependence on the parameter choice of ALADIN, we compare the performance of the ALADIN implementation for different initial choices for ρ and for different choices for the scaling matrices Σ_i. The total number of iterations for different parametrizations solving Problem `0174.4`, i.e. the complete weekly profile and a time step size of $\Delta t = 900\,\text{s}$, is given in Table 5.3. As described before the Hessian matrices of the previous iteration $H^{(k-1)}$ are adaptively convexified by the parameter δ_c. We denote by $B_i(\delta) = A^T A + \delta I$ the convexified scaling matrices inspired by ADMM.

The fails include exceeding of the maximal number of 100 iterations or the maximal computing time of $2\,\text{h}$ as well as failures in the solution of the subproblems. We can observe that the best results for these problems are obtained for the moderately convexified scaling matrices $A^T A$ and not too big penalty parameters ρ. The results indicate the difficulties to generalize them to rules how to get a reliable choice for the parameters for other problems. In this table these problem appears as "holes" in the area of successful runs. For example the choice for the scaling matrices $\Sigma_i = B_i(0.05)$ fails for $\rho = 35$ and $\rho = 50$, whereas the runs for $\Sigma_i = B_i(0.01)$ as well as for $\Sigma_i = B_i(0.1)$ are successful for both selected penalty parameters. Beginning with certain iteration numbers with iterates still far away from the reference solution both failed runs only apply the pure dual update. According to the global convergence strategy at some point the current solutions $\boldsymbol{y}$ should satisfy the coupling equations. There is no observable progress w.r.t. this measure for these runs which are finally stopped by the time limit.

Finally, we comment on the runs for the parametrization $\rho = 5$ and $\sigma_i = A_i^T A_i + 10^{-2} I$ on problems `048.5` and `0174.5`. This parametrization appeared as one of the best for all other time discretizations but fails to solve the problem for the finest discretization. However, the reason of failure is difficult to isolate. Applied to Problem `048.5` the solver gets stuck at some point unable to compute search directions that yield progress measured by the merit function as well as compared to the reference solution. The run for Problem `0174.5` is finished by the time limit as well but the distance of the last iterates to the reference solution is already very small. However, the implementation is not able to improve the iterate such that the termination criteria in Step 2 are satisfied. This numerical issue can partly be attributed to the solution tolerance provided by Ipopt as solver for the decoupled stage problems. Additionally, during the run some steps which would yield progress towards the reference solution are refused by the merit function. This indicates that a better choice for the penalty parameters for the merit function (5.13) could improve the performance here. Indeed, choosing smaller penalty parameters initially leads to faster convergence, but still the solution cannot be proven to be optimal by the termination criteria.

Further Tests and Outlook

The experiences made for the OPAL pipeline test case can be best summarized by the nonsensical statement that the implementation of Algorithm 1 works well if it works well. The results for the coarser time discretization show impressively lower iteration numbers compared with Ipopt. The successful runs are almost all characterized by not requiring the line search procedure of Step 4, i.e. taking only full steps. Whenever the third alternative with only dual update is invoked more than very few times, what is likely the case for more complicated instances, the algorithm does not provide acceptable performance on our test cases.

In addition to the experiments for the OPAL pipeline, we applied our implementation to the network test introduced in Section 4.2.2. The model was assembled for the coarse discretization of one time step per hour on a time horizon of two days. The constant cost profile that has been used for the earlier comparisons has been applied here as well. Even for the relaxed limits on iteration number (25 000) and computation time (24 h) none of the tested parametrizations of ALADIN has been able to compute an optimal solution. On the other hand, Ipopt solved this problem in 40 iterations requiring less than 45 s. Most of the tested runs are again canceled by the time limit, which already allows for a waste of computation time. All final iterates are not even close to the reference solution. However, it proved to be difficult to identify the reasons for these failures. The network test case differs from the OPAL case in not starting from a feasible point. Only the stationary state of the

network corresponding to the boundary values at the initial time point is available. The boundary values, which are part of the description of the feasible sets $\mathcal{F}_i$ of the problems for every stage, vary. Hence, the stationary state as starting point is not feasible w.r.t. these constraints. In all cases, the line search frequently rejects the full step and only a partial primal step or even the pure dual step is selected in Step 5. For many of these iterations the QP (5.7) does not even provide a dual ascent direction which has to be computed by an extra linear solve. Clearly, these problems are not part of the favorable instances, solved for any small penalization with ρ without requiring a globalization routine. Since the ALADIN algorithm shares many ideas with dual decomposition approaches, which are expected to perform well far from the solution, we did not expect such a poor performance, anyway.

The failures could be related to different difficulties hidden in the abstract description of Algorithm 1. In Step 1 the vector $\boldsymbol{y}$ is set to be the minimizer of the augmented stage problems. There is no further specification which solution concept is required here. Nevertheless, for the global convergence proof it is assumed that this step is equivalent to the evaluation of the dual function of the problem (5.21). This indicates, that a global optimal solution is necessary in this context. However, most NLP solvers that are usually applied to the decoupled problems (5.4) compute solutions that may or may not be the global optimum. Since they use local information only, no guarantees are made with respect to global solutions. This could possibly yield to problems for the global convergence of the algorithm. As a remedy so-called global solvers could be employed for the stage problems but this would imply a much bigger computational effort for each stage problem and hence contradict the assumption, that the small decoupled problems are solved rather fast.

Additionally, the theory at different points assumes that chosen constants are "sufficiently large". It is well known that satisfying these assumptions is involved from a numerical point of view. It is usually not desired to choose these parameters very large initially since this probably interferes with the algorithms performance. Finding the best strategy of when and how to increase or even decrease these parameters is known to be very challenging. We have already commented on this issue for ALADIN and presented our algorithmic choices which however again depend on new parameters to select. Hence, the complexity is further increased, which makes it still more difficult to understand the behavior. However, in comparison with established solver implementations like Ipopt our implementation still lacks heuristics and other techniques that improve the reliability of the algorithm, like e.g. non-monotone techniques. The determination of the current active set and the associated approximation for the Jacobian matrix of the constraints also deserves further attention since we believe that in some iterations bad search direction are computed from the QP solution. This may be related to the selection of the working set.

Hence, there are various open questions and tasks to make our implementation of Al-

gorithm 1 a reliable alternative. Beside the above stated problems, the computational performance could be improved. So far our experimental implementation does not solve the decoupled parts of the algorithm in parallel. Additionally, problem specific linear solvers for the gas network problem as presented in [64] could be tested as replacement for the general purpose solver, currently used.

We selected the ALADIN approach because it would provide a good basis for further structure aware solver development for the optimization on gas transmission networks. The separation between the nonlinear stage models and the solution of the possibly approximated coupling QP allows for a combination of more detailed stage descriptions with tractable coupling QPs. In addition to the time structure, the gas network optimization problem also inherits the structure of the underlying network, which could be exploited in this context. Nevertheless, without a remedy for the reliability problems of the algorithm in general and, in particular, of our ALADIN implementation, no further steps have been possible.

Chapter 6

Conclusions and Outlook

In this thesis a transient optimization model for gas networks has been presented and discussed. We employed mathematical optimization techniques to this model for realistic networks to evaluate the new proposal to use gas transmission networks as storage for electric energy.

The isothermal Euler equation account for the principal contribution to the model, characterizing the flow inside pipelines. We showed that this governing PDEs satisfy the typical assumption to be treated as strict hyperbolic system on a network. Based on these results the finite volume framework ADER has been applied to the model. By a novel comparison of these high order schemes with a finite difference approximation, commonly utilized for the mathematical optimization on gas networks, we could show that the typical dynamics in gas transmission networks is described sufficiently well by the approximation obtained by an implicit box scheme. The numerical results showed visible differences only in the presence of large variations in the solution which stay acceptably small. Thus, the usage of such discretizations schemes, using implicit time steps, is justified and recommended for complete transmission networks, especially comparing the computational effort, which make the finite volume approach intractable in an optimization context, yet.

Using this optimization model, we have shown that the existing gas transmission infrastructure can play a role for storage of renewable electric energy. The presented case studies indicate that the operation of electric compressor drives having the electricity network under consideration can be beneficial even for just one compressor station. Nevertheless, we have also presented results that show that the potential is strongly dependent on the price as indicator as well as on the network structure and the capacity to operate the network away from the state required for the normal operation. Of course, there are still various open questions to complement. In addition to an embedding economic study it would be very interesting to verify the promising results for real operation data of network operators. Having a better data basis, the model could also be enhanced to include the network structure with more details. However, we are positive that the essential conclusion has not to be changed incorporating a more detailed network model. Moreover, there are various directions to

extend the model coverage on the neglected effects. One could include to the model, for example, temperature effects, discrete control decisions as well as the effects of uncertainty concerning the energy prices and the external in- and outflow to the networks. All these lead to very challenging optimization problems that require further investigation.

Additionally, our implementation of the distributed algorithm ALADIN [39] and its application to the optimization problem, trying to exploit the problem structure originating from the underlying time discretization, has been presented. This algorithm was selected because of its potential to serve as a starting point for the development of structure exploiting solvers not only for the transient optimization of gas networks but also others fitting in a separable structure. With our implementation we could show promising performance of this approach compared to an established interior-point solver on models for a simple network and coarse time discretizations. On the other hand, poor reliability has been observed for finer discretizations and furthermore it has not been possible to apply the implemented algorithm successfully to more complicated networks. The algorithm's performance appears to be strongly related to the involved choice of parameters and subalgorithms which makes its application to challenging problems very difficult.

Bibliography

[1]   M. K. Banda and M. Herty. "Multiscale modeling for gas flow in pipe networks."
       In: *Mathematical Methods in the Applied Sciences* 31 (08/2008), pp. 915–936. DOI:
       `10.1002/mma.948`.

[2]   D. P. Bertsekas. *Constrained Optimization and Lagrange Multiplier Methods.* Computer
       Science and Applied Mathematics. New York, London: Academic Press, 1982.

[3]   D. P. Bertsekas. *Nonlinear programming. 2nd ed.* English. 2nd ed. Belmont, MA: Athena
       Scientific, 1999, pp. xiv + 777.

[4]   H. G. Bock, E. Kostina, H. X. Phu, and R. Rannacher, eds. *Modeling, Simulation and
       Optimization of Complex Processes.* Berlin: Springer, 2005.

[5]   R. Borsche and J. Kall. "ADER schemes and high order coupling on networks of
       hyperbolic conservation laws." In: *Journal of Computational Physics* 273 (2014), pp. 658–
       670. DOI: `10.1016/j.jcp.2014.05.042`.

[6]   S. Boyd, N. Parikh, E. Chu, B. Peleato, and J. Eckstein. "Distributed Optimization and
       Statistical Learning via the Alternating Direction Method of Multipliers." In: *Found.
       Trends Mach. Learn.* 3.1 (01/2011), pp. 1–122. DOI: `10.1561/2200000016`.

[7]   A. Bressan. *Hyperbolic Systems of Conservation Laws: The One Dimensional Cauchy
       Problem.* English. Vol. 20. Oxford Lecture Series in Mathematics and Its Applications.
       Oxford University Press, 2000.

[8]   A. Bressan, S. Čanić, M. Garavello, M. Herty, and B. Piccoli. "Flows on networks:
       recent results and perspectives." In: *EMS Surveys in Mathematical Sciences* 1.1 (2014),
       pp. 47–111. DOI: `10.4171/EMSS/2`.

[9]   J. Burgschweiger, B. Gnädig, and M. C. Steinbach. "Optimization Models for Operative
       Planning in Drinking Water Networks." In: *Optim. Eng.* 10.1 (2009). Published online
       2008, pp. 43–73. DOI: `10.1007/s11081-008-9040-8`.

[10]   R. H. Byrd, N. I. M. Gould, J. Nocedal, and R. A. Waltz. "An Algorithm for Nonlinear
       Optimization Using Linear Programming and Equality Constrained Subproblems." In:
       Math. Program., Ser. B 100.1 (05/2004), pp. 27–48.

[11] R. H. Byrd, J. Nocedal, and R. A. Waltz. *Feasible Interior Methods Using Slacks for Nonlinear Optimization.* Tech. rep. OTC 2000/11. Argonne National Laboratory, 2000.

[12] R. G. Carter. "Pipeline Optimization: Dynamic Programming after 30 Years." In: *30th Annual Meeting.* Paper 9803. Pipeline Simulation Interest Group. 1998.

[13] G. Cerbe. *Grundlagen der Gastechnik.* Hanser, 2008.

[14] R. M. Colombo, G. Guerra, M. Herty, and V. Schleper. "Optimal control in networks of pipes and canals." In: *SIAM Journal on Control and Optimization* 48.3 (2009), pp. 2032–2050.

[15] R. M. Colombo, M. Herty, and V. Sachers. "On 2\times2 conservation laws at a junction." In: *SIAM Journal on Mathematical Analysis* 40.2 (2008), pp. 605–622.

[16] A. R. Conn, N. I. M. Gould, and P. L. Toint. "A Globally Convergent Augmented Lagrangian Algorithm for Optimization with General Constraints and Simple Bounds." In: *SIAM J. Numer. Anal.* 28.2 (1991), pp. 545–572.

[17] R. Courant, K. Friedrichs, and H. Lewy. "Über die partiellen Differenzengleichungen der mathematischen Physik." German. In: *Mathematische Annalen* 100.1 (1928), pp. 32–74. DOI: 10.1007/BF01448839.

[18] H. Derlien and J. Müller-Kirchenbauer. "Elektromobiles Erdgas - Stromspeicherung und Steigerung der Energieeffizienz durch elektrische Verdichterantriebe." German. In: *gwf Gas Erdgas* 152.9 (2011), pp. 558–563.

[19] Deutsche Energie-Agentur GmbH. *Strategieplattform Power to Gas.* 2017. URL: http://www.powertogas.info/power-to-gas/pilotprojekte-im-ueberblick/ (visited on 10/08/2017).

[20] A. S. Drud. *CONOPT: A System for Large Scale Nonlinear Optimization, Reference Manual for CONOPT Subroutine Library.* Tech. rep. ARKI Consulting and Development A/S, Bagsvaerd, Denmark, 1996.

[21] I. S. Duff. "MA57—a Code for the Solution of Sparse Symmetric Definite and Indefinite Systems." In: *ACM Trans. Math. Softw.* 30.2 (06/2004), pp. 118–144. DOI: 10.1145/992200.992202.

[22] K. Ehrhardt and M. C. Steinbach. "KKT Systems in Operative Planning for Gas Distribution Networks." In: *Proc. Appl. Math. Mech.* 4.1 (2004), pp. 606–607. DOI: 10.1002/pamm.200410284.

[23] K. Ehrhardt and M. C. Steinbach. "Nonlinear Optimization in Gas Networks." In: *Modeling, Simulation and Optimization of Complex Processes*. Ed. by H. G. Bock, E. Kostina, H. X. Phu, and R. Rannacher. Berlin: Springer, 2005, pp. 139–148. DOI: `10.1007/3-540-27170-8_11`.

[24] R. Fletcher and S. Leyffer. *Nonlinear Programming without a Penalty Function*. Preprint NA/171. Dundee, DD1 4HN, Scotland, U. K.: University of Dundee, 09/1997.

[25] A. Forsgren. "Inertia-controlling factorizations for optimization algorithms." In: *Applied Numerical Mathematics* 43.1 (2002). 19th Dundee Biennial Conference on Numerical Analysis, pp. 91–107. DOI: `https://doi.org/10.1016/S0168-9274(02)00119-8`.

[26] Fraunhofer-Institut für Solare Energiesysteme ISE. *Stromproduktion und Börsenstrompreise in Deutschland*. 2017. URL: `https://www.energy-charts.de/price_de.htm` (visited on 10/08/2017).

[27] A. Fügenschuh, B. Geißler, R. Gollmer, A. Morsi, M. E. Pfetsch, J. Rövekamp, M. Schmidt, K. Spreckelsen, and M. C. Steinbach. "Physical and technical fundamentals of gas networks." In: *Evaluating Gas Network Capacities*. Ed. by T. Koch, B. Hiller, M. E. Pfetsch, and L. Schewe. SIAM-MOS series on Optimization. SIAM, 2015. Chap. 2, pp. 17–43. DOI: `10.1137/1.9781611973693.ch2`.

[28] M. Garavello and B. Piccoli. *Traffic flow on networks.* English. Springfield, MO: American Institute of Mathematical Sciences (AIMS), 2006, pp. xvi + 243.

[29] C. Geiger und C. Kanzow. *Theorie und Numerik restringierter Optimierungsaufgaben.* Springer, 2002.

[30] B. Geißler. "Towards Globally Optimal Solutions for MINLPs by Discretization Techniques with Applications in Gas Network Optimization." PhD thesis. Friedrich-Alexander Universität Erlangen-Nürnberg, Germany, 2011.

[31] P. E. Gill, W. Murray, and M. S. Saunders. "SNOPT: An SQP Algorithm for Large-Scale Constrained Optimization." In: *SIAM J. Optim.* 12.4 (2002), pp. 979–1006.

[32] M. Gugat. "Boundary Controllability between Sub- and Supercritical Flow." In: *SIAM J. Control Optim.* 42 (2003), pp. 1056–1070.

[33] M. Gugat and M. Herty. "Existence of classical solutions and feedback stabilization for the flow in gas networks." In: *ESAIM: Control, Optimisation and Calculus of Variations* 17.01 (2011), pp. 28–51.

[34]   M. Gugat, M. Herty, A. Klar, G. Leugering, and V. Schleper. "Well-posedness of Networked Hyperbolic Systems of Balance Laws." English. In: *Constrained Optimization and Optimal Control for Partial Differential Equations*. Ed. by G. Leugering, S. Engell, A. Griewank, M. Hinze, R. Rannacher, V. Schulz, M. Ulbrich, and S. Ulbrich. Vol. 160. International Series of Numerical Mathematics. Basel: Springer, 2012, pp. 123–146. DOI: `10.1007/978-3-0348-0133-1_7`.

[35]   M. Gugat and G. Leugering. "Global boundary controllability of the de St. Venant equations between steady states." In: *Annales de l'Institut Henri Poincare (C) Non Linear Analysis* 20.1 (2003), pp. 1–11. DOI: `10.1016/S0294-1449(02)00004-5`.

[36]   N. Heinecke, U. Gotzes, B. Hiller, J. Rövekamp, and T. Koch. "Regulatory rules for gas markets in Germany and Europe." In: *Evaluating Gas Network Capacities*. Ed. by T. Koch, B. Hiller, M. E. Pfetsch, and L. Schewe. SIAM-MOS series on Optimization. SIAM, 2015. Chap. 3, pp. 45–64. DOI: `10.1137/1.9781611973693.ch3`.

[37]   M. Herty and V. Sachers. "Adjoint calculus for optimization of gas networks." In: *Networks and heterogeneous media* 2.4 (2007), pp. 733–750. DOI: `10.3934/nhm.2007.2.733`.

[38]   M. Herty and M. Seaïd. "Simulation of transient gas flow at pipe-to-pipe intersections." In: *International Journal for Numerical Methods in Fluids* 56.5 (2008), pp. 485–506. DOI: `10.1002/fld.1531`.

[39]   B. Houska, J. Frasch, and M. Diehl. "An Augmented Lagrangian Based Algorithm for Distributed NonConvex Optimization." In: *SIAM Journal on Optimization* 26.2 (2016), pp. 1101–1127. DOI: `10.1137/140975991`.

[40]   HSL. *A collection of Fortran codes for large scale scientific computation*. URL: `http://www.hsl.rl.ac.uk/`.

[41]   *HSL MA57 Package Specification*. The HSL Mathematical Software Library. 03/2013.

[42]   J. Hübner. "Distributed Algorithms for Nonlinear Tree-Sparse Problems." PhD thesis. Gottfried Wilhelm Leibniz Universität Hannover, 2016.

[43]   J. Kall. "ADER Schemes for Systems of Conservation Laws on Networks." PhD thesis. Technische Universität Kaiserslautern, 2016.

[44]   T. Koch, B. Hiller, M. E. Pfetsch, and L. Schewe, eds. *Evaluating Gas Network Capacities*. SIAM-MOS series on Optimization. SIAM, 2015. xvii + 364. DOI: `10.1137/1.9781611973693`.

[45] O. Kolb, J. Lang, and P. Bales. "An implicit box scheme for subsonic compressible flow with dissipative source term." English. In: *Numerical Algorithms* 53.2-3 (2010), pp. 293–307. DOI: 10.1007/s11075-009-9287-y.

[46] J. Králik, P. Stiegler, Z. Vostrý, and J. Závorka. "A Universal Dynamic Simulation Model of Gas Pipeline Networks." In: *IEEE Trans. Syst., Man, Cybern.* 14.4 (1984), pp. 597–606.

[47] J. Králik, P. Stiegler, Z. Vostrý, and J. Záworka. "Modeling the Dynamics of Flow in Gas Pipelines." In: *IEEE Trans. Syst., Man, Cybern.* SMC-14.4 (1984), pp. 586–596.

[48] R. J. LeVeque. *Numerical methods for conservation laws. 2nd ed.* English. 2nd ed. Basel: Birkhäuser, 1992, pp. x + 214. DOI: 10.1007/978-3-0348-8629-1.

[49] R. J. Leveque. *Finite Volume Methods for Hyperbolic Problems.* University Press, 2002.

[50] A. Martin and M. Möller. "Cutting Planes for the Optimization of Gas Networks." In: *Modeling, Simulation and Optimization of Complex Processes.* Ed. by H. G. Bock, E. Kostina, H. X. Phu, and R. Rannacher. Berlin: Springer, 2005, pp. 307–329. DOI: 10.1007/3-540-27170-8_24.

[51] H. Mittelmann. *Decision Tree for Optimization Software.* 2017. URL: http://plato.asu.edu/guide.html.

[52] B. A. Murtagh and M. A. Saunders. *MINOS 5.4 USER'S GUIDE.* Tech. rep. SOL 83-20R. Stanford University, CA 94305: Department of Operations Research, Stanford, 1993.

[53] NEL Gastransport GmbH. *Webpage OPAL Gastransport GmbH & Co. KG.* 2017. URL: https://www.nel-gastransport.de/en/our-network/ (visited on 09/14/2017).

[54] J. Nocedal and S. J. Wright. *Numerical Optimization.* 2nd. Berlin: Springer, 2006. DOI: 10.1007/978-0-387-40065-5.

[55] OPAL Gastransport GmbH & Co. KG. *Webpage OPAL Gastransport GmbH.* 2017. URL: https://www.opal-gastransport.de/en/our-network/ (visited on 09/14/2017).

[56] I. Papay. *OGIL Musz. Tud. Kozl.* Budapest, 1968.

[57] R. Z. Ríos-Mercado, S. Kim, and A. E. Boyd. "Efficient Operation of Natural Gas Transmission Systems: A Network-Based Heuristic for Cyclic Structures." In: *Computers & Operations Research* 33.8 (2006), pp. 2323–2351. DOI: 10.1016/j.cor.2005.02.003.

[58] D. Rose. "An Elastic Primal Active-Set Method for Structured QPs." submitted. PhD thesis. Gottfried Wilhelm Leibniz Universität Hannover, 2017.

[59] A. Ruszczyński. *Nonlinear Optimization.* Princeton University Press, 2006.

[60] D. Scheibe and A. Weimann. "Dynamische Gasnetzsimulation mit GANESI." In: *GWF Gas / Erdgas* 9 (1999), pp. 610–616.

[61] M. Schmidt. "A Generic Interior-Point Framework for Nonsmooth and Complementarity Constrained Nonlinear Optimization." PhD thesis. Gottfried Wilhelm Leibniz Universität Hannover, 2013.

[62] M. Schmidt, M. C. Steinbach, and B. M. Willert. "High detail stationary optimization models for gas networks." In: *Optim. Eng.* (2014), pp. 1–34. DOI: `10.1007/s11081-014-9246-x`.

[63] M. Schmidt, M. C. Steinbach, and B. M. Willert. "The precise NLP model." In: *Evaluating Gas Network Capacities.* Ed. by T. Koch, B. Hiller, M. E. Pfetsch, and L. Schewe. SIAM-MOS series on Optimization. SIAM, 2015. Chap. 10, pp. 181–210. DOI: `10.1137/1.9781611973693.ch10`.

[64] M. C. Steinbach. "On PDE Solution in Transient Optimization of Gas Networks." In: *J. Comput. Appl. Math.* 203.2 (2007), pp. 345–361. DOI: `10.1016/j.cam.2006.04.018`.

[65] E. F. Toro. "Riemann solvers with evolved initial conditions." In: *International Journal for Numerical Methods in Fluids* 52.4 (2006), pp. 433–453. DOI: `10.1002/fld.1186`.

[66] E. F. Toro. *Riemann solvers and numerical methods for fluid dynamics. A practical introduction. 3rd ed.* English. 3rd ed. Berlin: Springer, 2009, pp. xxiv + 724. DOI: `10.1007/b79761`.

[67] F. Tröltzsch. *Optimale Steuerung partieller Differentialgleichungen. Theorie, Verfahren und Anwendungen.* German. 2nd revised ed. Wiesbaden: Vieweg + Teubner, 2009, pp. x + 311. DOI: `10.1007/978-3-8348-9357-4`.

[68] R. J. Vanderbei and D. F. Shanno. "An Interior-Point Algorithm For Nonconvex Nonlinear Programming." In: *Comput. Optim. Appl.* 13 (1997), pp. 231–252.

[69] Y. Villalobos-Morales, D. Cobos-Zaleta, H. J. Flores-Villarreal, C. Borraz-Sánchez, and R. Z. Ríos-Mercado. "On NLP and MINLP Formulations and Preprocessing for Fuel Cost Minimization of Natural Gas Transmission Networks." In: *Proceedings of the 2003 NSF Design, Service and Manufacturing Grantees and Research Conference.* Birmingham, USA, 01/2003.

[70] A. Wächter and L. T. Biegler. "On the Implementation of an Interior-Point Filter Line-Search Algorithm for Large-Scale Nonlinear Programming." In: *Math. Program.* 106.1 (2006), pp. 25–57. DOI: `10.1007/s10107-004-0559-y`.

[71]   R. A. Waltz, J. L. Morales, J. Nocedal, and D. Orban. "An interior algorithm for nonlinear optimization that combines line search and trust region steps." In: *Math. Program.* 107.3 (07/2006), pp. 391–408. DOI: 10.1007/s10107-004-0560-5.

[72]   A. Weimann. "Modellierung und Simulation der Dynamik von Gasnetzen im Hinblick auf Gasnetzführung und Gasnetzüberwachung." Ph. D. dissertation. Technische Universität München, 1978.

[73]   J. F. Wilkinson, D. V. Holliday, E. H. Batey, and K. W. Hannah. *Transient Flow in Natural Gas Transmission Systems.* American Gas Association, New York, 1964.

[74]   P. J. Wong and R. E. Larson. "Optimization of Natural-Gas Pipeline Systems Via Dynamic Programming." In: *IEEE Trans. Automat. Contr.* 13 (10/1968), pp. 475–481. DOI: 10.1109/TAC.1968.1098990.

[75]   P. J. Wong and R. E. Larson. "Optimization of Tree-Structured Natural-Gas Transmission Networks." In: *J. Math. Anal. Appl.* 24 (3 1968), pp. 613–626. DOI: 10.1016/0022-247X(68)90014-0.

[76]   S. Wu. *Steady-State Simulation and Fuel Cost Minimization of Gas Pipeline Networks.* Thesis (Ph.D.)-University of Houston. ProQuest LLC, Ann Arbor, MI, 1998, p. 153.

Lebenslauf

Jan Thiedau

geboren am 25.03.1987 in Gehrden

06/2006	Abitur an der Marie-Curie-Schule Ronnenberg
10/2006–09/2009	Studium im Bachelor of Science Studiengangs Mathematik mit Anwendungsfach Physik, Leibniz Universität Hannover
03/2009–12/2009	Auslandssemester an der Universidad del Norte, Barranquilla, Kolumbien
05/2009	Bachelorarbeit: *Non-Conforming Finite Element Methods for Electromagnetic Problems*, Institut für Angewandte Mathematik, Prof. Dr. Stephan
10/2009–03/2012	Studium im Master of Science Studiengangs Mathematik mit Anwendungsfach Meteorologie, Leibniz Universität Hannover
01/2012	Masterarbeit: *Ein NLP-Ansatz zur Betriebsoptimierung in Abwassernetzen*, Institut für Angewandte Mathematik, Prof. Dr. Steinbach
03/2012–12/2017	Wissenschaftlicher Mitarbeiter am Institut für Angewandte Mathematik, AG Algorithmische Optimierung (Prof. Steinbach), Leibniz Universität Hannover